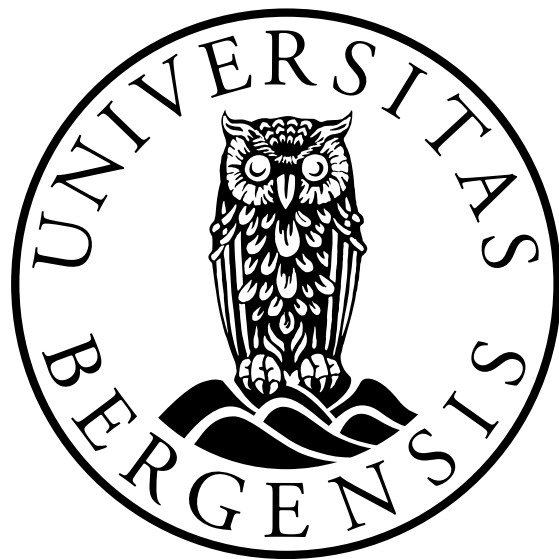


Extreme Precipitation in Nepal - Trends and Key Processes

Patrik Bohlinger



Dissertation for the degree of Philosophiae Doctor (PhD)

Geophysical Institute
University of Bergen

November, 2017

Scientific environment

My work for this thesis was carried out at the Geophysical Institute (GFI), University of Bergen (UiB), Norway. I was employed on a four year university PhD position, funded by the UiB. The PhD position included one year of duty work which was spent on being teaching assistant at the GFI for the courses GEOF328 Mesoscale Dynamics and GEOF321 Numerical Weather Prediction, and outreach via the Turspor-project (turspor.buib.no, ut.no). Computational resources for processing and analysing data were provided from the UiB in form of two minor local work station clusters capable of parallel computing. For model runs and data processing, I had access to the high performance computing environment Hexagon, a 204.9 TFlops Cray XE6m-200 cluster provided by Notur, the national infrastructure for High-Performance Computing. During my overseas stay at the National Center for Atmospheric Research, Boulder, US and after I used NCAR's Yellowstone 1.5-petaflops high-performance IBM iDataPlex cluster for model runs and data processing. As a PhD-student, I was part of the Norwegian Research School in Climate Dynamics (ResCLIM) and the Research School on Changing Climates in the Coupled Earth System (CHESS). With funding from the research schools, I could attend numerous courses helping me to develop technical skills and widening my horizon. The financial support from The Research Council of Norway through the Klimaforsk program enabled my overseas stay at NCAR. I was active in the Bjerknes Centre for Climate Research as a member of the Research Group 2: Climate predictions from global to regional scales, and the Bjerknes Research Group on Climate Hazards.

Acknowledgements

I would like to thank my principal supervisor Asgeir Sorteberg for our valuable scientific discussions, his visit in Boulder, the baby equipment, and the fun skiing trip in the Rocky Mountains. I am grateful to my second supervisor Roy Rasmussen for his scientific input and perspective, hosting me at NCAR, and inviting me to Thanksgiving and Easter celebration with his family. It was also very interesting for me to listen to both supervisors sharing more general views on science, climate, meteorology, and life outside of my PhD topic. I thank Changhai Liu for his help with the WRF simulations, Ethan Gutmann for the opportunity to work with his new model ICAR and useful programming advices, Harald Sodemann for valuable comments and the training in his water source diagnostic tool, Buwan Bhatt for discussing results of station data in Nepal, and Anak Bhandari for helping me to purchase the rain gauge data from Nepal. I thank the Graduate schools, ResClim and CHESS, for interesting courses, Klimaforsk for financing my stay at NCAR, the summer school on “Extreme Value Modeling and Water Resources” 2016 in Lyon for the best block course I have ever attended, the meteorology group at the GFI and the Bjerknes RG2 group for providing me a platform to present and discuss my results. I am grateful to my research group at the Meteorological Institute in Bergen “Oceanography and Maritime Meteorology” for offering me a great researcher position before I delivered my thesis and for taking it easy on me while I was finishing my PhD. I would also like to thank Astrid Fremme for discussions on water sources, the Friday Soccer group for being a great therapy and Kjetil Våge for reminding me that there is nothing more important than soccer on Friday noon, the Beer Brewing group for the fun time when brewing and tasting, and the GFI band for some fun gigs where I was equally surprised every single time that we managed to play some songs in the end. Further, I thank the PhDs and postdocs at GFI and NCAR for the great social environment, the Friday-Inside group with Takaya Saito, Torge Lorenz, Erwin Lambert, Lander R. Crespo, and Arne Klein for knowing how to switch off my brain, Valerie Kumer, Stefan Keiderling, Stephan Kral, Line Båserud, Omar El Guernaoui for being great office mates, and Mathew Stiller-Reeve, Tim Dunker, Aleksi Nummelin, Erwin Lambert, and Lisbeth Håvik for being awesome reviewers. I thank my parents and sisters for supporting me in my decision to move to Norway. And, to my superduper Lisbeth: thank you for your support, for keeping the house together and taking good care of our babygirl Johanna while I was finishing my PhD, and of course for reading through my stuff again and again; I am a lucky man having you two in my life.

Abstract

Nepal is located at the rim of the Himalayas and houses the highest mountains of the world. Owing to the complex topography and a seasonal monsoon climate, Nepal experiences precipitation events of considerable intensity. Large amounts of rain lead to natural hazards like landslides, floods, infrastructure damage, agricultural losses, and human casualties. It is therefore important to understand whether there are changes in extreme precipitation in Nepal, and which physical processes lead to an extreme event while taking into account the spatial variability of rainfall.

To approach these questions the setup of this thesis is threefold. First, a measurement based climatology of precipitation was established and trends in extreme precipitation were detected. Second, synoptic scale conditions associated with extreme precipitation in Nepal were revealed, and third, a case study was used to proceed to the process level and obtain a better understanding of how involved processes interact and finally end in an extreme event.

The first manuscript (Paper I) aims to assess the rainfall climatology and trends in extreme precipitation based on rain gauge data in Nepal from 1971-2010. Rain gauge data show that most of the annual precipitation is recorded during the Indian summer monsoon with considerable variability in time and space. Upper quantiles and annual maxima occur mainly during the Indian summer monsoon. The seasonal precipitation varies with the El Niño-Southern Oscillation (ENSO). This correlation vanishes with increasing quantiles. Trends in precipitation extremes were assessed using linear regression, quantile regression, and non-stationary extreme value theory. Moreover, parameter estimation for the non-stationary extreme value distribution was performed applying a maximum likelihood and a Bayesian approach. Multiple approaches add information regarding the method sensitivity of the trends. The study concludes that despite high spatial variability in the trends of extreme precipitation, Far-West Nepal shows a robust positive trend in extreme precipitation across the different methods.

The significant changes in extreme precipitation found in Paper I urge a better understanding of the involved physical processes, which motivates the second and third manuscript (Paper II and Paper III). Paper II investigates atmospheric synoptic scale conditions and moisture sources related to extreme precipitation events in Nepal. The high spatial variability in daily rainfall was taken into account by clustering daily precipitation from rain gauges using K-means clustering. As a result, spatial patterns of daily rainfall were established dividing Nepal into West, Central, and East Nepal. The study focuses on extreme precipitation events during which the 99.5 percentile was exceeded at least at five stations at the same time in one cluster. Based on the resulting set

of extreme precipitation events, a composite study was conducted for each cluster using meteorological fields from Era-Interim reanalysis. The study shows that large scale atmospheric flow was angled toward the Himalayas at the cluster location during an extreme event following mid- and upper-tropospheric trough structures in geopotential height. Tracking of low pressure systems indicates that the large scale flow conditions guided the low pressure systems toward the Himalayas where they rain out. These results show that the large scale flow conditions mainly determined the location of the extreme event. A Lagrangian moisture source diagnostic reveals anomalously abundant moisture sources over land, particularly over the Indo-Gangetic plain, along the path of the low level flow. The moisture was likely provided by foregone precipitation events over this region preconditioning the soil moisture for additional uptake. It was further found that monsoon break conditions were prevailing during 25 %-43 % of all extreme events during July and August.

To go deeper into the responsible physical processes and their interplay, Paper III focuses on one case, the extreme precipitation event on 19 July 2007 in Nepal. This extreme event was part of a sequence of precipitation events contributing to the South Asia flood 2007 affecting 20 million people. The study is based on rain gauge data, TRMM 3B42, Era-Interim reanalysis, Lagrangian trajectories, and a high resolution numerical simulation. The combination of these different datasets allows a multiscale analysis of the considered extreme precipitation event. The evolution of the extreme event started with individual convective cells forming over Nepal that were invigorated by moist low-level inflow with high convective available energy. The individual cells organized upscale into an intense wide convective system and resulted in torrential rain with over 250 mm within 24 hours. The synoptic scale conditions were similar to Paper II, permitting and orchestrating the development of this extreme event. The following conditions were identified: prior to the extreme event precipitation events preconditioned the soil moisture along the Indo-Gangetic plain, anomalously high moisture sources were available along the path of the low level flow which was characteristic for monsoon break periods, abundant moisture sources enabled the formation of moist airmasses fueling the convective system, and the airmasses were destabilized by topographic and quasi-geostrophic forcing where the final trigger mechanism was probably the upslope flow. Besides investigating an interesting extreme precipitation event, this study shows how synoptic conditions can co-exist and interact to form a system of unusual intensity.

Together, the three studies provide the basis for a comprehensive understanding of extreme precipitation events in Nepal. The interplay between atmospheric circulation and moisture sources are of particular importance. The conditions, as described in Paper II and III, have to be just right to provoke an extreme event and should therefore be useful to increase the ability of forecasting an extreme event. Challenges resulting from the pronounced changes in extreme precipitation (Paper I) can be approached supported by the conditions found in Paper II and III. The involved processes can be pursued in future studies to gain further insights which will hopefully foster new research and useful findings for Nepal.

List of papers

1. Bohlinger, P., Sorteberg, A., 2017: *A comprehensive view on trends in extreme precipitation in Nepal and their spatial distribution*, Int. J. Climatol., doi: 10.1002/joc.5299
2. Bohlinger, P., Sorteberg, A., and Sodemann, H.: *Synoptic conditions and moisture sources actuating extreme precipitation in Nepal*, accepted for publication in J. of Geophys. Res. Atmospheres, doi: 10.1002/2017JD027543
3. Bohlinger, P., Sorteberg, A., Liu, C., Rasmussen, R., Sodemann, H., and Ogawa, F.: *Multiscale characteristics of an extreme precipitation event over Nepal*, submitted to Q. J. R. Meteorol. Soc.

Prologue

The Indian summer monsoon affects over a billion of people. For the societies that are fine-tuned toward economic profit depending on precisely clocked and appropriate amounts of the seasonal monsoon precipitation, small variations can bring about severe consequences. Variations that were not anticipated, can considerably impact crops and hence the gross domestic product of countries in the affected region. As a result of this, authorities of concerned countries supported and advocated research aiming at increasing the understanding and predictability of the monsoon, which, for good and bad, is a remarkably complex circulation entangled in multiple components of the Earth system. It is therefore not surprising that the amount of research conducted on the countless aspects of the monsoon is overwhelming, featuring considerable scientific efforts and important results.

While I was reading up on the literature about the Indian summer monsoon, I found myself confronted with three challenges: the literature is endless, abstract and presumably complex mechanisms are often taken as given, and their origin and explanation is sometimes hard to trace back. This makes it challenging to both find out how processes work and whether someone actually had explored those. I noticed that oftentimes a bridge was missing between a climatic scale occurrence of events and the processes responsible for the occurrence of these events. With my work, I hope to shed light, not only on prevailing conditions during extreme precipitation events in Nepal, but also on the processes that need to co-exist and interact to make a precipitation event extreme. I attempted to perform a transition from a climatic perspective, quite common in monsoon literature, to get beyond the *what* and end with the process oriented perspective *why*. In this way, I strived to build this bridge connecting the climatic scale to the processes. I wanted to obtain an idea about the important mechanisms and a comprehensive understanding of how the mechanisms work without being chained to one single process.

Since I was dealing with extreme events, I soon asked myself what that really meant; What is an extreme event? It turned out that the answer to this essential question was not simple. An extreme event could be defined in myriad of ways, customized to the region, process, and needs of the study. In the literature, authors justified different ways on how to define extremes and how to detect changes in extremes. The approaches varied from basic statistics to very advanced statistical methods claiming that the simple methods were not appropriate. I felt it difficult to judge what would be appropriate and hence, right from the start of my PhD, I had a tenacious itching, urging me to better understand statistics of extreme values. I believed this to be crucial for understanding published work and interpreting changes in extreme events; I ended up with so much

more. Diving into extreme value statistics was very instructive and helped me to better understand famous scientific results e.g. from the *International Panel on Climate Change* on the future of extreme weather. I met statisticians at the National Center of Atmospheric Research in Boulder (NCAR), US, and at a summer school on extreme value statistics in Lyon, France, that had both an enormous knowledge and the patience and gift to communicate it. During the summer school in Lyon, I noticed that, although statistical methods are widely used in climate science and meteorology, the language is not nearly the same. Together with a french mathematician, I tried to discuss problems in statistics and likewise his questions about atmospheric physics. It took about two weeks of laughing and aching stomach muscles due to misunderstandings before we reached a state, where we could efficiently convey our questions and answers in connected sentences. Learning to communicate across the borders of those disciplines together with understanding Bayesian statistics were eureka experiences for me as a non-statistician.

My stay at NCAR was important in many more aspects. In my research group at NCAR and outside, I met very capable and helpful people that got me closer to the world of numerical models and their development. I was lucky enough to work with the developer of the model ICAR, Ethan Gutmann, and discuss parameterization issues with a main developer of the WRF-model, Jimi Dudhia. Due to their comments, I could improve my understanding of numerical models as well as the efficiency of my programming. I inhaled every bit of what the fruitful scientific environment had to offer. Above all, the nature in the Rocky mountains and its fantastic snow conditions really was the icing on the cake. Together with other PhD-students and postdocs I enjoyed the best skiing experience of my life.

The research environment at the Geophysical Institute in Bergen and the Bjerknes Center for Climate Research together was a great place to spend the time of my PhD. It was a special time for me, not only professionally but also in my private life. I am grateful for my colleagues, the people I met, and that I could learn so much. Motivated by scientists crafting impressive publications, I am looking forward to continue my learning process in the future.

Contents

Scientific environment	i
Acknowledgements	iii
Abstract	v
List of papers	vii
Prologue	ix
1 Introduction	1
1.1 Setting the scene	1
1.2 Availability of precipitation measurements in Nepal	2
2 Scientific background	5
2.1 Main processes governing precipitation along the Himalayas	5
2.2 Spatial variability of precipitation in Nepal	8
2.3 Temporal variability of precipitation in Nepal	9
2.3.1 The Indian summer monsoon	10
2.3.2 Other sources of temporal variability	12
3 Objectives	15
4 Key findings and discussion	17
5 Concluding remarks and outlook	19
6 Data and methods	21
6.1 Data	21
6.2 Methods	22
6.2.1 Statistical approaches	22
6.2.2 Physical approaches	30
7 Scientific results	37
7.1 Summary of the papers	37
7.2 A comprehensive view on trends in extreme precipitation in Nepal and their spatial distribution	39

7.3	Synoptic conditions and moisture sources actuating extreme precipitation in Nepal	55
7.4	Multiscale characteristics of an extreme precipitation event over Nepal .	117

Chapter 1

Introduction

1.1 Setting the scene

Over the recent years, extreme weather events and particularly extreme precipitation events have become increasingly prevalent in scientific literature. Since extreme weather events are of societal importance, the Intergovernmental Panel on Climate Change issued a Special Report on Extreme Events [[Field et al., 2012](#)], together with the Fifth Assessment Report [[Stocker et al., 2013](#)], state that the magnitude of precipitation extremes and their frequency of occurrence have been increasing over most of the globe.

[Chalise and Khanal \[2002\]](#) conclude that in Nepal, extreme weather entailing heavy precipitation is the primary cause of natural disasters. The most common hazards in Nepal connected to extreme precipitation are glacier lake outburst floods, landslides, dam breaks, and flash floods [[Chalise and Khanal, 2002](#)] with severe consequences including human casualties, agricultural loss, pests and diseases, and infrastructure damage.

Climate projections for the future suggest an enhancement of the existing global spatial pattern, meaning dryer regions become dryer and wetter regions become wetter [[Field et al., 2012; Stocker et al., 2013](#)]. Moreover, extreme events are projected to become more pronounced in the future over most of the globe [[Sillmann et al., 2013a,b](#)]. It is clear that for socioeconomic reasons, changes in the hydrological cycle and its extremes, processes leading to extremes, and inherent spatial patterns need to be understood. While there exists the rather univocal notion of precipitation extremes becoming more extreme on a global scale, the trends of extreme precipitation in Nepal are not yet clearly determined.

Various authors conducted studies of changes in extremes over Nepal and South Asia [[Shrestha, 2005; Baidya et al., 2008; Caesar et al., 2011](#)]. However, the focus was either not on extreme precipitation or it was not on Nepal in particular. Recently, [Shrestha et al. \[2016\]](#) assessed changes of extreme temperatures and precipitation in the Koshi river basin in Nepal. Changes in other parts of the country remain to be explored.

Not only trends in extreme precipitation but also processes leading to extreme precipitation in Nepal were not yet systematically investigated. For surrounding countries such as India and Pakistan, case studies could reveal processes that were critical for the development of precipitation systems entailing floods (e.g. [Houze Jr et al. \[2011\]](#), [Rasmussen and Houze Jr \[2012\]](#), [Kumar et al. \[2014\]](#), [Rasmussen et al. \[2015\]](#), [Houze Jr et al. \[2017\]](#)). Due to the high spatial and temporal variability of rainfall along the Himalayas (Section [2.2](#) and [2.3](#)) it was not clear whether the same processes and conditions would occur, and if, lead to an extreme precipitation event.

In my dissertation, I therefore concentrate on establishing a comprehensive overview of trends in extreme precipitation in Nepal and the physical processes causing extreme precipitation events. This set of physical processes then hopefully provides a basis for future research on extreme precipitation in Nepal.

1.2 Availability of precipitation measurements in Nepal

Nepal is located right at the rim of the Himalayas (Fig. [1.1](#)) and houses the highest peaks of the world. The extreme topographic features, the inaccessibility of many regions, and the poverty of a developing country had suppressed the installation of a network of meteorological stations for a long time [[Nandargi and Dhar, 2011](#)]. On this issue, [Nandargi and Dhar \[2011\]](#) illustrate the availability of rain gauge data in countries along the Himalayas (Fig. [1.2](#)). Unfortunately, for Nepal they used only data from 1921 to 1990. Nonetheless, compared to the entire Himalaya region, Nepal has very little coverage along most of the depicted time line where only during the last 60 years significant improvements have taken place. Because measurement stations were deployed and maintained at that time, we can now harvest the fruits of these efforts as the record reaches a time scale relevant for climate related research.

A critical step forward in assessing rainfall over the Himalayas was the possibility to measure rainfall with satellites. The precipitation radar on board the Tropical Rainfall Measurement Mission (TRMM) satellite provided coverage of rainfall over these remote areas for the first time. The extended coverage made it possible that also precipitation in deep inaccessible valleys became visible. Rainfall in these valleys would have been shadowed by the surrounding mountains when using a ground based radar [[Houze Jr et al., 2007](#)]. The TRMM datasets span a, in a climatological sense, rather short period of time (active from 1997). Nonetheless, multiple studies successfully utilized TRMM output to investigate precipitation systems, climatological rainfall, and the hydrological budget in the Himalayas [[Lang and Barros, 2002](#); [Bookhagen and Burbank, 2006](#); [Houze Jr et al., 2007](#); [Romatschke et al., 2010](#); [Bookhagen and Burbank, 2010](#); [Bookhagen, 2010](#); [Romatschke and Houze Jr, 2011](#)].

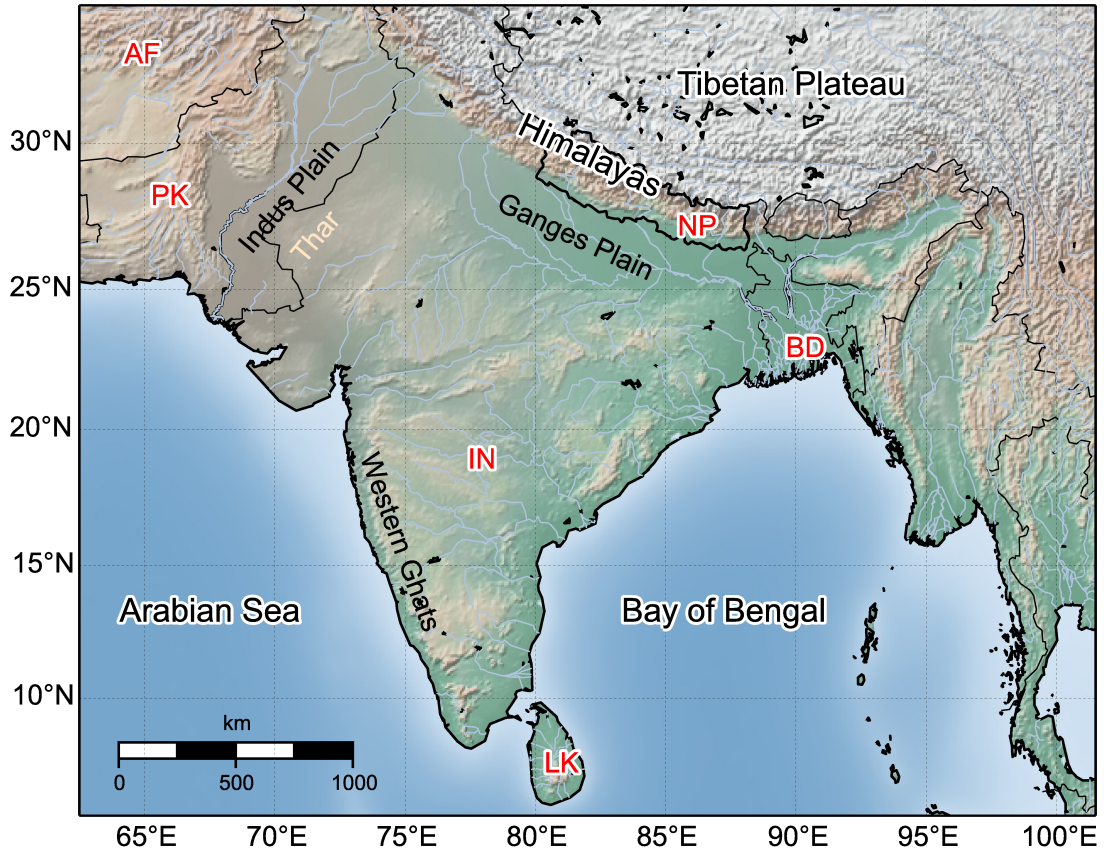


Figure 1.1: Overview map for South Asia. Country abbreviations are displayed in red (ISO 3166-1 alpha-2) for NP = Nepal, IN = India, AF = Afghanistan, PK = Pakistan, BD = Bangladesh, LK = Sri Lanka. The main topographic features Tibetan Plateau, Himalayas, and Western Ghats are marked to serve the discussion in this thesis. The Thar desert is indicated as its arid nature is important for the second manuscript. The main river plains, the Indus Plain and the Ganges Plain, as well as the location of the Arabian Sea and the Bay of Bengal are highlighted for orientation purposes. Major rivers are indicated in blue.

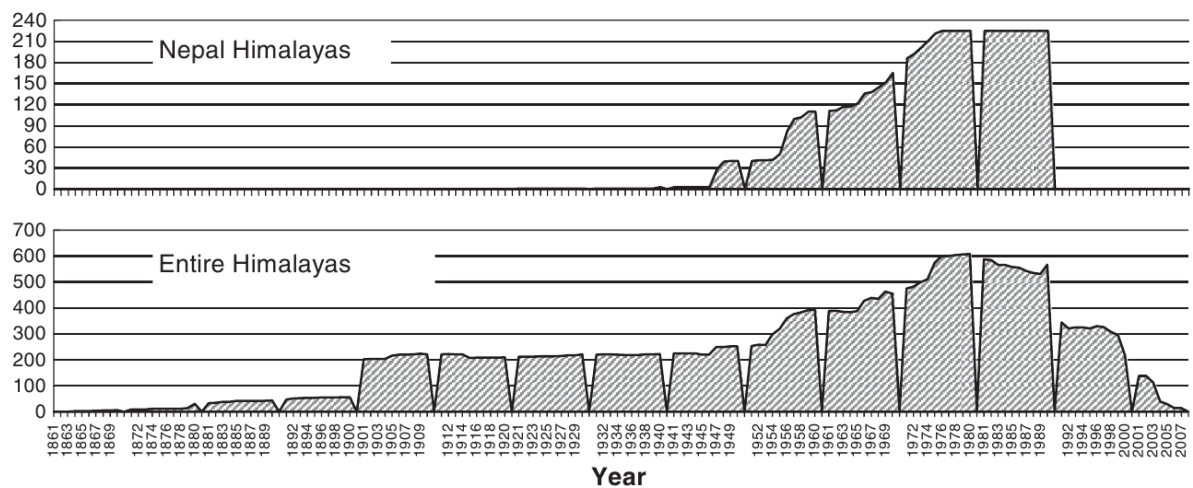


Figure 1.2: Two panels from Figure 4. from [Nandargi and Dhar \[2011\]](#) displaying the rainfall data availability in terms of number of stations for Nepal and the entire Himalaya region.

Chapter 2

Scientific background

2.1 Main processes governing precipitation along the Himalayas

There are various types of precipitation systems along the Himalayas for which different processes cause precipitation. [Houze Jr et al. \[2007\]](#) went about the challenge of systematically addressing these processes, by defining different types of convective systems. Facilitating TRMM measurements, they divided precipitation systems into deep intense convective cores, wide intense convective cores, and broad stratiform systems. Deep intense convection was defined as a system containing a core of more than 40 dBZ exceeding an altitude of 10 km. To be classified as wide intense convective system, the 40dBZ echo core needed to exceed an area of 1000 km^2 at its level of maximum extent. These studies opened up for systematically determined insights into three-dimensional characteristics of convective systems along the Himalayas [[Houze Jr et al., 2007](#); [Romatschke et al., 2010](#)].

Existing hypotheses and conceptual models were tested which could help to explain the preferred region of occurrence of convective systems [[Sawyer, 1947](#); [Houze Jr et al., 2007](#); [Medina et al., 2010](#); [Rasmussen and Houze Jr, 2012](#); [Kumar et al., 2014](#)]. [Sawyer \[1947\]](#) introduced a conceptual model (Fig. 2.1) connecting the monsoonal atmospheric environment to the location of convection over the northwestern Indian subcontinent. [Houze Jr et al. \[2007\]](#) added to this model an explanation for the location of the convective systems in this region as defined in their work. Sawyer's conceptual model is illustrated in Figure 2.1. During the Indian summer monsoon, moist low-level air from the Arabian Sea is directed toward the Himalayas, following the Indus-Plain. The moist low-level flow is capped by warm and dry continental air from the Hindu Kush mountains in Afghanistan, creating an inversion. This inversion layer prevents premature convection, as the moist low-level flow gains buoyancy due to insolation over the warm and arid region. Finally, the low-level air can penetrate the inversion layer and deep convection develops explosively.

[Medina et al. \[2010\]](#) confirmed this conceptual model with a high resolution numerical modeling study for a single event over Pakistan. They showed that topographic lifting, rather than increasing buoyancy due to sensible heat fluxes, was the most efficient process to overcome the inversion layer and consequently triggering deep convection. When the moist low-level air is heading north toward the Himalayas, it will

finally be trapped in a concave region in Northwest India and North Pakistan where it accumulates as it breaks against the mountain ridge. Developing convective cells can tap into abundant moisture and develop extreme intensities [Houze Jr et al., 2007].

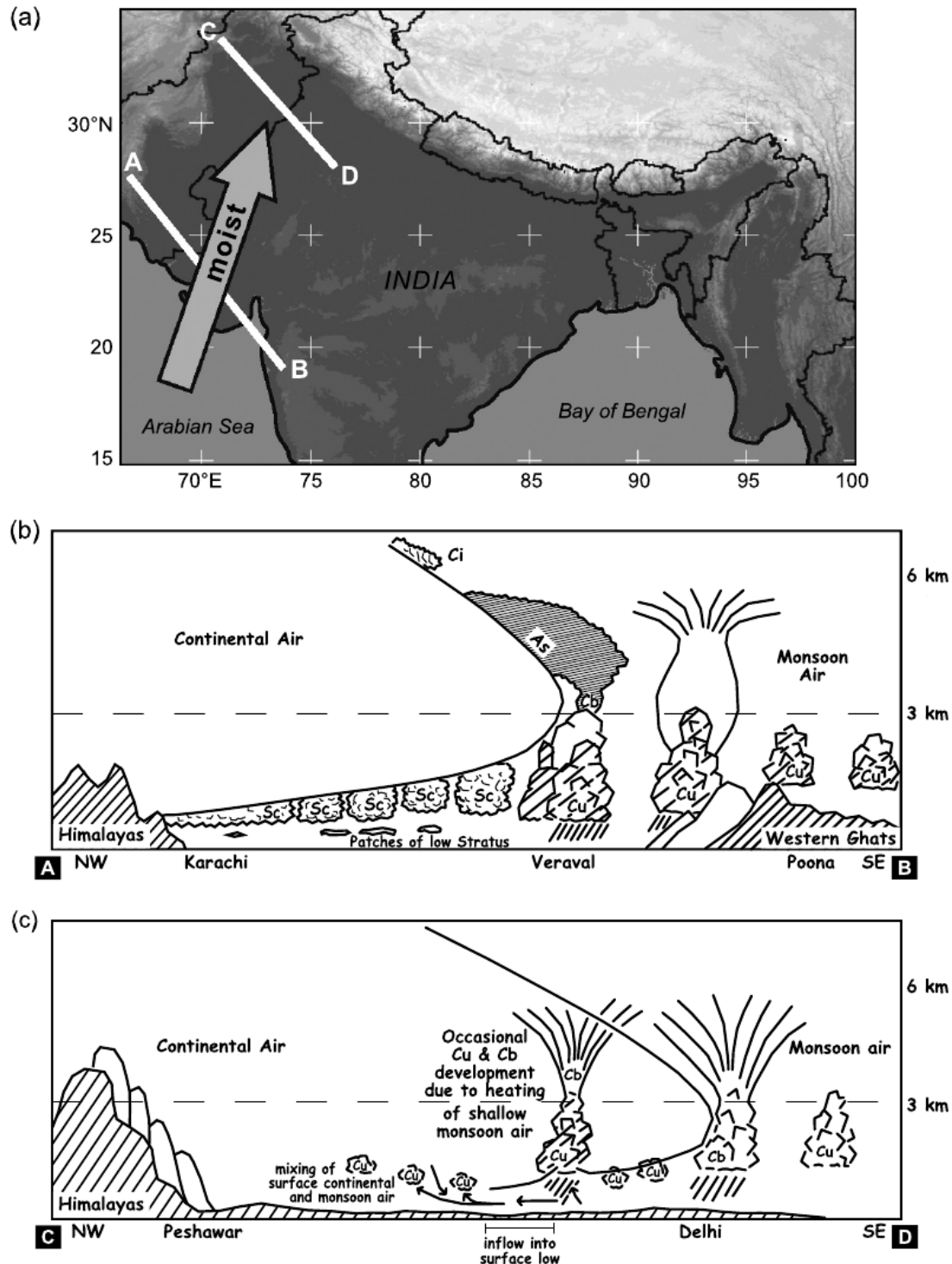


Figure 2.1: Illustration from [Houze Jr et al. \[2007\]](#) displaying the conceptual model from [Sawyer \[1947\]](#). a) shows South Asia with a low-level moist inflow from the Arabian Sea crossing the Thar desert. Two cross sections are indicated and schematically illustrated in b) for distance \overline{AB} and c) for distance \overline{CD} .

Rasmussen and Houze Jr [2012] investigated a flash flood event in Northwest India over the city Leh, introducing a conceptual model for the intensification of mesoscale convective systems that formed over the Tibetan Plateau. A constant jet over the Tibetan Plateau organized the individual convective cells into a squall line structure and directed them off the Plateau toward Leh. Synoptic conditions provided two low-level streams of moist air toward Leh, one from the Arabian Sea and one from the Bay of Bengal, invigorating the convective systems as they moved over Leh down from the Tibetan Plateau. This has been confirmed by *Kumar et al.* [2014] who performed a high resolution numerical simulation of this event. The movement of the mesoscale convective systems was set up by a quasi-stationary situation featuring a wide area of high geopotential at 500 hPa over the Tibetan Plateau.

Similar large scale conditions accompanied the Pakistan flood 2010. A blocking high over the Tibetan Plateau and two low pressure anomalies conveyed moist air from the Bay of Bengal along the Himalayas and from the Arabian Sea to Pakistan [*Houze Jr et al.*, 2011; *Rasmussen et al.*, 2015]. These highly unusual conditions led to the development of a large stratiform system which is usually more common in the humid environment over the Eastern Himalayas and the Bay of Bengal [*Houze Jr et al.*, 2011]. The arid region was not prepared to take up the large amount of moisture resulting in a flooding event [*Houze Jr et al.*, 2011]. During a flood in Pakistan in 2012, no stratiform echoes were identified [*Rasmussen et al.*, 2015]. The high variability in the nature of the flood producing precipitation systems over South Asia, even over one subregion e.g. Pakistan, indicates a high complexity of the involved processes, determining whether an event can develop the intensity needed to entail severe societal consequences.

Comprehensive studies like those introduced above were absent for Nepal in the published literature. Rather, single processes and conditions and their impact on rainfall in Nepal were investigated. For instance, *Lang and Barros* [2002] described onset monsoon low pressure systems that created an upslope flow followed by a mixture of stratiform and convective precipitation. Large amounts of rainfall up to 462 mm were recorded over two days. *Nandargi and Dhar* [2011] summarized meteorological situations, like monsoon low pressure systems, related to heavy precipitation along the Himalayas of which some could be assumed to be relevant for Nepal.

Additional to monsoon low pressure systems, *Nandargi and Dhar* [2011] mention monsoon break periods. Monsoon break periods are found to coincide with less precipitation over central India (therefore the name *break period*) and excess precipitation along the Himalayas [*Rajeevan et al.*, 2010]. Break periods coincide with a low-level flow split at the Western Ghats where the flow bifurcates into a northern and a southern branch [*Joseph and Sijkumar*, 2004]. Consequently, the moist flow is no longer directed over Central India which decreases the amount of rainfall in that region. Instead, the northern branch is directed toward the Himalayas supporting rainfall in Northern India. Another large scale mechanism influencing seasonal precipitation in Nepal is the El Niño-southern oscillation (ENSO) although the robustness of this correlation is still under debate [*Trenberth*, 1997; *Kumar et al.*, 1999; *Shrestha*, 2000; *Ichiyanagi et al.*, 2007; *Sigdel and Ikeda*] (more in Section 2.3).

After introducing research conducted for Nepal it becomes apparent that the studies are scattered across different topics but can be categorized under the subject *variability* of rainfall in Nepal. Let us therefore continue to bundle the studies into *spatial* and *temporal variability* to make the existing research on Nepal more accessible.

2.2 Spatial variability of precipitation in Nepal

Large spatial variability in precipitation has been observed along the Himalayas [Bookhagen and Burbank, 2006, 2010; Bookhagen, 2010]. This can be partly caused by various precipitation systems occurring in different regions. Various types of precipitation systems were characterized and observed by e.g. Houze Jr et al. [2007], Romatschke et al. [2010], Romatschke and Houze Jr [2011], and Nandargi and Dhar [2011]. To the west of Nepal deep convective systems prevail whereas to the east stratiform precipitation systems are most common. Nepal, however, can experience both stratiform and convective precipitation systems of varying sizes [Romatschke et al., 2010; Romatschke and Houze Jr, 2011].

The fact that Nepal is located in this transition zone highlights the importance of considering spatial variability when investigating processes leading to extreme precipitation events in Nepal. In particular, the complex topography in Nepal can strongly interact with precipitation systems. This has been shown e.g. for monsoon low pressure systems during the onset of the Indian summer monsoon [Lang and Barros, 2002]. Lang and Barros [2002] found that years without low pressure systems colliding with the Himalayas depict considerably less seasonal rainfall. Studies of low pressure systems [Lang and Barros, 2002; Krishnamurthy and Ajayamohan, 2010; Sørland and Sorteberg, 2015a] suggest large variability in their trajectories which consequently affects the rainfall variability in Nepal. On smaller spatial scales, Barros and Lang [2003] suggest that the diurnal cycle of the precipitation is determined by the diurnal change in thermally driven circulation. During the night the upslope winds stall and the flow converges upstream in front of the mountain range lifting the air column and causing precipitation.

The topography varies considerably along the Himalayas and in Nepal, which makes the described effects of topography even more important for the rainfall distribution. Bookhagen and Burbank [2010] describe the difference between a one-step and two-step topography. A one-step topography means that the mean topography rises to the Greater Himalayas without a break in the slope. A two-step topography describes a gradual rise to the lesser Himalayas with a subsequent break in relief followed by a second rise to the Greater Himalayas. These features translate directly into the amount of annual rainfall with one peak at places with a one-step topography and two peaks at places with a two-step topography. In the West and East Himalayas the one-step topography is prevailing whereas in the Central Himalayas the two-step topography is characteristic. However, within Nepal, although located in the Central Himalayas, both features can occur.

The close relationship between rainfall amounts and topography raises the question whether we can see spatial patterns of rainfall in Nepal associated with topographic features. [Kansakar et al. \[2004\]](#) clustered climatological rainfall using a dataset containing 222 rain gauge stations. They found considerable different rainfall regimes which aligned with main river basins and the physiographic regions of Nepal (Fig. 2.2). These results from [Kansakar et al. \[2004\]](#) support the previously discussed findings that the complex topography in Nepal influences considerably the rainfall distribution in Nepal, resulting in a high spatial variability.

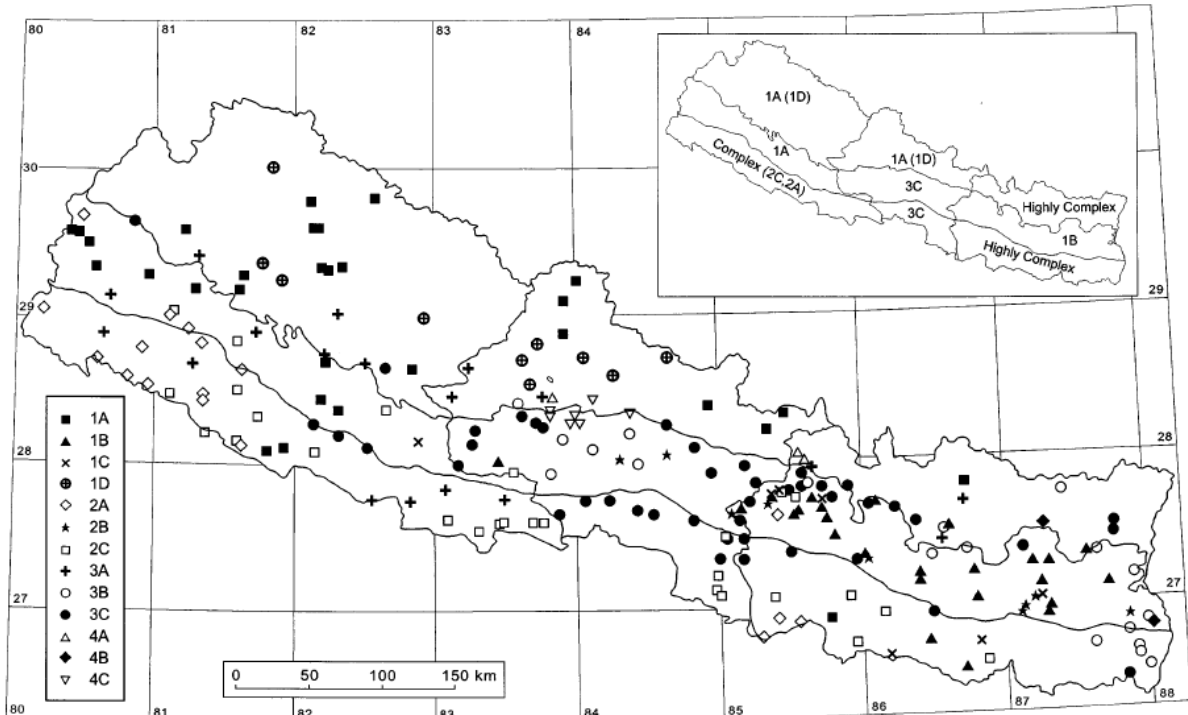


Figure 2.2: Summary figure from [Kansakar et al. \[2004\]](#) depicting regions dominated by different clusters of rain gauges. Clusters are oriented along physiographic regions and major river basins.

2.3 Temporal variability of precipitation in Nepal

Precipitation in Nepal experiences strong temporal variability from an intra-seasonal to a decadal time scale [[Webster et al., 1998](#)]. Climate in Nepal as well as in entire South Asia is largely determined by the South Asian summer monsoon responsible for most of the intra-annual variability in rainfall [[Nayava, 1980](#)]. The society and economy in monsoon climates are highly depending on the seasonal monsoon rainfall and consequently slight changes can have severe socio-economic consequences [[Gadgil and Kumar, 2005](#)]. [Webster et al. \[1998\]](#) and [Gadgil and Kumar \[2005\]](#) show the socio-economic importance of the monsoon performance for India. There is a significant correlation between crops production and the performance of the Indian summer monsoon [[Webster et al., 1998](#)]. During *bad* monsoon years, meaning deficient rainfall, India produces considerable less crops than during *good* monsoon years, years with

abundant rainfall. Changes in crops production directly translates into India's gross domestic product. Given the importance of the Indian summer monsoon, I will introduce basic concepts and mechanisms influencing the temporal variability of the monsoon precipitation in Nepal.

2.3.1 The Indian summer monsoon

The Indian summer monsoon can be seen as a regional monsoon, part of a complex global monsoon system consisting of a varying thermally driven overturning circulation close to the equator [Trenberth et al., 2000]. The overturning circulation strives to remove the energy imbalance created by unevenly distributed radiation received from the sun. In places with a more pronounced Coriolis force as in mid-latitudes, this task is accomplished by baroclinic instabilities [Trenberth et al., 2005].

There is no agreement on the main driver of the Indian summer monsoon circulation in the literature, hence, I will briefly describe the most prominent hypotheses. Differential heating due to land sea distribution in the horizontal and the Tibetan plateau in the vertical can modulate the position of the overturning circulation comparable to a land-sea breeze system. The Tibetan plateau and its function as elevated heat source was thought to be a significant driver on the South Asian monsoon circulation [Webster et al., 1998]. However, in a modeling study it was shown that the pattern of the monsoon circulation was hardly impaired when removing the Tibetan plateau, only retaining the Himalayas [Boos and Kuang, 2010]. Only the strength of the circulation was reduced resulting in locally reduced precipitation. The large scale monsoon circulation was unaffected. Consequently, elevated heating as the main driver for the Indian summer monsoon dropped out entailing a void of explanations.

A possible mechanism that could fill this void is latent heat release. Various studies indicated that latent heat release could be the motor maintaining the monsoon circulation. Vertical velocity fields coincide with the moisture sinks and regions of precipitation supporting this idea [Trenberth et al., 2005]. Other diabatic effects like radiative cooling in the descending branch of the overturning heated by adiabatic compression, can strengthen the circulation as a feedback but can hardly be thought of as the driving mechanism [Trenberth et al., 2005]. Boos and Kuang [2010] show that the subcloud entropy maximum, illustrated by the equivalent potential temperature maximum, is aligned with the Himalayas, underlining the importance of moist processes.

In Nepal, the Indian summer monsoon precipitation accounts for approximately 80 % of the annual precipitation with considerable variations across the country [Nayava, 1980; Marahatta et al., 2009]. Typically, Far-West Nepal is less dominated by the monsoon than East Nepal [Marahatta et al., 2009]. This is due to the development of the wind field and the propagation of the moist monsoonal air coming mainly from the Bay of Bengal. During the monsoon season the monsoon gradually advances to the west over the subcontinent and retreats until the end of the season. This advance can be seen in terms of the timing of the monsoon onset [Webster et al., 1998]. However, the monsoon onset and its progression highly depends on the definition of the

monsoon and is a complicated issue on its own (e.g. [Stiller-Reeve et al. \[2015\]](#)).

The Indian summer monsoon can be characterized e.g. by the reversal of the wind system over South Asia. Following the winds, also the propagation of precipitation can be better understood. As the Inter-Tropical Convergence Zone (ITCZ) moves to the north, the atmospheric flow funnels moisture to the land, fueling the monsoon precipitation. [Trenberth et al. \[2005\]](#) illustrate the reversal of the low-level winds comparing the winter season (December to February) with the summer season (June to August). During the boreal winter, low-level winds are aligned with the Himalayas and point toward the east before they turn to the south and west in the Bay of Bengal. They subsequently cross the Indian subcontinent and continue to the south-west toward the coast of Africa where they turn again toward the equator. Upper tropospheric winds exhibit a strong band of westerlies over Nepal. The moisture in the atmosphere follows the low-level winds and converges south of the equator consistent with the main precipitation band during winter [[Trenberth et al., 2005](#)].

During the boreal summer the low-level flow is organized in the opposite direction (Fig. 2.3). Manifested as the Somali Jet, the low-level flow curves northeast along the Somali coast and the Arabian peninsula crossing the Arabian Sea and finally reaching India. The first barrier is the Western Ghats along the west coast of India (Fig. 1.1) where a precipitation band is visible due to the topographic forcing (Fig. 2.3a). After crossing India the flow veers north again, where it pushes moisture from the Bay of Bengal in over land, mainly over India, Bangladesh, and Nepal (Fig. 2.3b). Precipitation forming over India during summer is part of the Indian summer monsoon, which gradually progresses until it reaches the Himalayas in the north and Pakistan in the west [[Webster et al., 1998](#)]. The Himalayas stand out as an insurmountable barrier, preventing the moisture to pass (Fig. 2.3b) and leaving parts of the Tibetan plateau arid [[Wang and Gaffen, 2001](#)]. The topographic forcing and the abundance of moisture along the Himalayas allow for the formation of intense convective systems [[Houze Jr et al., 2007](#)].

The direct moisture sources for rain events in Nepal (Fig. 2.3c) are very interesting to examine as they differ considerably from what one would expect based on the moisture flux (Fig. 2.3b) (investigated and discussed in my second manuscript). I could find hardly any research done on moisture transport to Nepal. Some studies explored the origin of moisture for the Indian subcontinent during the monsoon season concluding with the Arabian Sea as an important moisture source [[Ghosh et al., 1978](#); [Cadet and Reverdin, 1981](#); [Cadet and Greco, 1987a,b](#)]. However, since these studies used a budget approach comparing precipitation against evaporation, only a pattern of general moisture sources and sinks could be established. It is not straight forward nor given that the established regions hold when considering direct moisture sources for Nepal. [Sodemann et al. \[2008\]](#) developed a moisture source diagnostic to represent the direct moisture sources for precipitation events. A glimpse of the distribution of moisture sources for Nepal could be caught in [Läderach \[2016\]](#) where Kathmandu was the target region for a case study. However, a study comprehensively analyzing this issue was still missing.

2.3.2 Other sources of temporal variability

Break monsoon periods [Rajeevan *et al.*, 2010] and the occurrence of monsoon low pressure systems [Lang and Barros, 2002] can impose intra-seasonal variability. During years where no monsoon depression collides with the Himalayas there can be considerably less monsoon rainfall in Nepal [Lang and Barros, 2002]. The All-India Rainfall is also significantly decreased during monsoon break periods as precipitation amounts over Central India are reduced [Rajeevan *et al.*, 2010]. In South India, over Sri Lanka, and in the north close to the Himalayas, precipitation is enhanced [Rajeevan *et al.*, 2010]. Monsoon break periods are associated with a split of the low-level flow at the Indian west coast with a southern branch around the southern edge of the Indian subcontinent and a northern branch along the Indo-Gangetic plain toward the Himalayas [Joseph and Sijkumar, 2004].

Variability on inter-annual and decadal time scales can be related to the ENSO [Trenberth, 1997; Webster *et al.*, 1998; Kumar *et al.*, 1999; Shrestha, 2000; Ichiyangagi *et al.*, 2007; Sigdel and Ikeda]. During El Niño years, negative ENSO phase and positive Southern Oscillation index (SOI), less rainfall is expected, whereas during La Niña years more rainfall occurs. A physical relationship is assumed to exist between the Walker Circulation and the lateral and traverse monsoon circulation as illustrated in Webster *et al.* [1998], or between the monsoon circulation and the Eastern- and Western Walker Cell as in Yang and Lau [2005]. Modulations of these circulation patterns can alter the location of precipitation systems. Such a modulation could be imposed for instance by changes in the Indian Ocean Dipole [Ashok *et al.*, 2001]. On a decadal time scale the Pacific Quasi-Decadal Oscillation (QDO) was recently found to affect precipitation in Nepal by modulating moisture fluxes toward the Himalayas [Wang and Gillies, 2013].

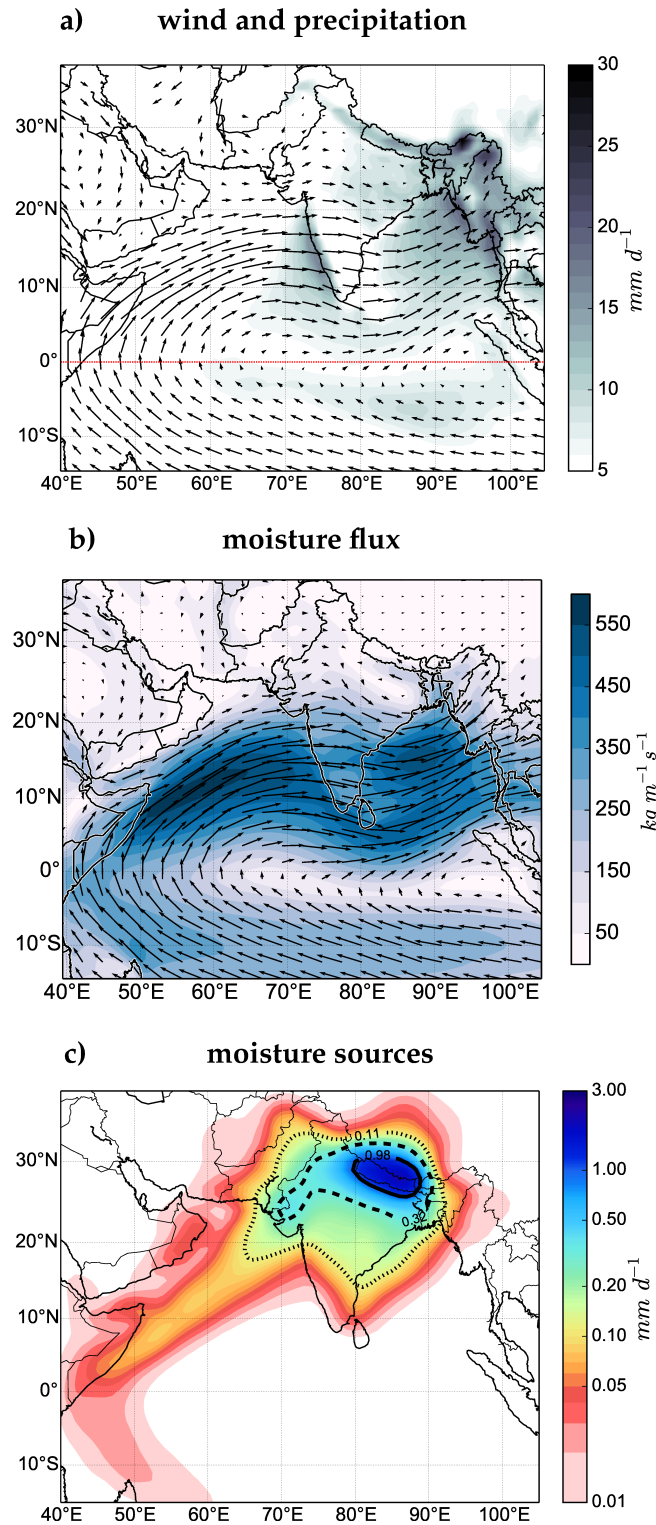


Figure 2.3: Illustrating the similarities and differences between the following climatologies for the months June to August. a) depicts wind at 850 hPa and mean daily precipitation. The equator is marked with a red line. b) shows total column water vapor flux. c) illustrates direct moisture sources for precipitation events in Nepal obtained with the method from [Sodemann et al. \[2008\]](#). The percentiles 75, 50, and 25 are marked with a dotted, a stippled, and a solid line.

Chapter 3

Objectives

In my thesis, I aimed at finding ingredients for extreme precipitation events in Nepal. The knowledge gaps mentioned in Chapter 1 reflect the structure of how I went about the task of finding these ingredients. Studying the scientific literature, I identified the main gaps as follows: there was no coherent picture of climatic trends in extremes in Nepal based on measurements, a systematic study on synoptic conditions leading to extreme precipitation in Nepal was missing, direct moisture sources and their role for extreme precipitation events had not yet been investigated in that region, and a comprehensive case analysis as existing for neighboring regions was not yet conducted. Against this background, the following objectives evolved:

1. Investigate whether there are regions in Nepal exhibiting consistent trends in extreme precipitation (Paper I)
2. Find synoptic-scale key processes actuating extreme precipitation in Nepal using composites of events (Paper II)
3. Explore the location and role of moisture sources supplying additional moisture during the extreme events (Paper II)
4. Perform high resolution study for one extreme case and proceed to a process level of understanding (Paper III)
5. Add mesoscale characteristics of the precipitating system on top of synoptic scale characteristics (Paper III)
6. Assess the composite results for the investigated event (Paper III)

These objectives effectively manifest in a top-down approach, proceeding from the general to the specific. First, obtaining an overview over the rainfall climatology, variability, and trends in rainfall. Second, identifying processes actuating extreme precipitation in Nepal and establishing a conceptual understanding of the interplay and effect of the involved processes. Third, seeking the physical link between the processes and determine their effect for one extreme event. The top-down approach is also reflected in the choice of datasets and methods. Starting with rain gauge records to obtain a measurement based view on rainfall in Nepal, I moved from global reanalysis and global trajectory datasets, to finer-scale satellite data and finally high-resolution modeling.

Chapter 4

Key findings and discussion

The main findings are condensed in three manuscripts. The first manuscript provides an overview over rainfall climatology, variability, and trends in extremes in Nepal. The second manuscript consolidates synoptic-scale key processes and associated moisture sources in a conceptual sketch (representing the ingredients mentioned in Chapter 3). The third manuscript reveals how the processes interact and provoke an extreme precipitation event based on a case study. Moreover, the third manuscript adds mesoscale characteristics to the synoptic-scale processes found in the second manuscript.

The most prominent findings in the first manuscript are twofold. First, I can show that the linear correlation between ENSO and the number of extremes vanishes with increasing percentiles. This means that extreme precipitation events are equally likely to occur during a La Niña and an El Niño event. Second, modeling trends in extreme precipitation with quantile regression and extreme value theory results in a robust positive trend in Far-West Nepal answering to the first objective. For the whole of Nepal, however, there is no consistent trend in the occurrence of extreme precipitation events.

The second manuscript presents a conceptual sketch of the synoptic-scale key processes and moisture sources actuating extreme precipitation in Nepal. During extreme precipitation events, the large-scale atmospheric flow was directed against the Himalayas at the location of the extreme precipitation. Anomalies in geopotential height and winds illustrate this for most of the troposphere. The atmospheric flow was further shown to be able to guide low pressure systems toward the Nepal Himalayas. Consequently, it seems that the atmospheric flow can determine the location of the extreme event to a considerable degree (second objective). During the extreme events, unusually high moisture flux was present where the extreme event occurred. The additional moisture was provided by anomalously abundant moisture sources predominantly over land (73%-77%), in particular along the Indo-Gangetic plain. The moisture stemmed probably from foregone precipitation events moistening the soil along the pathway of the low-level atmospheric flow (third objective). Between 25% and 43% of the extreme events during July and August occur during monsoon break periods which take up about 24% of the days in July and August. Since this fraction is likely underestimated, monsoon break periods considerably affect the probability of occurrence of extreme events.

In the third manuscript a single extreme event on 19 July 2007 in Central Nepal is examined to assess and understand physical links between the key processes from the second manuscript. The synoptic conditions and moisture source pattern from the conceptual sketch in the second manuscript can be recognized, enabling the intense development of the extreme event investigated in the third manuscript. A monsoon break period with the associated low-level flow conditions were evoked by the Western Ghats blocking the westerly flow. The northern branch of the resulting bifurcation of the low-level flow ingested moisture mostly over land, provided by foregone precipitation events. The moist low-level flow, containing large CAPE, was directed against the Himalayas in Central Nepal. Topographic forcing destabilized the airmasses releasing the CAPE. Invigorated by the moist inflow a wide intense convective system developed resulting in torrential rain. The prevailing synoptic conditions created a favorable environment with a traversing trough aligning the flow against the Himalayas and exerting weak quasi-geostrophic forcing over Nepal. By recognizing and connecting the processes from the second manuscript and characterizing the mesoscale structure, objectives four to six were met.

The value of the studies lies not only in the key findings but also in contrasting these results with existing findings in other regions along the Himalayas. Various features distinguish extreme precipitation in Nepal from high impact events in Pakistan and Northwest India (e.g. [Houze Jr et al. \[2011\]](#), [Rasmussen and Houze Jr \[2012\]](#), [Kumar et al. \[2014\]](#), and [Rasmussen et al. \[2015\]](#)). For the flooding events described in those studies the atmospheric circulation exhibited a blocking event over the Tibetan Plateau. Together with low pressure systems in the Bay of Bengal and the Arabian Sea moisture could be funneled to the location of the respective precipitating system. The low-level flow was directed along the Himalayas from east to west with an additional branch from the Arabian Sea. For the extreme precipitation events in Nepal considered in this thesis, the low-level flow is directed in the opposite direction, from west to east, along the Himalayas. At the location of the extreme precipitation event the flow turns north against the mountain barrier. The moisture sources were located along this flow mainly in the Indo-Gangetic plain. Interestingly, although different dynamical situations prevailed, the same target was met, namely funneling moisture to the location of the precipitating system. In the recently accepted paper by [Houze Jr et al. \[2017\]](#), an eastward propagating trough merged with a low pressure system and organized the flow against the Himalayas leading to a flooding event in Uttarakhand, India, just west of Nepal. This result for a region close to Nepal supports the conceptual sketch in the second manuscript where the guiding role of the upper-level trough as well as the merging of a trough and a low pressure system is described.

Chapter 5

Concluding remarks and outlook

The three manuscripts resolve the objectives of the thesis providing a comprehensive picture of trends and key processes of extreme precipitation in Nepal. With my work, I hope to provide a basis of findings that can foster new research in the future and that can be evaluated against new results. However, this thesis is by no means exhaustive and there are many ways to extend the included studies. Given that the moisture sources for extreme precipitation in Nepal differ considerably from what one would expect from the column integrated water vapor transport and results from [Ghosh et al. \[1978\]](#) and [Cadet and Reverdin \[1981\]](#), the moisture sources should be investigated considering non-extreme precipitation events in Nepal. This could then include the seasonal cycle and elucidate the variability of the moisture sources. Having in mind the key processes for extreme precipitation from the second and third manuscript, one can now try to explore the potential to increase predictability of the extreme events by recognizing similar conditions in model forecasts. The precipitation event described in [Houze Jr et al. \[2017\]](#) in Northeast India resulted from the interaction of an eastward propagating trough and a low pressure system similar to the case described in the second manuscript. It would be interesting to investigate whether the prevailing precipitation system in the second manuscript exhibited similar characteristics. In my third manuscript, I use a Q-vector analysis to assess the contribution of quasi-geostrophic forcing which is useful for comparison with [Martius et al. \[2013\]](#) and [Houze Jr et al. \[2017\]](#). However, the region, season, and respective thermodynamic environment this technique is used in, is not optimal for the use of quasi-geostrophic theory. The extreme differences in elevation and the governing diabatic processes during the Indian summer monsoon could distort the results. It would thus be useful to asses the importance of the quasi-geostrophic theory for this region and the monsoon season in general.

Chapter 6

Data and methods

6.1 Data

For this thesis, five datasets were used: rain gauge data, TRMM 3B42 [[Huffman et al., 2007](#)], Lagrangian trajectories [[Läderach and Sodemann, 2016](#)], simulations with the Weather Research and Forecasting (WRF) model [[Skamarock et al., 2008](#); [Skamarock and Klemp, 2008](#)], and Era-Interim reanalysis [[Dee et al., 2011](#)]. In the following, I give a brief introduction to these datasets, the setup for the WRF simulation is described in Section [6.2.2](#).

The measurement network consists of US standard 8 inch diameter manual rain gauges and are maintained by the Department of Hydrology and Meteorology (DHM) in Nepal [[Talchabhadel et al., 2016](#)]. An overview map of the rain gauges used in this thesis can be found in Paper I (Fig. 1b). The DHM performs basic quality control including the removal of outliers and negative values (personal communication with Ramchandra Karki, working in the DHM data management section at the time of the purchase). When considering extremes, the removal of outliers could potentially be problematic. However, this was done in a standard procedure and could not be influenced. Meta data was unfortunately not available such that I could not find out whether stations have been moved (personal communication with Ramchandra Karki). In the first manuscript, testing for homogeneity in the time series is performed to account for this issue. Due to the harsh environment in the mountainous regions in Nepal there are a lot of data gaps and sometimes stations are not recording for multiple seasons. Nonetheless, this is a unique dataset giving insights into rain events and climate in Nepal. Moreover, it allowed me to evaluate model results with ground based measurements, a rare and valuable opportunity for this region.

The TRMM 3B42 product [[Huffman et al., 2007](#)] is a result from a joint mission between NASA and the Japan Aerospace Exploration Agency (JAXA) to study the distribution and variability of tropical and subtropical precipitation. The TRMM satellite was launched in November 1997 and re-entered the Earth's atmosphere on 15 June 2015 over the South Indian Ocean (<https://pmm.nasa.gov/trmm>). Although originally designed with a lifetime of three years the TRMM satellite provided valuable data for 17 years. The TRMM 3B42 product is a level 3 product meaning that the satellite derived raw data has undergone considerable post-processing to result in rainfall

estimates. In this thesis, the 3-hourly TRMM 3B42 product is used which has a spatial resolution of 0.25° covering the latitudes 50°N to 50°S . TRMM 3B42 is a combined microwave and infrared rainfall estimate with rain gauge adjustment. Rain gauges as part of the TRMM hydrological network are installed in Central Nepal and evaluated in [Barros et al. \[2000\]](#). The network consists of 16 meteorological stations ranging from 500 m.a.s.l. to 4400 m.a.s.l.. [Barros et al. \[2000\]](#) found that TRMM derived precipitation matched station values better at low elevation compared to high elevation where values above a rain rate of 0.5 mm h^{-1} were found to be reliable.

The Era-Interim reanalysis dataset [[Dee et al., 2011](#)] is a global reanalysis based on the version Cy31r2 of the Integrated Forecast System (IFS) from the European Centre for Medium-Range Weather Forecasts (ECMWF). Through assimilating observations into the simulations, the model is pushed towards measured values which results in a best guess for the state of the atmosphere. For this thesis, 6-hourly data is retrieved from Era-Interim's data server (apps.ecmwf.int/datasets/data/interim-full_daily) on a horizontal resolution of 0.75° .

To compute moisture sources (Section [6.2.2](#)) the global trajectory dataset from [Läderach and Sodemann \[2016\]](#) is used for the period 1979 to 2010. After dividing the atmosphere into five million air parcels of equal mass, they computed the trajectory dataset with the Lagrangian dispersion model FLEXPART [[Stohl et al., 2005](#)] driven with winds, specific humidity, and boundary layer height from Era-Interim interpolated on a $1^\circ \times 1^\circ$ horizontal grid.

6.2 Methods

In this thesis, several methods were utilized to approach extreme precipitation in Nepal from different angles. These methods included various statistical techniques as well as tools and theory that is more based on the physics and dynamics of processes. In the following, I describe the different methods and tools to provide a more thorough introduction and deeper understanding than is possible in the short explanations of the manuscripts. To keep the thesis to a reasonable size, I focus on explaining the more advanced techniques which are necessary to reproduce my results. This means that e.g. a mean value or an ordinary linear regression technique is not explained in detail.

6.2.1 Statistical approaches

Quantile regression

Quantile regression [[Koenker and Hallock, 2001](#)] is more flexible than ordinary least square regression (OLSR) because it offers the possibility to explore the impact of covariates on all quantiles of a dataset. It is robust to outliers and leads to reasonable estimates when the error distribution is non-Gaussian. Quantile regression can be described similarly to the OLSR. When performing OLSR the relationship between one or more covariates and the conditional mean of a response variable is modeled. In quantile regression the conditional quantiles of the response variable are modeled mak-

ing the analysis more flexible and independent from assumptions about the parametric probability distribution of the residuals. Hence the goal is to minimize the sum of the asymmetrically weighted absolute residuals, and not the squared residuals as is done in OLSR. The residuals are weighted asymmetrically because, in addition to the absolute residuals, there is a penalty term considering what is above and below the chosen quantile if it is not the median. This means that the penalty term penalizes for under- and over-prediction. A comparison with the median regression, also known as least-absolute-deviation (LAD) regression, makes this point clearer. In LAD regression (50^{th} percentile) the sum of the absolute errors $\sum_i |e_i|$ have to be minimized. An asymmetric case is just the extension of this using a different quantile (q) than the median and penalizing under-prediction $q|e_i|$ and over-prediction $(1-q)|e_i|$. This results in the objective function Q (Eq. 6.1) which can be minimized using linear programming methods.

$$Q(\beta) = \sum_{i:y_i \geq \beta x_i}^N q|y_i - \beta x_i| + \sum_{i:y_i < \beta x_i}^N (1-q)|y_i - \beta x_i| \quad (6.1)$$

q is the chosen quantile, β the parameter to be estimated which consists of an offset plus a trend, y_i represents the response variable and x_i the covariate (in this case time). The sum is taken over all i to N with respect to the potentially asymmetric weighting. For this thesis, the simplex method is used for minimization. In the first manuscript, quantile regression is illustrated with rainfall datasets from two exemplary stations.

Non-stationary extreme value statistics

The extreme value statistics in this thesis are based on work from [Coles et al. \[2001\]](#) and [Katz et al. \[2002\]](#) who describe applications for a hydrometeorological framework. Extreme value statistics differ from the standard statistics as the argument is not an empirical one. In fact, it cannot be since extremes are rare by nature. Instead of an empirical argument, extreme value theory is based on an asymptotic rational. However, this implies that estimates can be made for levels that have never occurred before which is also what is most criticized. As [Coles et al. \[2001\]](#) points out, at least there is a rational for extreme value theory, and there is no other competing theory existing. From the *Extremal Types Theorem*, it turns out that the only possible distributions for modeling block maxima are the Gumbel, Frechet, and Weibull distributions regardless of the original distribution of the population where the maxima stem from. These three distribution families can be combined into one single distribution, the Generalized Extreme Value (GEV) distribution.

Block maxima values, like annual or seasonal maxima, follow the GEV distribution which is defined by a set of three parameters, location (μ), scale (σ), and shape (ξ). From a data set of block maxima these parameters can be estimated for instance by maximum likelihood or Bayesian approaches. Using time as a covariate, a linear trend can be imposed on the location parameter to capture changes of block maxima for the

observation period. The GEV including a time dependent location parameter looks as follows:

$$GEV(x; \mu(t), \sigma, \xi) = e^{-1 \left[1 + \xi \left(\frac{x - \mu(t)}{\sigma} \right) \right]^{-\frac{1}{\xi}}} \quad (6.2)$$

$\mu(t)$ is expressed using a linear relationship with time (Eq. 6.3) but any arbitrary function could be used.

$$\mu(t) = \mu(years) = \mu_0 + a \cdot years \quad (6.3)$$

Compared to the stationary case the parameter a is now an additional parameter that needs to be estimated to determine the best statistical model.

Since we now have a statistical model, we can compare the starting value with the end value of all time series to assess changes in extremes over a certain period of time. This is illustrated in the example below (Fig. 6.1), depicting annual precipitation maxima of an exemplary station (s1111) in Nepal (Fig. 6.1a). Including the temporal change in extremes (Fig. 6.1c) looks much more appropriate to the eye than the stationary model (Fig. 6.1b). More objectively, also the model evaluation, represented by the p-value of a likelihood-ratio test ($p = 0.006$), suggests that including the trend improves the model significantly. This means that the uncertainty in estimating the probability of an extreme event is reduced by a better model.

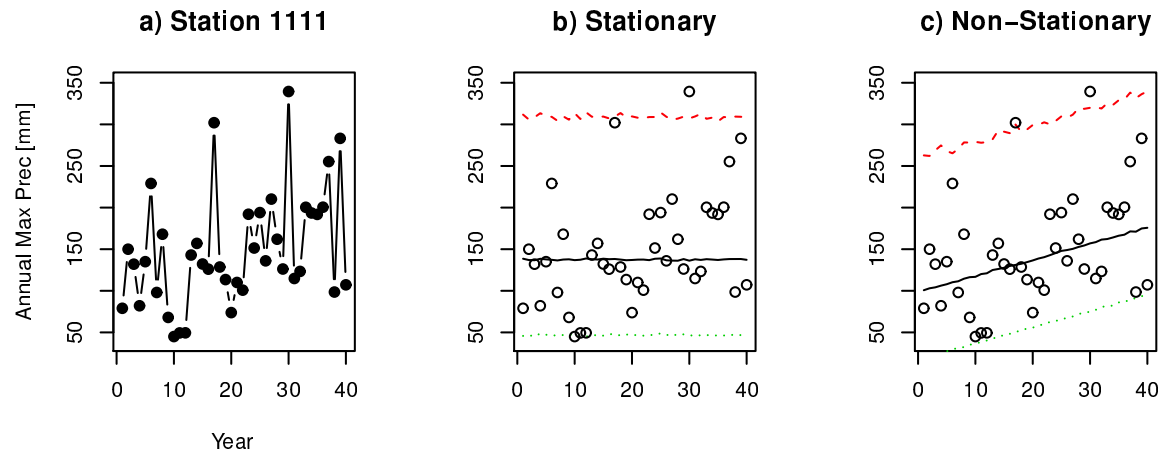


Figure 6.1: Figure illustrating the improvement obtained using a non-stationary extreme value model for modeling extreme precipitation block maxima. The station s1111 in Nepal is chosen as an example station. a) depicts the time series of annual maxima over 40 years. b) a stationary GEV-model is used. c) a non-stationary GEV-model is applied with time as covariate. The black line represents the evolution for the median, the green line the 0.025 quantile and the red line the 0.975 quantile.

Bayesian statistics

Additional to the quite standard maximum likelihood estimates, Bayesian statistics were applied to model trends in extremes in the first manuscript. Bayes' Theorem

(Eq. 6.4) forms the basis of the Bayesian approach.

$$P(A|B) = \frac{P(A \cap B)}{P(B)} = \frac{P(B|A)P(A)}{P(B)} \quad (6.4)$$

This formula comprises the conditional probabilities $P(A|B)$ and $P(B|A)$, the joint probability $P(A \cap B)$, and the marginal probabilities $P(A)$ and $P(B)$. Hence, Bayes' Theorem provides a powerful tool to efficiently manipulate conditional probabilities. An often used example (e.g. in [Bolstad \[2007\]](#)) is adopted with slight changes to illustrate the applicability for a binary variable:

Example: Let's assume 1% of a population has a disease ($P(\text{disease}) = 0.01 \Rightarrow P(A)$) and under a clinical test 95% ($P(\text{positive}|\text{disease}) = 0.95 \Rightarrow P(B|A)$) of infected persons are tested positively for the disease. However, the imperfect test indicates a positive result also for 3% of the healthy population ($P(\text{positive}|\text{notdisease}) = 0.03 \Rightarrow P(B|\text{not}A)$). A person being tested might now wonder what is the probability of having the disease when tested positively ($P(\text{disease}|\text{positive}) = ? \Rightarrow P(A|B)$).

The solution can be obtained with the Bayes' Theorem:

$$P(A|B) = \frac{P(B|A)P(A)}{P(B|A)P(A) + P(B|\text{not}A)P(\text{not}A)} = \frac{0.95 \cdot 0.01}{0.95 \cdot 0.01 + 0.03 \cdot 0.99} \cong 24\% \quad (6.5)$$

Instead of inserting a known distribution, a probability distribution expressing the personal belief can be incorporated in the equation. For instance, if you were the person that spread the disease and knew that there should be 5% of the population infected and not 1% you could incorporate this knowledge into the prior distribution ($P(A) = 0.05$ instead of $P(A) = 0.01$). This is how incorporating your belief in parameter estimation works in a Bayesian framework.

The following example applies this for the estimation of the parameter θ of the Poisson distribution using a Poisson distributed example dataset from Benjamin Renard's lecture in the summer school *Extreme Value Modeling and Water Resources* 2016 in Lyon. Of course, any Poisson distributed dataset could be used. The explicit calculation is done using Eq. 6.4 for an array encompassing a range of possible values for θ . Further, a uniform distribution is chosen to be the prior distribution, expressing our lack of knowledge about the outcome, and evaluated for the same range of values. The unnormalized posterior distribution can be computed explicitly with equation 6.6.

$$\text{post} = \exp(\ln \mathcal{L}(\theta, \text{stationvalues}) + \ln \text{prior}(\theta)) \quad (6.6)$$

$$f(y_1, \dots, y_n | \theta) = \prod_{i=1}^n f(y_i | \theta) = \mathcal{L}(\theta | y) \Rightarrow \ln \mathcal{L}(\theta | y) = \sum_{i=1}^n \ln f(y_i | \theta) \quad (6.7)$$

where the log-likelihood ($\ln \mathcal{L}$) of the proposed θ is the sum of the logarithms of the probability densities ($f(y_i | \theta)$) from the Poisson distribution for the proposed θ -values

evaluated at the station values y_i ¹ (Eq. 6.7). We do not need to normalize the posterior because the location of the maximum, which is what we are after, is the same as for the normalized posterior.

To illustrate this example more clearly, let us compute the maximum value of the unnormalized posterior distribution. The choice of the maximum is arbitrary but convenient since it is easily detectable (Fig. 6.2a). We proceed to fill in values in Equation 6.6. First, we compute the prior distribution of one possible θ . The chosen $\theta=1.94$ is on the location of the maximum of the posterior distribution and indicated with a red dot in Figure 6.2a. With the definition of our uniform distribution ($\min=0$, $\max=366$, $\theta=1.94$) we obtain $\text{Inprior} = -5.9$. Now, we need to determine the log-likelihood for our θ . $\ln \mathcal{L}(1.94|y) = \sum_{i=1}^n \ln f(y_i|1.94) = -70.1$. In the final step, we sum Inprior and the log-likelihood and compute the posterior with Equation 6.6. This yields an unnormalized posterior $\text{post} = 9.85184 \cdot 10^{-34}$, which is consistent with Figure 6.2a. Computing the posterior for each θ value, here 501 values from 0 to 5 with steps of 0.01, will result in the posterior distribution in Figure 6.2a.

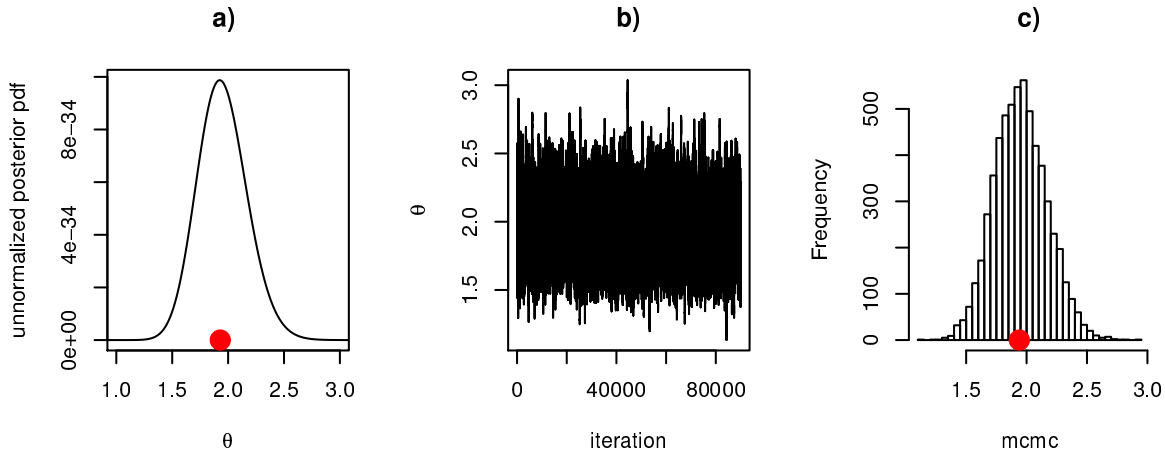


Figure 6.2: Figure illustrating different methods to estimate the parameter λ for the Poisson distribution on example rainfall data. The explicitly calculated unnormalized posterior is displayed in a), the MCMC draws are in (b), and the sampled unnormalized posterior is depicted in c). The location of the maximum is highlighted with a red dot and is in both cases 1.94.

The above demonstrated analytical or explicit approach is only feasible for such simple distributions featuring one parameter. For more complicated distributions sampling of the posterior distribution is a very efficient way to obtain the parameter estimates. Figure 6.2 illustrates the above described explicit approach (Fig. 6.2a) versus the Metropolis-Hastings algorithm (Fig. 6.2c), a widely used Markov chain Monte Carlo (MCMC) method. An instructive explanation of MCMC sampling and the Metropolis-Hastings algorithm can be found in [Renard et al. \[2013\]](#). The results of the explicitly computed unnormalized posterior and the sampled posterior are consistent and depict maxima at the same location. This value can then be chosen to be the best guess for our

¹ y_i : 1, 1, 0, 3, 3, 1, 0, 5, 3, 0, 2, 2, 2, 1, 5, 0, 1, 4, 2, 2, 1, 0, 0, 2, 2, 4, 3, 2, 0, 1, 7, 1, 2, 3, 2, 2, 3, 1, 1

distribution parameter θ with confidence intervals based on the obtained distribution of θ . These confidence intervals are called credible intervals in Bayesian statistics. The histogram of the posterior distribution (Fig. 6.2c) is obtained by the sampled values presented in (Fig. 6.2b). These values reflect the Markov chain randomly walking through the posterior distribution. Before computing the parameter estimate based on the sampled values from the Markov chain, the first values should be removed until convergence is assumed (burn-in period). Auto-correlation is a known artifact of the Markov chain where thinning of the values can be applied to remove this auto-correlation if existing.

The above mentioned Metropolis-Hastings algorithm uses a Markov chain to sample from the posterior distribution. Using the Bayes' Theorem, the prior distribution for each θ is multiplied with the Poisson distribution (\mathcal{P}) for each θ (Eq. 6.9). θ has to be initialized and is subsequently derived from a proposal (or jumping) distribution which is the normal distribution with θ as its mean $\mathcal{N}(\mu = \theta, \sigma_{const})$. The meaning of the proposal distribution is to determine the next step of the Markov chain and by this successively sample the posterior distribution. Drawing from the proposal distribution represents the Monte Carlo contribution in MCMC sampling. The proposal distribution changes every time a new θ is accepted. θ_{new} becomes then θ_{old} and is plugged into the proposal distribution. Using the newly accepted θ for the next step a new θ is drawn from $\mathcal{N}(\theta_{old}, \sigma)$. If a new θ is rejected the old θ is used. A new θ is accepted if the acceptance probability α is larger than 1 (Eq. 6.10). If this is not the case, the acceptance probability is compared against a draw u from a uniform distribution $\mathcal{U}(0, 1)$ (Eq. 6.11). The new value of θ is kept when $u < \alpha$, if not, the new θ is rejected and the old θ is used (Eq. 6.12). The reason for comparing α against u is that we accept the newly proposed θ with a probability P that u is less than α , meaning that we have a rule for this decision. The described decision making process ensures that, given the data, always the most likely θ is picked. The steps of the Metropolis-Hastings algorithm, as implemented for the first manuscript, are visualized below using a uniform distribution as prior.

Step 0: Monte Carlo based step in the Markov chain

$$\theta_{new} \leftarrow \mathcal{N}(\theta_{old}, \sigma_{const}) \quad (6.8)$$

Step 1: Compute ratio of posteriors

$$r(\theta_{new}, \theta_{old}) = \frac{P_{post}(\theta_{new})}{P_{post}(\theta_{old})} = \frac{\mathcal{U}_{prior}(\theta_{new}) \cdot \mathcal{P}(\theta_{new})}{\mathcal{U}_{prior}(\theta_{old}) \cdot \mathcal{P}(\theta_{old})} \quad (6.9)$$

Step 2: Compute acceptance probability

$$\alpha(\theta_{new}, \theta_{old}) = \min \{r(\theta_{new}, \theta_{old}), 1\} \quad (6.10)$$

Step 3: Draw from \mathcal{U} to compare with α

$$u \leftarrow \mathcal{U}(0, 1) \quad (6.11)$$

Step 4: Decide on which θ to use

$$\theta = \begin{cases} \theta_{new}, & \text{if } u < \alpha(\theta_{new}, \theta_{old}) \\ \theta_{old}, & \text{otherwise} \end{cases} \Rightarrow \begin{array}{l} \text{accepted} \\ \Rightarrow \text{rejected} \end{array} \quad (6.12)$$

K-means clustering and cluster sensitivity

The purpose of clustering technique is to reveal patterns in large datasets in a systematic and automated way. There are two basic approaches: hierarchical and non-hierarchical clustering. In this thesis, the K-means algorithm is adopted. K-means is a non-hierarchical cluster technique, relatively simple to use and can be adopted for various distance metrics. A distance metric is a function defining a distance between pairs of elements and can be used to measure similarity or dissimilarity of two elements. The K-means algorithm seeds centroids and computes distances from the centroids to each object. The distance metric is a matter of choice and often the squared Euclidean distance is activated by default. After comparing distances an object can be attributed to its presumed cluster. The smaller the distance between an object and a centroid the higher the probability that the object belongs to that centroid. The seeding process occurs multiple times where the cluster membership is not fixed and also the centroids are re-computed. In the following, I discuss some factors that can influence the outcome of the clustering.

Observational data typically exhibit missing values, challenging statistical methods. In terms of clustering, missing values have to be dealt with in order to use the cluster algorithm. There are two basic approaches: fill in missing values (imputation) or ignore them (marginalization). The rain gauge data used in this thesis had missing values on different dates and time periods. Therefore, when applying marginalization instead of imputation, there would be a substantial loss of information. The example given in the second manuscript shows that for only 4% of missing data, marginalization would result in a reduction of the dataset by approximately 43%. Clustering with missing values using no imputation is possible, described in [Wagstaff \[2004\]](#). However, they also show that substituting with reasonable values, for example using the mean, should not lead to distorted results when only few data is missing. For reducing the loss of information imputation was chosen for the second manuscript. In general, introducing artificial values could distort the clustering results which is why in the second manuscript a sensitivity tests was performed comparing the results after imputing the mean, the median, and an arbitrary value. The test result only showed negligible sensitivity to those changes.

It is indicated above that different distance metrics for the clustering can be chosen. The choice of the distance metric can influence the outcome of clustering. The sensitivity is tested for the clusters in the second manuscript revealing that only stations at the cluster rims might switch cluster memberships. The general structure of the clusters remains robust. The following different distance metrics were tested with similar

outcomes: squared Euclidean, correlation, cosines, and the city-block metric. In this thesis only correlation as a distance metric is used as this is most intuitive and little sensitive to non-Gaussian distributed values. Since the number of clustered stations can impact the cluster results, its sensitivity was tested and found to be very low. For instance, clustering only stations that have consistent records for 40 years, instead of the final dataset of 112 stations, results in a very similar grouping of stations.

Deciding on the number of clusters

Cluster algorithms usually expose the user to the dilemma of choosing the number of clusters beforehand. Various techniques approach this problem where the alleged objective methods still need subjective judgment. The methods used to decide whether a chosen number of cluster was suitable were: comparison of silhouettes [Rousseeuw, 1987] aiming for high silhouette coefficients, and applying gap statistics [Tibshirani et al., 2001]. In the following, I give a brief description of the methods but recommend reading the original citations for more information.

A silhouette $s(i)$ (Eq. 6.13) is a measure for how well a cluster member is assigned to its cluster based on a dissimilarity measure. $a(i)$ is the average distance from the i^{th} object to all other objects in the same cluster. $b(i)$ represents the minimum distance from the i^{th} object to objects in the closest cluster. $s(i)$ can range from -1 to 1 where a value of 1 means that the object lies perfectly in the cluster it is assigned to. Let us use a simple example to illustrate this logic: if an object o is closer to its own cluster members compared to members of other clusters, the silhouette $s(o)$ will be larger than 0. If the object o has a larger average distance to its own cluster than to members of another cluster, the fraction $\frac{a(o)}{b(o)}$ becomes larger than 1 and $s(o) < 0$. $s(o) = 0$ means that the point lies exactly between two clusters. The silhouette coefficient is the average of all silhouettes and gives an impression of how well cluster members are attributed. A high silhouette coefficient for a certain amount of clusters indicates that in average the silhouette values were high which is a sign for well separated clusters.

$$s(i) = \begin{cases} 1 - \frac{a(i)}{b(i)}, & \text{if } a(i) < b(i) \\ 0, & \text{if } a(i) = b(i) \\ \frac{b(i)}{a(i)} - 1, & \text{if } a(i) > b(i) \end{cases} \Rightarrow s(i) = \frac{b(i) - a(i)}{\max(a(i), b(i))} \quad (6.13)$$

Gap statistic [Tibshirani et al., 2001] is a more sophisticated method where not only dissimilarity measures are considered but also whether using more clusters contributes with additional information. This is measured by calculating the gap (Eq. 6.14) between the natural logarithm of the within cluster dispersion W_k and the expected value of a set of natural logarithms of W_k of a reference distribution from Monte Carlo replicates. Although the reference dataset could be drawn from any distribution a uniform distribution was chosen as recommended in [Tibshirani et al. [2001]].

$$G_n(k) = E_n^* \{ \ln W_k \} - \ln W_k \quad (6.14)$$

The final step is to determine, depending on the gap, which number of clusters k should be chosen. In [Tibshirani et al. [2001]], this is decided with the rule in Equation

6.15, where s_{k+1} is a measure expressing the standard deviation of the dispersion of the reference distribution.

$$k = \text{smallest } k \text{ such that } G(k) \geq G(k+1) - s_{k+1} \quad (6.15)$$

6.2.2 Physical approaches

Tracking of low pressure systems

In the second manuscript, trajectories of low pressure systems are obtained using the tracking algorithm TRACK from [Hodges \[1994\]](#), [Hodges \[1995\]](#) and [Hodges \[1999\]](#). This algorithm works in multiple steps. At first, the data is divided into objects which are defined e.g. by local maxima or minima in a meteorological field. This results in a binary map of objects and background field and the data obtains a hierarchical data structure. Identified objects are tracked minimizing a cost function to serve the purpose of smoothness of the trajectories. The cost function is constructed consulting three consecutive time steps and computing the deviation of the positions of feature points. Abrupt changes are not allowed or would result in high costs and are therefore omitted. This tracking algorithm is an established algorithm applied in multiple studies also in South Asia [[Sørland and Sorteberg, 2015a,b](#); [Hodges and Emerton, 2015](#); [Fine et al., 2016](#)].

For this thesis, we applied TRACK on the vorticity field at 850 hPa. The level of 850 hPa was chosen because monsoon depressions tend to have their vorticity maximum in that level in the lower troposphere [[Tyagi et al., 2012](#)]. Further constraints were that the low pressure systems must have traveled at least 1000km and exhibit a vorticity threshold of $5 \cdot 10^{-6} \text{ s}^{-1}$. The regions of genesis and depletion are consistent with [Sørland and Sorteberg \[2015a\]](#) and [Sørland and Sorteberg \[2015b\]](#). However, probably due to the additional constraints in these studies some low pressure systems were not detected, e.g. the case described in the second manuscript on 25 September 2005. With the constraints in my thesis, the trajectory of the low pressure system causing precipitation in West Nepal on 25 September 2005 becomes visible.

Lagrangian moisture source diagnostics

Moisture sources were computed using the moisture source diagnostics from [Sodemann et al. \[2008\]](#) on a global trajectory dataset from 1979 to 2010 [[Läderach and Sodemann, 2016](#)]. This dataset was computed with the Lagrangian dispersion model FLEXPART [[Stohl et al., 2005](#)] with input data from Era-Interim [[Dee et al., 2011](#)]. The moisture source diagnostics from [Sodemann et al. \[2008\]](#) is illustrated in Figure 6.3. An air parcel is traced back in time while its moisture content is monitored. Every change in moisture is assumed to be caused by either evaporation or precipitation. Another monitored quantity is the height of the parcel to distinguish whether the parcel is in the free troposphere or the boundary layer, both defined by Era-Interim. Once these quantities are known, one can compute changes in moisture and attribute those changes to evaporation or precipitation. As illustrated in Figure 6.3 the method takes

into account the history of the air parcel. Hence, this approach prevents the overestimation of sources and sinks along the trajectory and focuses on the moisture sources directly related to the precipitation event. Taking into account the history of the trajectory is also a major difference and advantage (as introduced in [Sodemann et al. \[2008\]](#)) to the evaporation minus precipitation (E-P) approach and therefore used in this thesis. [Winschall et al. \[2014\]](#) and [Läderach and Sodemann \[2016\]](#) evaluated the method from [Sodemann et al. \[2008\]](#) against Eulerian tracers and concluded that both results were consistent. Hence, the moisture diagnostics represents a computational efficient method to determine moisture sources for precipitation events.

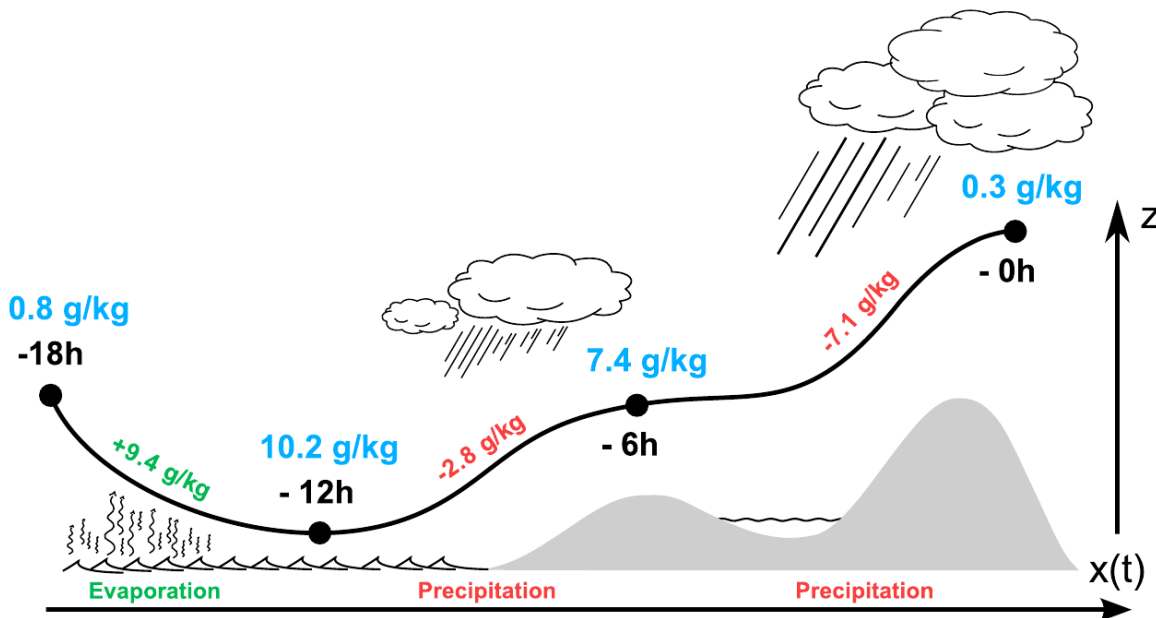


Figure 6.3: Figure 1 from [Läderach and Sodemann \[2016\]](#) illustrating the moisture source diagnostics from [Sodemann et al. \[2008\]](#). Along the trajectory (black line) of an air parcel the moisture content is evaluated every 6 hours. Red numbers indicate moisture loss, green numbers indicate moisture uptake, and blue numbers the moisture content for every time step.

Numerical modeling

In the third manuscript the physics and dynamics of the considered extreme precipitation event are in the focus. To overcome poor resolution, convection parameterization and large time steps, we simulate the event with the Weather Research & Forecasting (WRF) model where we use the Advanced Research WRF (ARW) [[Skamarock et al., 2008](#); [Skamarock and Klemp, 2008](#)]. The WRF-model is a numerical model which solves the moist, compressible, non-hydrostatic Euler equation in flux form along with the diagnostic equations for inverse density and the equation of state. In the final equations the map projection is included and the equations are transformed into perturbation equations to minimize truncation errors. The model is designed with a terrain-following hydrostatic-pressure vertical coordinate η which is a classical σ -coordinate [[Laprise, 1992](#)]. The WRF-model is integrated forward in time using the Runge-Kutta time integration scheme [[Wicker and Skamarock, 2002](#)] with two time step modes, where the

Table 6.1: Model setup for WRF-ARW v.3.7.1.

Horizontal Resolution	4 km
Horizontal grid	612 x 502 grid boxes
Number of Vertical Levels	50
Microphysics	Thompson graupel scheme
Planetary Boundary Layer Scheme	MYNN 2.5 level TKE
Surface Layer	MYNN
Land Surface Scheme	unified Noah LSM

short acoustic time step is separated from the lower frequency integration. In the ARW solver, the spatial discretization is approached staggering variables on an Arakawa C-grid.

In this thesis, the simulation was subject to spectral nudging [[Waldron et al., 1996](#)], applied to the wavenumber 1 in the horizontal wind field. Spectral nudging was only applied above the 12th model level. The lowest model levels were not nudged to retain the advantage of resolving fine scale topographic structures and associated physical processes. Due to the complex topographic features in the Himalayas, high resolution and the resulting dynamics and thermodynamics developing in the model can add value to the simulation.

In the third manuscript a simulated radar reflectivity is derived from the model. The corresponding computations were done in the Thompson microphysic scheme [[Thompson et al., 2004, 2008](#)] which makes use of libraries from [Blahak \[2008, updated June 2012\]](#) to compute quantities related to Rayleigh scattering. The libraries are summarized in *module_mp_radar.F* in the WRF physics code. This is only possible for a selection of microphysic schemes as can be seen in the freely available WRF code. In the Thompson scheme, the reflectivity is derived assuming a radar with a wavelength $\lambda = 10\text{ cm}$ applying the Rayleigh approximation to imitate the use of USA NEXRAD radars (described in *module_mp_radar.F*). When using the Rayleigh approximation one assumes that the diameter of the hydrometeors are much smaller than the wavelength. In order to be able to measure as many different drops as possible a comparably large wavelength is chosen ($\lambda = 10\text{ cm}$). The computation of the radar reflectivity factor (dBZ with Z in $\text{mm}^6\text{ m}^{-3}$) is performed for rain, graupel, and snow particles as well as for water-coated snow and water-coated graupel particles.

Assessing quasi-geostrophic forcing

Quasi-geostrophy is a useful diagnostic framework which, due to the inherent simplification, allows to better understand predominant forcing mechanisms in the atmosphere. The quasi-geostrophic momentum equation result from scale analysis applied on the general horizontal momentum equation (Eq. 6.16). When the atmospheric flow is divided into a geostrophic part and an ageostrophic part $\mathbf{V} = \mathbf{V}_g + \mathbf{V}_a$, it turns out that in the free troposphere the terms describing geostrophic effects are greater than the ageostrophic terms which therefore can be mostly neglected. I wrote *mostly*, because

there is in particular one term that tends to have a similar magnitude as the geostrophic terms. This term is the ageostrophic Coriolis term (term B 2 in Eq. 6.17). Since there is one ageostrophic component retained and the geostrophic components dominate the system, the framework is called *quasi-geostrophic*. Equations 6.16 and 6.17 show the transition from the horizontal momentum equation to the quasi-geostrophic form in pressure coordinates. Term A and A' describe the change of the horizontal winds and geostrophic winds, respectively. Term B is the Coriolis term which can be split up in its geostrophic component B 1 and its ageostrophic component B 2. Term C represents differences in the geopotential and term F is the friction term which can be removed when assuming free troposphere and large scale conditions.

$$\underbrace{\frac{D\mathbf{V}}{Dt}}_{A} = \underbrace{-f\hat{k} \times \mathbf{V}}_{B} - \underbrace{\nabla_p \Phi}_{C} + \underbrace{F}_{D} \quad (6.16)$$

$$\underbrace{\frac{D_g \mathbf{V}_g}{Dt}}_{A'} = \underbrace{-f\hat{k} \times \mathbf{V}_g}_{B 1} - \underbrace{\nabla_p \Phi}_{C} - \underbrace{f\hat{k} \times \mathbf{V}_a}_{B 2} \quad (6.17)$$

V_g is the geostrophic wind, V_a the ageostrophic wind, f the Coriolis parameter, \hat{k} represents the unit vector in the vertical, and Φ is the geopotential. Since the geostrophic wind, term B 1 and term C, is balanced (Eq. 6.17), it becomes clear that only the ageostrophic term can cause changes in the geostrophic wind. A change in the geostrophic wind field has to be compensated with an additional circulation to maintain continuity. Diagnosing the forcing responsible for the large scale ascent or descent is what we are looking for.

Manipulating the quasi-geostrophic thermodynamic energy equation and the quasi-geostrophic vorticity equation, derived from the quasi-geostrophic momentum equation [Bluestein, 1992], we can obtain the quasi-geostrophic ω -equation (Eq. 6.18), a diagnostic equation for the pressure tendency ω .

$$\underbrace{\left(\nabla^2 + \frac{f_0}{\sigma} \frac{\partial^2}{\partial p^2} \right) \omega}_{A} = \underbrace{\frac{f_0}{\sigma} \frac{\partial}{\partial p} [\mathbf{v}_g \cdot \nabla_p (\zeta_g + f)]}_{B} - \underbrace{\frac{1}{\sigma} \nabla_p^2 \left[(\mathbf{v}_g \cdot \nabla_p) \left(-\frac{\partial \Phi}{\partial p} \right) \right]}_{C} \quad (6.18)$$

f_0 is the Coriolis parameter on an f-plane, σ is the stability parameter $\sigma = -T(\partial \theta)(\partial p)^{-1}$ with the potential temperature θ , p is the pressure, ζ_g the quasi-geostrophic vorticity, and R the gas constant for dry air.

With the hydrostatic assumption, the definition of the geopotential, and the ideal gas equation we can arrive at the formulation of the ω -equation used in Bluestein [1992]:

$$\underbrace{\left(\nabla^2 + \frac{f_0}{\sigma} \frac{\partial^2}{\partial p^2} \right) \omega}_{A} = \underbrace{\frac{f_0}{\sigma} \frac{\partial}{\partial p} [\mathbf{v}_g \cdot \nabla_p (\zeta_g + f)]}_{B} - \underbrace{\frac{R}{\sigma p} \nabla_p^2 [\mathbf{v}_g \cdot \nabla_p T]}_{C} \quad (6.19)$$

The disadvantage of the ω -equation is the fact that it has, depending on its formulation, at least two forcing terms. These are under adiabatic conditions the vorticity advection (term B) and the air mass advection (term C). Both terms can amplify or dampen each other which can make it difficult to evaluate the combined effect. The forcing of each term has to be quantified and added to obtain the net-effect on the vertical motion (ω in term A).

[Hoskins et al. \[1978\]](#) expressed the quasi-geostrophic ω -equation in the Q-vector form. The derivation of the Q-vector form is outlined in [Bluestein \[1992\]](#) and results in Equation 6.20. The advantage now is that there is only one main forcing term (term B) which allows to evaluate whether there is rising or sinking motion.

$$\underbrace{\left(\nabla^2 + \frac{f_0^2}{\sigma} \frac{\partial^2}{\partial p^2} \right)}_{A} \boldsymbol{\omega} = \underbrace{-2\nabla_p \cdot \mathcal{Q}}_{B} - \underbrace{\frac{R}{\sigma p} \beta \frac{\partial T}{\partial x}}_{C} \quad (6.20)$$

Bearing in mind that we are almost in mid-latitudes, we can neglect the β -term (term C) due to scale analysis. Comparing magnitudes also suggests that we can neglect the vertical change in the pressure tendency (part of the operator in term A). Removing those two terms, we arrive at an elliptic equation for ω :

$$\nabla^2 \boldsymbol{\omega} = -2\nabla_p \cdot \mathcal{Q} \quad (6.21)$$

$$\mathcal{Q} = -\frac{R}{\sigma p} \begin{pmatrix} \frac{\partial v_g}{\partial x} \nabla_p T \\ \frac{\partial v_g}{\partial y} \nabla_p T \end{pmatrix} = \begin{pmatrix} Q_1 \\ Q_2 \end{pmatrix} \quad (6.22)$$

The Q-vectors are a mathematical construct and not real physical entities. It is a diagnostic that helps to combine the forcing terms from the quasi-geostrophic ω -equation to one forcing term, the divergence of Q-vectors. Considering the scales, we are operating on and the fact that we are rather far up in the troposphere (300 hPa), we assume a hydrostatic environment when transforming the vertical pressure tendency into the vertical velocity (Eq. 6.23):

$$\boldsymbol{\omega} = \frac{dp}{dt} = \frac{dp}{dz} \frac{dz}{dt} = \frac{dp}{dz} w \quad \Rightarrow \quad \text{insert: } \frac{dp}{dz} = -\rho g \quad \Rightarrow \quad \boldsymbol{\omega} = -\rho g w \quad (6.23)$$

Assuming that most moisture is in the lower troposphere, we obtain a more convenient form for the vertical velocity with the help of the ideal gas equation for dry air:

$$w = \frac{\omega R_d T}{pg} \quad (6.24)$$

Due to the applied simplifications, the elliptic equation for ω became a Poisson equation (Eq. 6.21) and can be solved e.g. by applying the Gauss-Seidel method or the Successive over relaxation (SOR) [[Press, 2007](#)]. To do this, we discretized equation Eq. 6.21 with central differences on a regular mesh with $\Delta x = \Delta y = h$. For better

comparison with [Press \[2007\]](#), I use the same notation where f represents the field to be filled with values initialized with zero, h is the horizontal resolution, and the source function $S = -2\nabla_p \cdot \mathcal{Q}$.

$$f_{i+1,j} + f_{i-1,j} + f_{i,j+1} + f_{i,j-1} - 4f_{i,j} = h^2 S_{i,j} \quad (6.25)$$

Rearranging for $f_{i,j}$ results in:

$$f_{i,j} = \frac{1}{4} [f_{i+1,j} + f_{i-1,j} + f_{i,j+1} + f_{i,j-1} - h^2 S_{i,j}] \quad (6.26)$$

The discretized equation shows that each node in our grid is defined by its neighboring nodes. This means also that we need some starting values for computing the value of the mid-node. Using the discretized equation, we can iterate through all nodes using already updated nodes in the vicinity (Eq. 6.27). This is also known as the Gauss-Seidel method.

$$f_{i,j}^{n+1} = \frac{1}{4} [f_{i+1,j}^n + f_{i-1,j}^{n+1} + f_{i,j+1}^n + f_{i,j-1}^{n+1} - h^2 S_{i,j}] \quad (6.27)$$

To speed up convergence, I applied the faster SOR method in Paper III. It makes use of the Gauss-Seidel method by combining the residual similar to Equation 6.27 and an additional relaxation parameter $1 < \omega < 2$. This ω is not to be confused with the pressure tendency described above. The letter ω is only used here to be consistent with [Press \[2007\]](#). The residual can be formulated in Equation 6.28. If this residual is larger than a predefined error margin the iteration continues and the field is updated with Equation 6.29.

$$Res = f_{i+1,j}^n + f_{i-1,j}^{n+1} + f_{i,j+1}^n + f_{i,j-1}^{n+1} - h^2 S_{i,j} - 4 \cdot f_{i,j}^n \quad (6.28)$$

$$f_{i,j}^{n+1} = f_{i,j}^n + \frac{\omega}{4} \cdot Res \quad (6.29)$$

Chapter 7

Scientific results

7.1 Summary of the papers

Paper I: *A comprehensive view on trends in extreme precipitation in Nepal and their spatial distribution*

We use multiple methods to assess trends in extreme precipitation in Nepal based on rain gauge stations. Previous studies had either poor station coverage of this region, did not apply extreme value theory, or did not take into account the possibility for a climatic change in their statistical model. We address these points by applying quantile regression and extreme value theory to assess trends in extreme precipitation events and compare those to trends in mean precipitation. This gives a new comprehensive picture on measurement based trends in extreme precipitation in Nepal. We find that almost all extreme precipitation events occur during the Indian summer monsoon reflecting the highly seasonal climate in Nepal. For Nepal in total, monsoon precipitation does not depict a significant trend nor does the number of extremes per station. In contrast to seasonal rainfall, extreme daily precipitation amounts are not linearly correlated with the El Niño-Southern Oscillation (ENSO). Despite high spatial variability of trends in extreme precipitation across Nepal, especially Far-West Nepal indicates considerable positive trends in extreme precipitation. This can be seen across the applied methods and thus indicate the robustness of our results.

Paper 2: *Synoptic conditions and moisture sources actuating extreme precipitation in Nepal*

Realizing in the first manuscript that extreme precipitation in Nepal is changing considerably, a better understanding of the involved physical processes becomes imperative. In paper II, we focus on direct moisture sources for the extreme events and the prevailing large scale meteorological conditions. The considered large scale conditions are divided into low pressure systems and mid-level troughs. Rain gauge data, reanalysis, and Lagrangian trajectories form the basis of this study. By clustering rain gauge data, we take into account the high spatial variability of the occurrence of precipitating systems along the Himalayas. We establish three cluster regions of similar daily precipitation characteristics, West Nepal, Central Nepal, and East Nepal. Subsequently, dates,

on which extreme precipitation occurred concurrently at multiple stations in each cluster region, are used to investigate atmospheric circulation patterns and moisture sources in a composite analysis. We find that the atmospheric flow is directed against the Himalayas at the location of the cluster accommodating the extreme event. Further, the large scale flow conditions guide low pressure systems toward the Himalayas where they rain out. Anonymously abundant moisture sources along the path of the low-level flow stems predominantly from land, particularly from the Indo-Gangetic plain. The additional moisture was likely provided by foregone precipitation events preconditioning the soil for enhanced moisture uptake. This complements previous studies in South Asia focusing on different regions. Moreover, we highlight differences in atmospheric circulation and moisture sources to flooding events in Pakistan and Northwest India.

Paper 3: Multiscale characteristics of an extreme precipitation event over Nepal

In the third manuscript, we investigate in more detail meteorological conditions and moisture sources revealed by our second manuscript. We now pick a single case, the extreme precipitation event on 19 July 2007. Using rain gauge data, TRMM 3B42, Era-Interim re-analysis, Lagrangian trajectories, and a high resolution numerical simulation allows us to scrutinize the interplay of the involved meteorological conditions and understand the physical processes that contribute to the development of an extreme precipitation event. To attain a comprehensive understanding, we perform a multiscale analysis covering large scale to mesoscale characteristics of the extreme event. The extreme event on 19 July started with initially separate convective cells over Nepal which were invigorated with moist low-level inflow housing high convective available potential energy. The individual convective cells organize upscale and an intense wide convective system with a simulated echo core of 40 dBZ exceeding a vertical extent of 12 km formed over Central Nepal during the late afternoon. The result was torrential rain with over 250 mm within 24 hours. We identify several synoptic scale conditions that lead to the intense development of the convective system: anomalously high moisture sources along the path of a low-level flow characteristic for monsoon break periods, this lead to moist airmasses feeding into the convective system, the additional available moisture was created by foregone precipitation events, and airmasses were destabilized by upslope flow and quasi-geostrophic forcing where the upslope flow was likely the main trigger mechanism. While the type of the convective system was not unusual for the Central Himalayas, its intensity was. This study shows how distinct synoptic scale conditions can create a system with unusual intensity.

Paper I

7.2 A comprehensive view on trends in extreme precipitation in Nepal and their spatial distribution

Patrik Bohlinger and Asgeir Sorteberg

International Journal of Climatology, (2017), doi: 10.1002/joc.5299

A comprehensive view on trends in extreme precipitation in Nepal and their spatial distribution

Patrik Bohlinger^{a,b*}  and Asgeir Sorteberg^{a,b}

^a Geophysical Institute, University of Bergen, Norway
^b Bjerknes Centre for Climate Research, University of Bergen, Norway

ABSTRACT: We investigate trends in monsoon and extreme precipitation in Nepal based on rain gauge measurements. We find that precipitation amounts in Nepal vary considerably in space and time. The number of occurring extremes and the amount of precipitation are controlled mainly by the Indian summer monsoon. Almost all extreme precipitation events, recorded by 98 considered meteorological stations, occur during the Indian summer monsoon with the maximum in July. For Nepal in general, we find that the amount of precipitation and number of extreme events per station are neither significantly increasing nor decreasing between 1971 and 2010. However, on a regional scale we identify areas with positive and negative trends. A comparison of the combined precipitation time series with the ENSO 3.4 index reveals a connection between ENSO and the variability in monsoon precipitation. The correlation with the number of monsoon extremes vanishes for increasing percentiles. We investigate trends of upper percentiles of daily precipitation which pinpoint regions of increasing and decreasing extremes. These patterns are similar to spatial patterns in mean monsoon precipitation trends, whereas the median of the precipitation distribution undergoes only minor changes. Further analysis using extreme value theory confirm the prevailing trends from quantile regression for most stations and depict strong changes in return levels. Especially for Far-West Nepal, we find robust evidence for a systematic increase in extreme precipitation.

KEY WORDS extreme precipitation; precipitation trends; Nepal; Himalaya; quantile regression; extreme value distribution; non-stationary

Received 10 October 2016; Revised 29 June 2017; Accepted 20 August 2017

1. Introduction

The Special Report on Extreme Events of the Intergovernmental Panel on Climate Change (Field *et al.*, 2012) and the Fifth Assessment Report (Stocker *et al.*, 2013) state that the magnitude of precipitation extremes and their frequency of occurrence have been increasing over most of the globe. They further conclude that a shift in the distribution, for instance a shift in the mean, can affect the extremes. For south Asia a change in return periods to more frequent extreme precipitation is projected for different emission scenarios. Bookhagen (2010) finds that the mountainous Himalaya has almost twice as many extreme events as the Ganges Plain or the Tibetan Plateau. Nepal, a country with complex topography, home to the highest peaks in the world, large glacier systems, and consequently great exposure to natural hazards like flash floods and landslides needs good estimates of changes in extreme temperature and precipitation for risk management. In this study, we comprehensively assess systematic changes in monsoon and extreme precipitation in Nepal. We hope that these findings will be useful to risk management which relies on correct estimations of changes in return values.

Natural variability has to be considered and explored to understand changes in precipitation and extremes. Several studies agree on the connection between the El Niño-Southern Oscillation (ENSO) and the magnitude of the monsoon precipitation. The strength of this connection has been subject to continuous debate (Trenberth, 1997; Kumar *et al.*, 1999; Shrestha, 2000; Ichiyangagi *et al.*, 2007; Sigdel and Ikeda, 2013). The general opinion condenses to a negative correlation between ENSO and the precipitation amount with a varying strength over time. Recently, also a lagged relationship between the Pacific quasi-decadal oscillation and the monsoon precipitation in Nepal was found (Wang and Gillies, 2013).

In order to homogenize the efforts to assess extremes worldwide and implement a common practice approach, the Expert Team on Climate Change Detection, Monitoring and Indices (ETCCDI) published a list of indices of climate extremes in the report WCDMP-No. 72 in 2009. In their report, they state that extreme weather phenomena are often not directly tied to environmental disasters. The impact of extremes depends to a large degree on the vulnerability and resilience of a system. A systematic change in extremes, however, is accompanied by a systematic change in hazardous weather situations leading to disasters with high socio-economic impact. An important piece of advice in the ETCCDI report is that changes in very rare extreme

*Correspondence to: P. Bohlinger, University of Bergen, Geophysical Institute, Allégaten 70, NO-5020 Bergen, Norway. E-mail: patrik.bohlinger@gsf.uib.no

P. BOHLINGER AND A. SORTEBERG

Table 1. Overview over conducted research on extreme precipitation in Nepal.

Study	Area	Years	Number of stations	Method	Trends in extremes
SH05	Basins in India Pakistan and Nepal	1971–2000	Nepal: 11	OLSR	✓
BD08	Nepal	1961–2006	26	ETCCDI, OLSR	✓
N09	Nepal	1976–2005	166	OLSR, EVT: Gumble Type 1	—
C11	Indo-Pacific	1971–2005	Nepal: 7	ETCCDI, OLSR	✓
SH16	Koshi River Basin	1975–2010	50	ETCCDI, OLSR	✓
BS17	Nepal	1971–2010	98	OLSR, QR, EVT: Full GEV	✓

Abbreviations of studies: SH05 = Shrestha (2005), BD08 = Baidya *et al.* (2008), C11 = Caesar *et al.* (2011), SH16 = Shrestha *et al.* (2017), BS17 = Bohlinger and Sorteberg (this study). Abbreviations for methods: ETCCDI = different ETCCDI climate indices for precipitation, OLSR = Ordinary Least Square Regression, QR = Quantile Regression, EVT = Extreme Value Theory.

events are not well represented by these indices and should be treated using the extreme value theory.

Utilizing ETCCDI indices for station-based research over central and south Asia, Tank *et al.* (2006) concluded with a warming signal but non-coherent precipitation trends. Zooming in on the Himalayas, limited work has been done assessing precipitation trends and possible future changes. This is partly due to limited availability of rain gauges compared to other surrounding countries (Dhar and Nandargi, 2000; Nandargi and Dhar, 2011). However, studies have shown evidence for a systematic increase in temperature and natural hazards (Shrestha *et al.*, 1999; Chalise and Khanal, 2001, 2002; Shrestha, 2005). Studies on changes in annual, seasonal, and extreme precipitation in Nepal produced less univocal results. Both increasing and decreasing trends have been reported at different sites across the country as well as a sensitivity to elevation, while no consistent trend could be found for the monsoon season over the entire country (Shrestha *et al.*, 2000; Shrestha, 2005; Ichiyanagi *et al.*, 2007). Nandargi and Dhar (2011) studied extremes along the Himalayas and stated that there was a sudden increase in the frequencies of extreme rainfall events in the 60s, but a decrease in the first decade from 2000. Nepal, however, was excluded since the respective dataset did not include the dates of occurrence of extreme events. Caesar *et al.* (2011) investigated changes in ETCCDI indices across the Indo-Pacific region. Nepal was only represented by seven stations which indicated an increase in east and west Nepal and a decrease in central Nepal. Due to data sparseness, however, caution should be taken when associating trends at single stations with larger regions of Nepal.

Few studies exist that focus on changes in extreme precipitation in Nepal. For instance, Shrestha (2005) found indications of an increasing trend in extreme precipitation in Nepal. Other studies computed least-square fits on ETC-CDI indices (Baidya *et al.*, 2008; Shrestha *et al.*, 2017). A quite comprehensive attempt on assessing rainfall and its extremes in Nepal was published in 2009 by the Practical Action Nepal Office in form of a report (hereafter N09) with the title ‘Temporal and spatial variability of climate change over Nepal (1976–2005)’ (Marahatta *et al.*, 2009). Spatial maps of precipitation, return levels and changes of

seasonal and annual rainfall were produced using Ordinary Least Square Regression (OLSR) for temporal changes and a Gumble type 1 distribution for computing stationary return levels. However, this report only computed trends for the means and not for extreme precipitation. The studies including Nepal are summarized in Table 1.

We highlight three issues which we complement in our study. First, we extend trends estimated with OLSR from N09 to different quantiles of daily precipitation. The reason being that OLSR is very sensitive to questionable values and outliers especially at the beginning and end of time series. Secondly, we estimate changes in return values for block maxima which has not yet been done. Thirdly, instead of a Gumble type 1 distribution we use the full Generalized Extreme Value (GEV) distribution, which, includes a shape parameter. This is because marginal rainfall distributions at the stations show shape parameters which despite large uncertainty, are likely to be different from zero. This in turn can have considerable impact on the distribution and consequently the estimation of return levels.

2. Data and methods

We start out with 278 meteorological stations from the Department of Hydrology and Meteorology (DHM) in Nepal (Figure 1). Purchased station data consist of 40 years of 24 h precipitation amounts (9 am previous day to 9 am local time, UTC/GMT +5:45 hours) for the years 1971 to 2010. Daily rainfall data analysed in this study was obtained using US standard 8 ‘diameter manual rain gauges and undergoes basic quality control like removing negative values and outliers.’ More information about the different measurement networks in Nepal can be found in Talchabhadel *et al.* (2016). Data is not continuously available and some stations are not measuring precipitation for the entire period but for some years only. Stations are well distributed over the country although the number of stations decreases with increasing elevation. Relatively densely populated areas like Kathmandu and Pokhara have a higher number of stations close-by while other areas, in particular the Mid-West and Far-West Nepal stations are more sparse. For describing regional characteristics in our

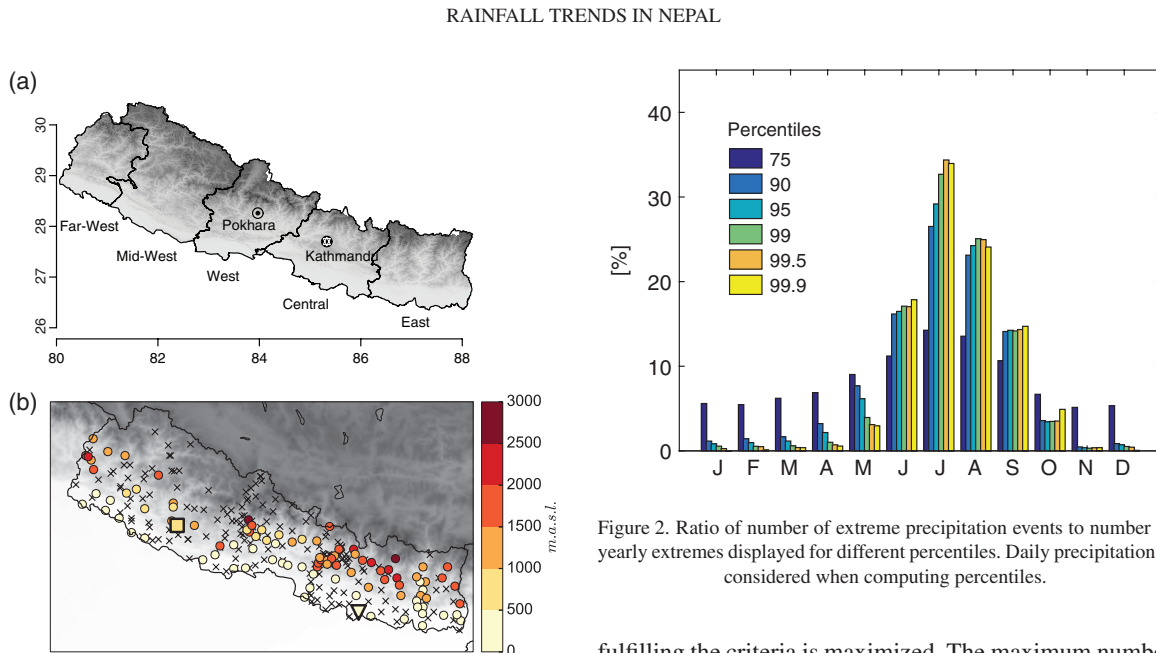


Figure 1. (a) Regions of Nepal with the location of two centres of high station density, Pokhara and the capital Kathmandu. (b) Location of the 98 meteorological stations from the Department Of Hydrology and Meteorology (DHM) in Nepal. Station elevation is in meters above sea level [m.a.s.l.]. Stations disregarded in this study are marked by a cross. Underlying topography is displayed in grey for orientation purposes. The stations 512 and 1111 are marked with a square and triangle, respectively.

results we use the names of the different regions in Nepal as shown in Figure 1.

Since there is a vast amount of missing values in the dataset, only stations offering a set of sufficiently representative data are chosen for further investigations (see Section 2.1 for details). We provide a complete table with station names and their basic meta-data as supporting information (Table S1, Supporting Information). In Section 3.4, two arbitrary stations are used to illustrate the applied concepts and findings. These two stations with the identification numbers 512 and 1111 are also marked in Figure 1.

2.1. Selection of appropriate stations

We selected stations based on a minimum amount of observations available and a desire to cover most of Nepal's climatic zones defined by elevation as sketched in Shrestha *et al.* (2017). Considering all available stations, strong precipitation events happen mostly during the Indian summer monsoon from June to September (Figure 2). Constraints for selecting suitable stations are therefore mainly based on these four months rather than the entire period. The challenge of choosing representative sites is approached by allowing only stations which have at least 75% data coverage for the period (1971–2010) in each monsoon month. Since too many stations disqualify when applying this constraint to the entire period of 40 years (100%) we ease the restriction to 30 years (75%) which is the second constraint. An optimal time period of 30 years from the total 40 years is chosen where the number of available stations

Figure 2. Ratio of number of extreme precipitation events to number of yearly extremes displayed for different percentiles. Daily precipitation is considered when computing percentiles.

fulfilling the criteria is maximized. The maximum number of stations is 112. Of these 112 stations at least 75% (84 stations) have to fulfil the quality criteria over the same time period (third constraint). The choice of 75% instead of 100% is due to the fact that with 75% we cover all regions in Nepal and all climatic zones but the High Himalayas which are higher than 2500 m.a.s.l. (Shrestha *et al.*, 2017). Choosing 30 years as a suitable reference period is mainly to retain time series that are somewhat representative for climate and long enough to level out variations that are associated with e.g. ENSO. In our case the reference period lasts from 1979 to 2008.

The availability of stations is sensitive to the constraints as illustrated in the following example. Keeping the second constraint untouched since we want to retain a 30 year data record, we can test the sensitivity to the remaining constraints. For instance, using 70% or 80% for the first criterion results in 112 and 111 stations, respectively. Changing only the third constraint to 70% or 80% would change the number of remaining stations to 122 and 100, respectively. The position of the optimal time period varies only by a few years when changing the constraints above as described. We note that our results are not very sensitive to the number of stations included. Ichiyanagi *et al.* (2007) demanded availability of 80% of the entire period (1987–1996). Choosing a certain degree of coverage for an entire period could mean less coverage in the monsoon months where most of the extremes are found and more coverage in the rest of the year. This is why we introduced an additional availability constraint for each monsoon month to avoid that potential bias on our results.

These constraints result in 112 stations which are rather uniformly spread over the country (Figure 1) and range from 72 m.a.s.l. to 2742 m.a.s.l. Higher mountain regions have unfortunately no stations fulfilling the requirements and were excluded from further investigations. It would be of course ideal to have close to full data coverage instead of 75%. This choice has to be made specifically

P. BOHLINGER AND A. SORTEBERG

for every study. We aimed for a balance between spatial and temporal availability. A uniform spatial spread gives confidence in capturing the total picture of precipitation in Nepal. Using the constraints we have chosen, we end up with a set of 112 stations that is largely a subset of the 166 stations used for the N09 report.

2.2. Homogeneity of time series

We tested the remaining 112 stations for homogeneity to reduce the risk to include artificially induced trends, e.g. by stations changing location. Due to the sparseness of stations in highly complex topography we did not find it feasible to test against a reference time series or nearby stations as suggested by Alexandersson (1986). Instead we used a penalized maximal F test (PMFT) (RHtestsV4, Wang (2008a,b)). This software for testing homogeneity is freely available and described in detail on the ETCCDI homepage (<http://etccdi.pacificclimate.org/software.shtml>). We did not adjust time series when a significant (5% significance level) break point was found but rather rejected the respective records. Additionally, time series were visually inspected and three more stations excluded. Two of them depicted break points that were not significant but to the eye a shift in mean seemed to be probable. The third station clearly depicted a strong, sudden change in variance and was excluded due to its heteroscedasticity. In total we rejected 14 stations and proceeded with a subset of 98 both plain area and hill stations (Table S1).

2.3. Trend analysis for extreme events

We used two methods to assess trends in extreme precipitation. Our approach using extreme value theory and specifications for the Bayesian estimation of the GEV distribution parameters are described in Appendix.

In order to determine the trend of different quantiles we performed a quantile regression on daily precipitation for each station following the method from Koenker and Hallock (2001). Advantages of quantile regression *versus* OLSR can be summarized as follows. Quantile regression is more flexible as it is possible to explore the impact of covariates on all quantiles within a given distribution, meaning that a different behaviour in different quantiles can be observed. Additionally, quantile regression is robust to outliers and leads to reasonable estimates when the error distribution is non-normal. Based on these advantages quantile regression is well suited for this study to investigate changes in different quantiles of daily precipitation. Fan and Chen (2016) illustrate some advantages of this method when calculating trends in extreme precipitation indices across China.

Block maxima values like annual or seasonal maxima follow the GEV distribution which is defined by the three parameters for location (μ), scale (σ), and shape (ξ). Given a set of values these parameters can be estimated for instance by maximum likelihood or Bayesian approaches which are both used in this study. We computed changes of the 100 year return level with 1 where Q_{99} represents the 99th quantile from a GEV with the location parameter for year 2010 *versus* 1971 for a single station s :

$$\text{CHANGE}_s = \left[\frac{Q_{99}(\text{GEV}(x, \mu(t=2010), \sigma, \xi)_s)}{Q_{99}(\text{GEV}(x, \mu(t=1971), \sigma, \xi)_s} \cdot 100\% \right] - 100\% \quad (1)$$

3. Results and discussion

The results presented in this chapter are computed with respect to the reference period explained in Section 2.1. For percental trends the respective climatological value is used. This allows us to directly compare stations and regions without biasing the results with records of different length. For the following analysis a day is considered a wet day when precipitation is recorded, irrespective of the amount.

3.1. Station monsoon climatology

Over a variety of high quantiles, almost all extremes were measured during the Indian summer monsoon period (Figure 2). The higher the percentiles the more likely it is that it is recorded during the monsoon. The distribution flattens out for lower percentiles. July claims most extreme events with a substantial difference compared to June, August, and September.

Most of the annual precipitation is measured during the Indian summer monsoon, ranging from 412 mm up to 4575 mm (Figure 3(a)). The contribution to the annual precipitation ranges from 54% to 88% depending on the station (Figure 3(b)). The monsoon mean precipitation indicates local maxima in the station cluster close to Pokhara in the north-west (Lumle), north-east of Kathmandu (Gumthang), and north in East Nepal (Num) (Figure 3(a)). The contribution of the monsoon precipitation to annual precipitation is highest close to the Indian border, close to Pokhara, Kathmandu and north-east of Kathmandu (Figure 3(b)). There are local minima in the contribution at the border between Far-West Nepal and Mid-West Nepal, and central in East Nepal. The spatial distribution of summer monsoon precipitation and the percentage of monsoon rainfall compared to annual rainfall is in agreement with findings from Shrestha (2000).

The spatial distribution for median values of wet days depict a similar pattern as described for mean monsoon precipitation (Figure 3(c)). The 99.5-percentiles of daily precipitation has the highest values along the Indian border, close to Pokhara, and north in East Nepal with maximum values of over 190 mm d⁻¹ (Figure 3(d)). Using only wet days for the extreme percentile calculation does not change the pattern qualitatively. Extreme values become higher towards India and seem to be rather constant along the Indian border where the topography is less complex.

The number of wet days combined with the rainfall amount indicates whether it rains often or seldom and if the events are strong or weak. The number of wet days increases towards China and further into the Himalayas (Figure 3(e)) with the highest values in West Nepal and Central Nepal. At stations close to Pokhara and in Central

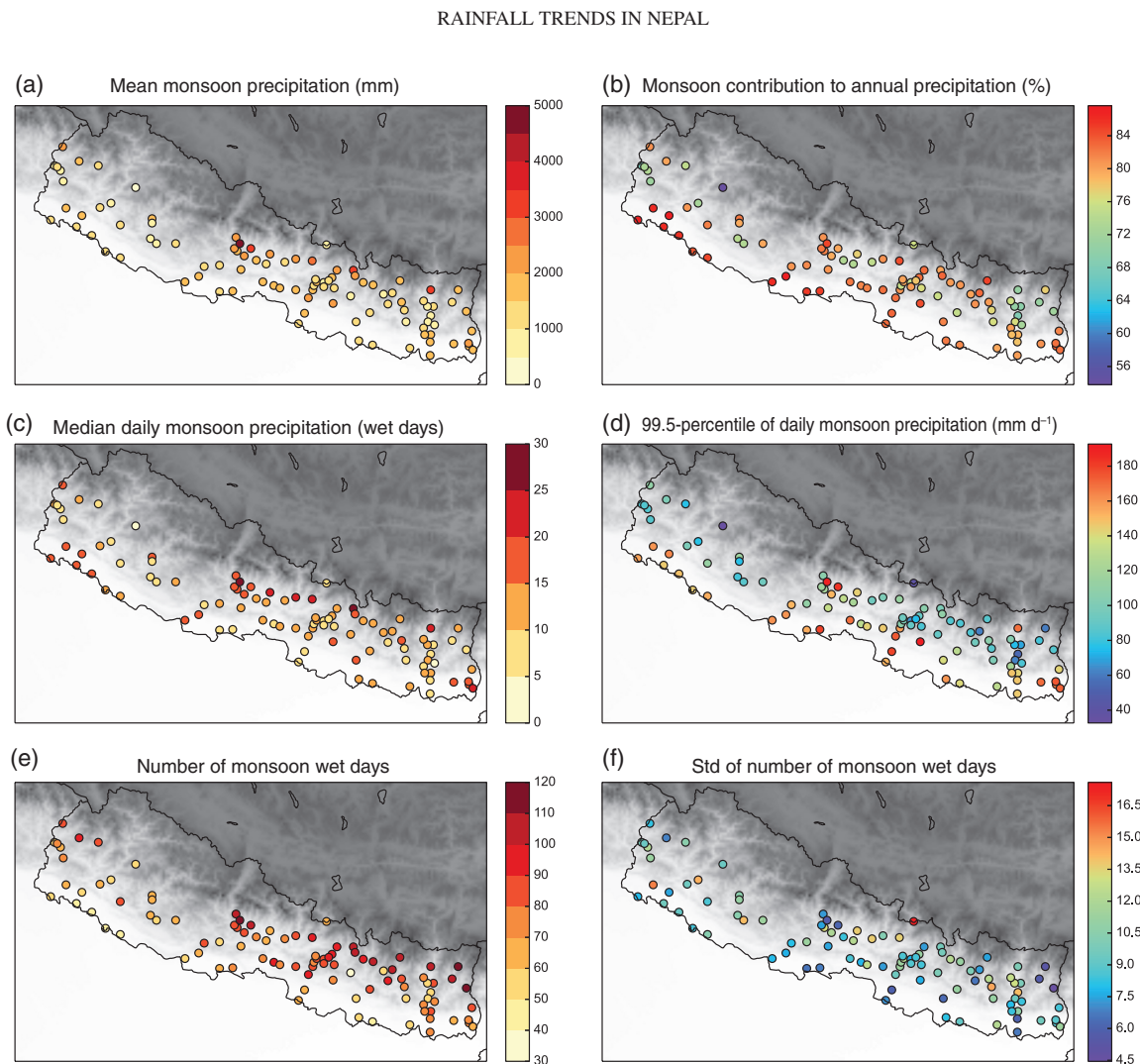


Figure 3. (a) Mean of monsoon precipitation for the months June to September (mm). (b) Ratio of monsoon precipitation to annual precipitation in (%). (c) Median of daily precipitation. (d) 99.5-percentile of daily precipitation. (e) Number of wet days (>0 mm) during monsoon season and (f) Standard deviation for the number of wet days. Topography is displayed in grey for orientation with darker colours indicating increasing elevation.

and East Nepal along the northern border, it rains almost every day on average, whereas at the southern border and Far-West and Mid-West Nepal there are stations that register rain on only half of the 122 monsoon days. The standard deviation of the number of wet days (Figure 3(f)) is probably highly influenced by local topography and spatially very variable.

3.2. Observed time series and trends

A shift in mean precipitation can affect extremes which is why we first explore possible changes in means of monsoon precipitation in Nepal. Precipitation records vary strongly in time and space. Variability ranges from strong fluctuations between single days to multi-year and multi-decadal oscillations. Trends of Indian summer monsoon precipitation and number of extreme events per station are challenging to calculate because data are heterogeneous and exhibits many data gaps. Different stations have the longest pseudo-continuous record in different time

periods. We use the word ‘pseudo-continuous’ because stations are used despite exhibiting data gaps as long as they fulfil the data availability and homogeneity criteria (Sections 2.1 and 2.2). Estimating OLSR trends for these different time slices makes the comparison and interpretation difficult. For this reason we choose only stations that have been measuring for the entire time period of 40 years and pass the homogeneity test. This results in a subset of 42 stations.

Figure 4(a) shows trends of the 42 remaining stations. Although the spatial coverage of stations in Nepal is sparse when using 42 stations, we still get an impression of the rainfall trends in various regions. The precipitation records show a high spatial variability with positive and negative trends. There are hardly any statistical significant trends (Figure 4(b)). The significance is estimated using the student *t*-test for the 0.05% significance level. The occurrence of a similar trend at several stations can indicate real changes in precipitation for a larger region. As

P. BOHLINGER AND A. SORTEBERG

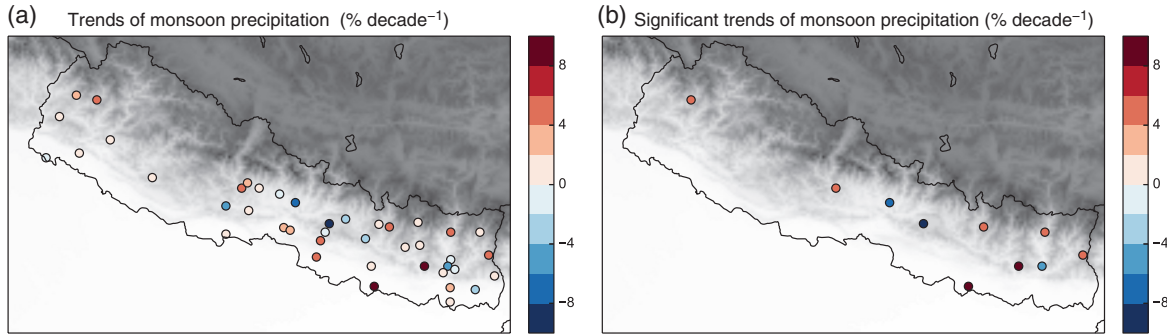


Figure 4. (a) Precipitation trends for 42 stations from 1971 to 2010. (b) Precipitation trends for only 10 stations which indicate a statistical significant trend on a 0.05% significance level obtained using a student *t*-test.

an example for this, around Kathmandu, several negative trends coincide indicating a decrease of monsoon precipitation in that area whereas trends close to the Pokhara region and in Far-West Nepal indicate an increase.

We merge the seasonal time series of all 98 stations to overcome data gaps and to obtain a precipitation trend that can be associated with Nepal. This is done by creating standard *z*-normal scores (*z*-scores) which make precipitation sums at different stations comparable. *z*-Scores are calculated for 40 years (1971–2010) using a reference period of 30 years to calculate a mean and a standard deviation for each station. The reference period consists of the 30 years where most stations fulfil the data availability criteria at the same time as explained in Section 2.1. *z*-Scores consist of precipitation anomalies, calculated from the difference between the seasonal value and the 30 years mean standardized by the standard deviation of the respective stations. Monsoon precipitation *z*-scores from different stations are merged, resulting in a time series for all of the 40 years (1971–2010).

The estimated trend for the combined time series is not significantly different from zero at a 95% confidence level using a student *t*-test. This means that there are no indications of a decline or increase in precipitation (Figure 5(a)). This is consistent with the high spatial variability of station-based trends and the existence of regions with a negative trend (around Kathmandu) and regions with positive trends like Far-West Nepal and close to Pokhara.

We explore the trends in the number of extremes (multiple upper percentiles) and count all extremes registered by stations from 1971 to 2010. The number of extreme events is normalized by the number of active stations at the time of the event. Normalization is necessary since the number of active stations varies substantially between 1971 and 2010 and thereby also the potential of measuring an extreme which would bias the result. Figure 5(b) shows time series of the amount of recorded extreme events with extreme defined as values higher than the displayed percentiles. We show results for the three percentiles 99.9, 99.5 and 99. The similarity between the time series of number of extremes and the combined precipitation time series increases as the percentiles decrease. We do not find a statistically significant trend. This suggests that occurrences of extremes have

neither increased nor decreased. This conclusion is consistent with findings from Shrestha *et al.* (2000).

3.3. Variability in the observed time series

The merged time series show strong inter-annual variability. In particular ENSO has been associated with variability in rainfall over India, Bangladesh and other places around the Indian subcontinent by changing large scale circulation patterns in the south Asian region (Pant and Parthasarathy, 1981; Rasmusson and Carpenter, 1983; Parthasarathy *et al.*, 1988; Kripalani and Kulkarni, 1997; Lau and Wu, 2001; Ashok *et al.*, 2001). The El Niño phase is usually associated with less precipitation whereas the La Niña phase coincides with heavy precipitation and floods. However, this correlation seems to be subject to temporal variability as described by Kumar *et al.* (1999) indicating the complexity of this relationship. Using the Niño 3.4 region bounded by 120°W–170°W and 5°S–5°N (Trenberth, 1997), Chowdhury (2003) investigated seasonal flooding in Bangladesh and shows that for strong El Niño events this relationship is valid, whereas an increase of precipitation is also observed during moderate El Niño years underlining the spatial differences in the impact of ENSO.

In this study, we investigate the relationship between ENSO and precipitation amounts and the number of extremes in Nepal. We use the cold and warm ENSO periods calculated by the NOAA Center for Weather and Climate Prediction (Climate Prediction Center Internet Team, 2016) over the Niño 3.4 region using the extended reconstructed sea surface temperature version 4 (ERSST. v4) (Huang *et al.*, 2015). We find a significant correlation ($r \approx -0.6$) between our combined seasonal time series and the ENSO signal (mean June to August, 3.4 region) (Figure 6(a)). This is consistent with other findings (e.g. Shrestha, 2000; Shrestha *et al.*, 2000) that related ENSO to the rainfall in Nepal using for instance the Southern Oscillation Index (SOI) which is derived from the mean sea level pressure difference measured in Tahiti and Darwin. Shrestha (2000) found a similar correlation of $r \approx 0.58$ between percentage departure of Nepal monsoon rainfall (PNMR) and Monsoon Southern Oscillation Index

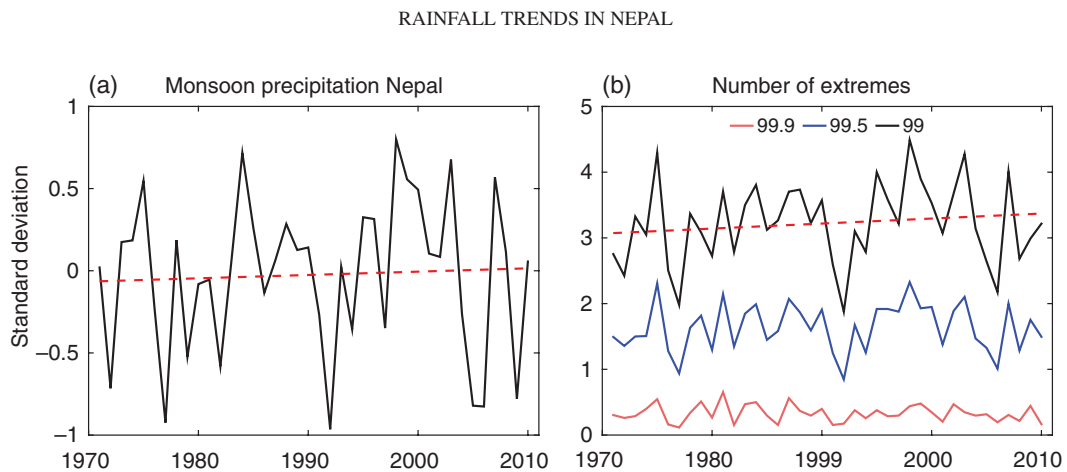


Figure 5. (a) Time series of monsoon z -scores merged from 98 stations. (b) Time series of number of extreme precipitation events (values above the respective percentiles: 99.9, 99.5, 99) normalized by number of active stations. The red dashed lines are linear regression lines.

(MSOI). For the monsoon months June to September a correlation between all-Nepal monsoon precipitation and SOI of $r \approx 0.43$ to $r \approx 0.63$ depending on the time period was found by Shrestha *et al.* (2000).

However, the correlation between ENSO and the number of extreme events per season requires a closer look (Figure 6(b)). As the percentile increases the correlation vanishes whereas for events lower than 99th percentile, the correlation starts to resemble the cross-correlation function of ENSO and the combined precipitation time series (Figure 6(a)). This shows that there is in fact a connection between ENSO and moderate extremes (here: lower than 99th percentile) but no linear correlation for percentiles even further out in the tail of the distribution.

3.4. Trends for extreme events

In this chapter, we use two different methods to assess changes of extremes. Comparing results from different methods gives a notion of sensitivity of observed trends to the method which goes beyond the obtained standard errors of a single method. We extend existing work using quantile regression to investigate and illustrate changes across a variety of high percentiles of daily precipitation. Finally, we use extreme value theory with the block maximum approach to make inference for very rare extreme events (100 year event) where the ETCCDI descriptive climate indices are not considered reliable anymore.

3.4.1. Investigating the evolution of quantiles over time using quantile regression

Temporal trends in extreme precipitation amounts are investigated by exploring changes of high quantiles of daily precipitation over the 40 year period from 1971 to 2010. This will answer questions like, does the value of the 99.5th percentile shift over time towards stronger or weaker extremes? Are the trends similar across multiple quantiles?

Considering station based trends of quantiles, spatial variability is strong (Figure 7). It is noteworthy that only negative trends are statistically significant. In a total Nepal

perspective there is no uniform increase or decrease of percentile values although some regions have several stations with similar trends indicating the presence of increasing or decreasing values for a given percentile in a larger area. The percentage of stations with positive and negative trends is summarized in Table 2. For example stations around Pokhara depict an increase of higher percentile values. A second region showing an increase of high percentile precipitation values is in most Far-West Nepal. Around Kathmandu a group of stations show negative trends. This pattern of regions of prevailing trends is consistent with the pattern in seasonal precipitation trends discussed in Section 3.2.

A tendency of stronger trends in the higher percentiles becomes visible when comparing trends of the 99.9, 99.5, 99, 95, 75 and 50th percentile. The median seems to be quasi constant for almost all stations which is consistent with a trend not significantly different from zero for the combined seasonal precipitation time series of all stations (Figure 5). Some stations even have a shift in sign for different percentiles. The result of the quantile regression reveals that the increase and decrease in seasonal precipitation (Figure 4) is not due to changes in the bulk of the distribution but rather caused by changes in the upper tail. Furthermore, this shows that the dispersion of precipitation amounts increases and decreases with time and that the conditional distribution of daily precipitation is positively skewed with a long upper tail.

Figure 8 illustrates the behaviour of a time-dependent increase and decrease of higher percentiles as described above for stations 512 and 1111. Both stations show different trends in their quantiles. For station 512, trend curves of different quantiles converge with increasing time. Quantiles at station 1111 are diverging over time, resulting in a positive trend in seasonal precipitation which is visible in Figure 4. The fact that the pattern for the trends in the higher quantiles is similar to the trends in seasonal precipitation for July to September indicates that seasonal precipitation trends are strongly influenced by trends in higher quantiles.

P. BOHLINGER AND A. SORTEBERG

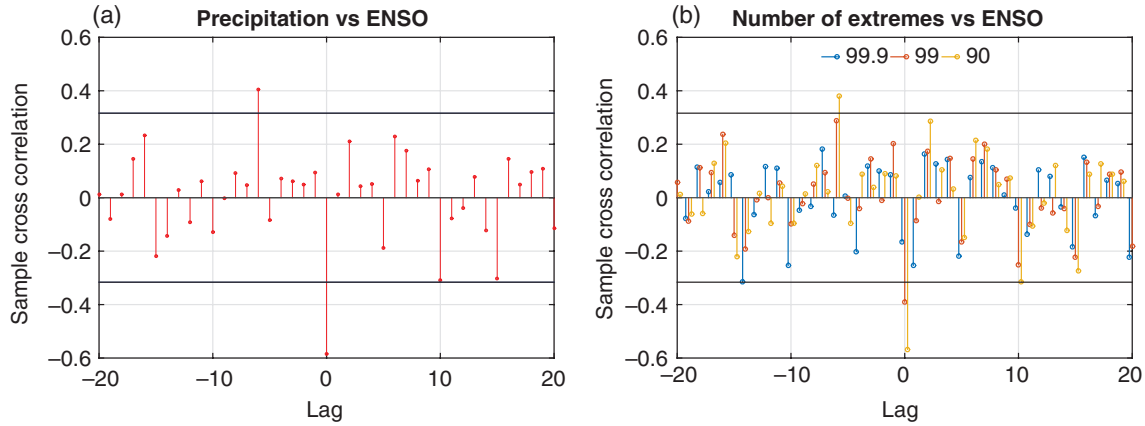


Figure 6. (a) Cross-correlation between the combined precipitation time series and the June to August mean of the ENSO signal from region 3.4. (b) Cross-correlation between ENSO and the number of extremes of upper tail percentiles. The black thin lines denote the 0.05 significance level.

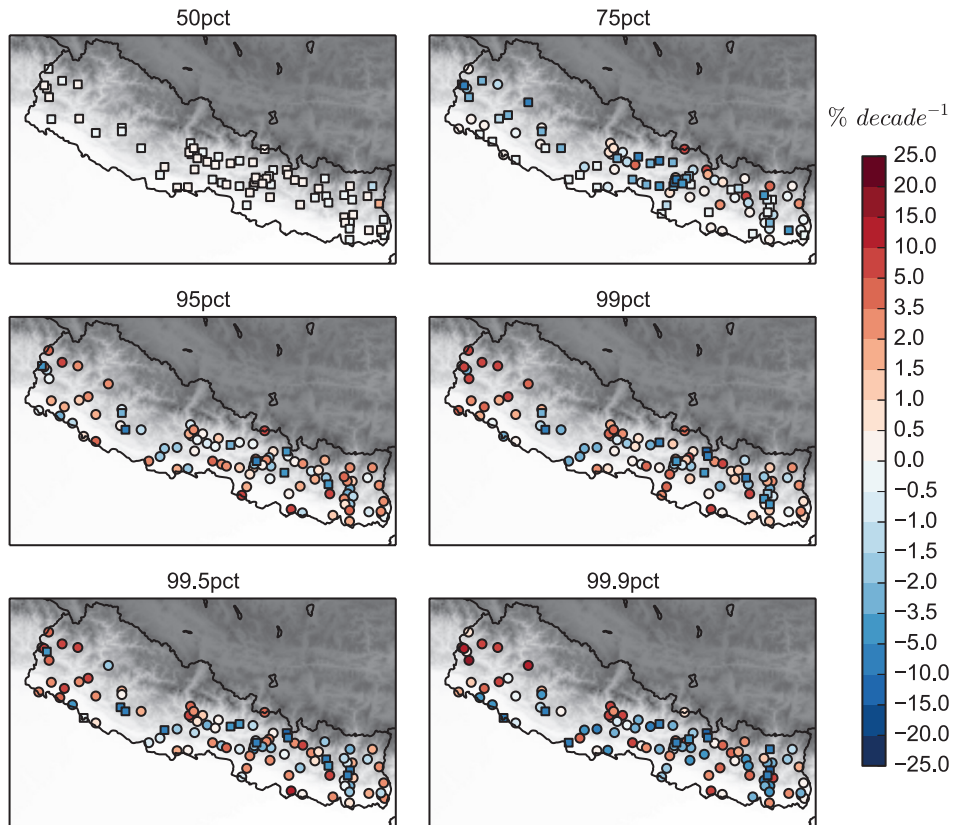


Figure 7. Trends from quantile regression for different stations based on quantiles obtained from daily precipitation. Stations that do not indicate a trend significantly different from zero at the 95% confidence level are marked using a circle, significant stations with a square. Confidence intervals are obtained using bootstrapping with 500 times of re-sampling. Results are little sensitive to the number of bootstrap samples. For trends in the median fewer stations are plotted because some have a median of zero which leads to division by zero when calculating the percental change. Their respective absolute trends are zero (of the order $|10^{-8}| \text{ mm decade}^{-1}$ or smaller) and therefore neglected.

3.4.2. Modelling trends of extremes using extreme value theory

We extend the previous analysis using a block maximum approach to detect return level changes and their spatial distribution over Nepal for 100 year events. For the block

maximum approach we use annual and monsoon maxima taken from our set of daily precipitation values. Results are obtained using Bayesian and maximum likelihood parameter estimation for the location, scale and shape parameters of the GEV distribution. Due to strong similarities between

RAINFALL TRENDS IN NEPAL

Table 2. The number and percentage (in parenthesis) of stations with positive and negative trends for different quantiles.

	99.9	99.5	99	95	75	50
Pos	52 (46%)	62 (55%)	67 (60%)	64 (57%)	36 (32%)	61 (54%)
Neg	60 (54%)	50 (45%)	45 (40%)	48 (43%)	76 (68%)	51 (46%)

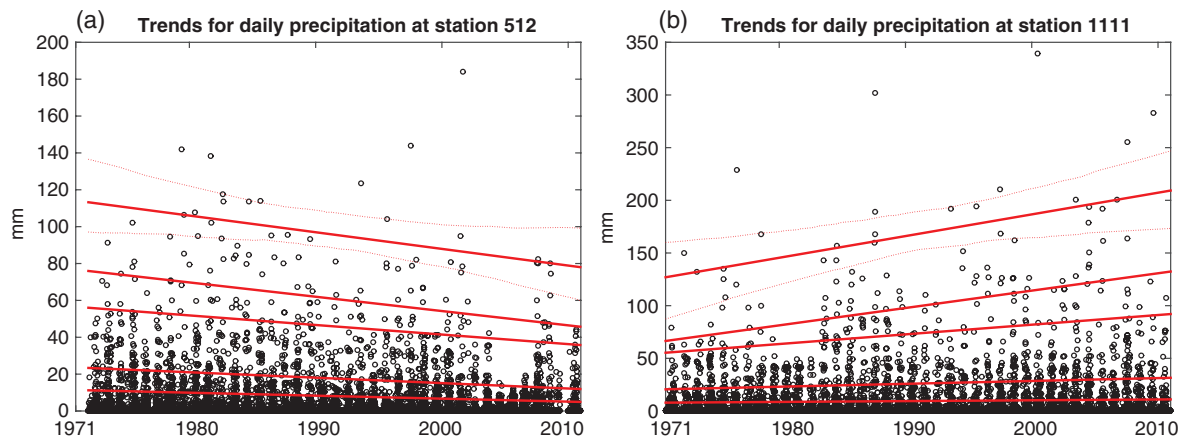


Figure 8. Daily precipitation (mm) are displayed as black circles. Trend curves (in red) for the percentiles 99.9, 99.5, 99, 95 and 90 depicting the respective trends. The line for the highest percentile is highest and so on. Dotted lines show the 95% confidence interval for the 99.9th percentile obtained using the bootstrap method with 500 times of re-sampling.

Bayesian and maximum likelihood estimated parameters we only use the results from the Bayesian estimation for illustrating consequences of using time as a covariate for the location parameter.

The systematic change over time which we described in the previous sections can also be seen by eye for the block maximum time series of the same stations 512 and 1111 (Figure 9). For both stations, the annual maximum daily precipitation depicts a change over time. At station 512 the annual maxima decrease and at station 1111 the extremes seem to increase over time, thus matches our assumption of an underlying linear trend in the location parameter. Starting from the year 1971 at station 512 a former 12-year event is now a 100-year event meaning that the probability of occurrence of such a high value has decreased. At station 1111 a 580-year event has become a 100-year event suggesting a higher probability of occurrence. The results from the block maximum approach are consistent with the trends in the high percentiles using quantile regression.

After illustrating our approach we fit a GEV distribution (Equation (A1)) to each station to assess the spatial distribution of trends in annual maxima. Since we are dealing with 98 stations we proceed with the same simple covariate for each station. We allow for a linear change in the location parameter at each station for the temporal evolution. The scale parameter is held constant as well as the shape parameter, which is notoriously difficult to estimate and comes along with large uncertainties. A linear change over time was chosen since many station-specific time series exhibit a somewhat linear trend, whereas for the variance we did not discover such systematic changes. Ideally a more physical covariate could be chosen. However,

this would require knowledge about the underlying mechanisms for the change which are not yet established. ENSO as a more physical covariate does not significantly improve the fit.

Figure 10 illustrates the change of the 100 year return level in 1971 compared to the same return levels in 2010. Data from each station have been fitted separately with the approach described above. The respective change of the 100 year return level in percent was calculated using Equation (1) in Section 2.3. For the maximum likelihood estimated models we performed a likelihood-ratio test to determine whether the trend contributes to improve the model. The null hypothesis is that the model without a linear trend in the location parameter is the same as the model including the trend. Rejecting this hypothesis therefore means that the models are significantly different from each other and the trend improves the model. Additionally, we compare the magnitude of the trend estimates and the respective standard errors. For the Bayesian estimation we decide on using the 95% credible intervals that come along with the MCMC sampling of the trend parameter. Since for the maximum likelihood estimation (MLE) the standard error approach and the likelihood-ratio test result in the same significant stations, except one, we just display the likelihood ratio test results with respect to 95% confidence interval. Bayesian and MLE estimations agree on the same significant stations, except one. This adds confidence to the robustness of the results which is supported by the fact that when considering only monsoon maxima instead of annual maxima the significant stations are the same.

In both estimation methods, the distribution parameters are very similar resulting in return values that are

P. BOHLINGER AND A. SORTEBERG

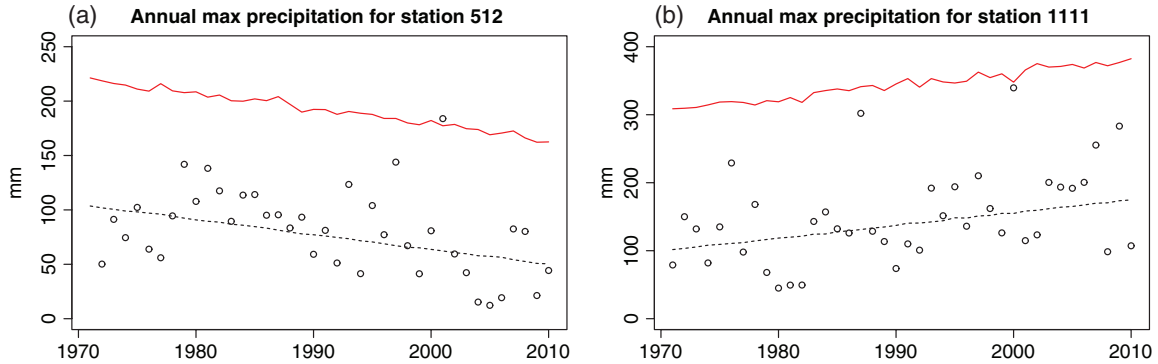


Figure 9. Annual maxima of daily precipitation (mm) are displayed as black circles. The black dashed line indicates the time dependent median and the red line the time dependent 100 year return level. Parameter estimates in this figure are obtained using Bayesian estimation.

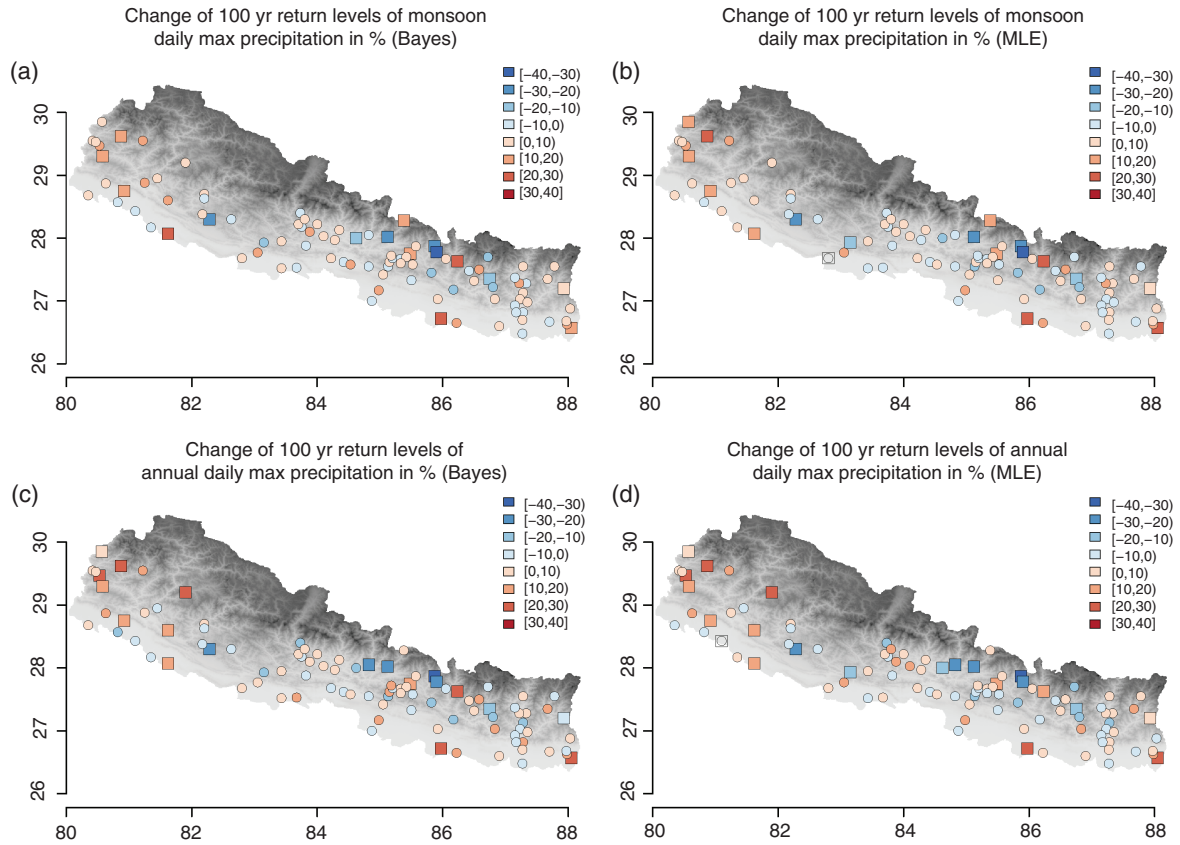


Figure 10. Change of the 100 year return level from 1971 to 2010 in % imposing a linear trend on the location parameter of the GEV-distribution at each site separately. (a) and (b) consider block maxima during the monsoon period using Bayesian and MLE estimation, respectively. Same for (c) and (d) but for annual block maxima. Squares depict stations with significant changes considering a 95% credible/confidence interval. For maximum likelihood figures there is one station indicated by a transparent circle and square for which the parameters could not be estimated and the change is set to NaN. Topography is displayed in grey shading for orientation purposes with darker grey indicating higher elevation.

much the same which in turn is reflected in the change of the return values over time. Comparing these methods reflects the sensitivity of the results to the use of different methods. The spatial pattern is consistent with the pattern obtained from quantile regression. Computed changes are substantial and typically range from -30% to $+30\%$ increase of the 100 year return level. Roughly

55% (Bayes: 53%, MLE: 56%) of the stations indicate a positive trend whereas 45% (Bayes: 47%, MLE: 44%) show a decline of annual maxima. Considering monsoon maxima instead of annual maxima, both methods agree on a ratio of ca. 61% (Bayes: 60%, MLE: 61%) of the stations indicating a positive trend. This is comparable with ratios obtained from quantile regression. The trend

RAINFALL TRENDS IN NEPAL

pattern shows an inhomogeneous trend distribution over Nepal where only smaller regions agree on the sign of a trend. For instance between Pokhara and Kathmandu there is an area with significant negative trends which is also visible in the results from quantile regression. The negative trend in the higher quantiles around Kathmandu is much less univocal in the block maxima. In Far-West Nepal there are almost exclusively positive trends. Another important finding is the robustness and significance of the positive trend in Far-West Nepal. A homogeneous region in terms of positive trends where some show statistical significance leads to strong indications for a systematic change towards higher extremes in western Nepal. Our results differ partly from the monsoon mean trends in N09 which underlines the importance of considering extremes in an own framework.

The trends do not seem to depend on the geographical parameters elevation, latitude and longitude. Using the parameters from the marginal distributions, we checked dependencies on geographical or physical parameters. Scatter plots reveal dependencies for the location offset and the scale parameter on latitude and elevation for both the MLE and Bayesian estimation (not shown here). Unfortunately, the observed dependencies are not enough to obtain a reliable fit of a spatial GEV using the mentioned covariates and creating a map of return values. The spatial model over- and underestimates return values compared to the marginal distributions at the station sites (not shown here). We conclude that a well-working spatial GEV-model probably has to be more complex, with spatially variable dependencies on physical variables.

4. Summary and conclusions

In this study, we investigated previously not considered elements of monsoon precipitation and extremes in Nepal on basis of rain gauge stations. We used quantile regression and extreme value theory to obtain a comprehensive view on trends in extreme precipitation.

Most events in the tail of the daily rainfall distribution occur during the Indian summer monsoon between the months June and September. The highest monsoon precipitation amounts were measured in the station cluster close to Pokhara in the north-west (Lumle), north-east of Kathmandu (Gumthang) and north in East Nepal (Num). Most of the monsoon contribution to annual rainfall is recorded close to the Indian border, around Pokhara, Kathmandu and north-east of Kathmandu. The highest absolute upper tail daily precipitation values can be found along the Indian border, close to Pokhara, and north in East Nepal.

Monsoon precipitation trends are heterogeneous across the country where a combined time series of 98 stations does not exhibit a significant trend. Seasonal monsoon precipitation is anti-correlated with ENSO ($r \approx -0.6$). The number of extremes throughout a variety of higher quantiles do not depict a significant trend. There is linear dependency between ENSO and the number of moderate

extremes (lower than 99th percentile). Percentiles above are not correlated with ENSO.

Quantile regression reveals a spread in the trends of different upper quantiles which can be responsible for trends in the seasonal precipitation time series at the same stations. This means that the upper tail undergoes a change rather than the bulk of the distribution. This in turn reflects in the characteristics of the distribution of daily rainfall. By computing sums or means of strongly skewed distributions, a trend in seasonal monsoon precipitation can occur.

Results using a block maximum approach from extreme value theory show a pattern similar to the one obtained by quantile regression. Especially Far-West Nepal depicts homogeneously positive trends throughout a variety of higher quantiles and block maxima where some show statistical significance at the 5% significance level. This concludes with robust evidence for a systematic change towards higher extremes in Far-West Nepal. It is important to note that trends in the annual and monsoon daily maxima differ in parts from the respective mean trends in the N09 report. This underpins the importance of considering extremes in an own framework and under non-stationarity which, due to the observed magnitude (change from -30% to $+30\%$), should also be included in a spatial model.

Acknowledgements

This work has been funded by the University of Bergen, Norway. The authors thank the Department of Hydrology and Meteorology (DHM) for sharing the rain gauge dataset. We thank Eric Gilleland and Richard Katz for a great introduction to extreme value theory, answering questions and for help with the respective R packages. We would also like to thank organizers and lecturers of the very informative summer school on ‘Extreme Value Modeling and Water Resources’ 2016 in Lyon and the time they took for individual discussions. Finally, we thank the anonymous reviewers for improving the manuscript.

Appendix

Extreme value theory in a non-stationary case

Coles (2001) and Katz *et al.* (2002) describe applications of extreme value theory in a hydrometeorological framework in a very approachable manner. This forms the basis of our approach where we estimated the distribution parameters with the software R. The Bayesian and MLEs were conducted with the support of the freely available R-packages *evd* and *extRemes* (Stephenson, 2002; Gilleland and Katz, 2011) where the latter was recommended by the ETCCDI report.

Block maxima values like annual or seasonal maxima follow the GEV distribution which is defined by the three parameters for location (μ), scale (σ) and shape (ξ). Given a set of values these parameters can be estimated for instance by maximum likelihood or Bayesian approaches which are both used in this study. In this study we use time as a covariate imposing a linear trend on the location

parameter to capture the visible changes of block maxima for the observation period. The GEV including a time dependent location parameter looks as follows:

$$GEV(x, \mu(t), \sigma, \xi) = e^{-1\left[1+\xi\left(\frac{x-\mu(t)}{\sigma}\right)\right]^{-\frac{1}{\xi}}} \quad (A1)$$

As priors for Bayesian estimation we used uniform distributions for the location offset and trend as well as for the scale and shape parameter. Additionally, the scale parameter is not allowed to become negative since that would make no physical sense. The posterior is obtained through sampling with a Markov chain Monte Carlo (MCMC) method where for the MCMC method the Metropolis–Hastings (MH) algorithm is used. Since station specific distributions can be very different the MH algorithm is initialized with the sample mean for the location parameter and the sample standard deviation for the scale parameter. The trend on the location parameter and the starting point for the shape parameter are both initialized with zero. For convergence we sample 90 000 times and use a burn-in period of 30 000 values. From the remaining values we skim every 10th value which is the basis for our final posterior distribution.

Supporting information

The following supporting information is available as part of the online article:

Table S1. Metadata of 98 rain gauge stations in Nepal including the 90th, 99th and 99.9th percentile of daily precipitation.

References

- Alexandersson H. 1986. A homogeneity test applied to precipitation data. *J. Climatol.* **6**(6): 661–675. <https://doi.org/10.1002/joc.3370060607>.
- Ashok K, Guan Z, Yamagata T. 2001. Impact of the Indian Ocean dipole on the relationship between the Indian monsoon rainfall and ENSO. *Geophys. Res. Lett.* **28**(23): 4499–4502. <https://doi.org/10.1029/2001GL013294>.
- Baidya S, Shrestha M, Sheikh M. 2008. Trends in daily climatic extremes of temperature and precipitation in Nepal. *J. Hydrol. Meteorol.* **5**(1): 38–51.
- Bookhagen B. 2010. Appearance of extreme monsoonal rainfall events and their impact on erosion in the Himalaya. *Geomat. Nat. Hazard. Risk Geomatics* **1**(1): 37–50. <https://doi.org/10.1080/19475701003625737>.
- Caesar J, Alexander L, Trewin B, Tse-ring K, Sorany L, Vuniyayawa V, Keosavang N, Shimana A, Htay M, Karmacharya J, Jayasinghearchachi DA, Sakkamart J, Soares E, Hung LT, Thuong LT, Hue CT, Dung NTT, Hung PV, Cuong HD, Cuong NM, Sirabaha S. 2011. Changes in temperature and precipitation extremes over the Indo-Pacific region from 1971 to 2005. *Int. J. Climatol.* **31**(6): 791–801. <https://doi.org/10.1002/joc.2118>.
- Chalise S, Khanal N. 2001. *An Introduction to Climate, Hydrology and Landslide Hazards in the Hindu Kush-Himalayan Region. Landslide Hazard Mitigation in the Hindu Kush-Himalayas*. ICIMOD: Kathmandu.
- Chalise S, Khanal N. 2002. Recent extreme weather events in the Nepal Himalayas. *The Extremes of the Extremes: Extraordinary Floods 271, 141–146*, IHAS Publ. no. 271.
- Chowdhury M. 2003. The El Niño–Southern Oscillation (ENSO) and seasonal flooding–Bangladesh. *Theor. Appl. Climatol.* **76**(1–2): 105–124. <https://doi.org/10.1007/s00704-003-0001-z>.
- Climate Prediction Center Internet Team. 2016. Cold and warm ENSO episodes for the Niño 3.4 region from the NOAA Center for Weather and Climate Prediction, Climate Prediction Center. http://www.cpc.ncep.noaa.gov/products/analysis_monitoring/ensostuff/ensoyears.shtml (accessed 22 February 2016).
- Coles S. 2001. *An Introduction to Statistical Modeling of Extreme Values*. Springer: London.
- Dhar O, Nandargi S. 2000. An appraisal of precipitation distribution around the Everest and Kanchenjunga peaks in the Himalayas. *Weather* **55**(7): 223–234. <https://doi.org/10.1002/j.1477-8696.2000.tb04065.x>.
- Fan L, Chen D. 2016. Trends in extreme precipitation indices across China detected using quantile regression. *Atmos. Sci. Lett.* **17**(7): 400–406. <https://doi.org/10.1002/asl.671>.
- Field C, Barros V, Stocker T, Qin D, Dokken D, Ebi K, Mastrandrea M, Mach K, Plattner G-K, Allen S, Tignor M, Midgley P (eds). 2012. *IPCC, 2012: Managing the Risks of Extreme Events and Disasters to Advance Climate Change Adaptation: Special Report of Working Groups I and II of the Intergovernmental Panel on Climate Change*. Cambridge University Press: Cambridge, UK and New York.
- Gilleland E, Katz RW. 2011. New software to analyze how extremes change over time. *Eos* **92**(2): 13–14.
- Huang B, Banzon VF, Freeman E, Lawrimore J, Liu W, Peterson TC, Smith TM, Thorne PW, Woodruff SD, Zhang H-M. 2015. Extended Reconstructed Sea Surface Temperature Version 4 (ERSST. v4). Part I: upgrades and Intercomparisons. *J. Clim.* **28**(3): 911–930. <https://doi.org/10.1175/JCLI-D-14-00006.1>.
- Ichiyaniagi K, Yamanaka MD, Muraji Y, Vaidya BK. 2007. Precipitation in Nepal between 1987 and 1996. *Int. J. Climatol.* **27**(13): 1753–1762. <https://doi.org/10.1002/joc.1492>.
- Katz RW, Parlange MB, Naveau P. 2002. Statistics of extremes in hydrology. *Adv. Water Resour.* **25**(8–12): 1287–1304. [https://doi.org/10.1016/S0309-0200\(02\)00056-8](https://doi.org/10.1016/S0309-0200(02)00056-8).
- Koenker R, Hallock K. 2001. Quantile regression: an introduction. *J. Econ. Perspect.* **15**(4): 43–56.
- Kripalani R, Kulkarni A. 1997. Rainfall variability over south-east Asia–connections with Indian monsoon and ENSO extremes: new perspectives. *Int. J. Climatol.* **17**(11): 1155–1168.
- Kumar KK, Rajagopalan B, Cane MA. 1999. On the weakening relationship between the Indian monsoon and ENSO. *Science* **284**(5423): 2156–2159. <https://doi.org/10.1126/science.284.5423.2156>.
- Lau K, Wu H. 2001. Principal modes of rainfall-SST variability of the Asian summer monsoon: a reassessment of the monsoon-ENSO relationship. *J. Climate* **14**(13): 2880–2895. [https://doi.org/10.1175/1520-0442\(2001\)014;2880:PMORSV;2.0.CO;2](https://doi.org/10.1175/1520-0442(2001)014;2880:PMORSV;2.0.CO;2).
- Marahatta S, Dangol BS, Gurung GB. 2009. Temporal and Spatial Variability of Climate Change over Nepal (1976–2005). Tech. Rep., Practical Action Nepal Office. https://practicalaction.org/file/region_nepal/ClimateChange1976-2005.pdf
- Nandargi S, Dhar O. 2011. Extreme rainfall events over the Himalayas between 1871 and 2007. *Hydrolog. Sci. J.* **56**(6): 930–945. <https://doi.org/10.1080/02626667.2011.595373>.
- Pant G, Parthasarathy SB. 1981. Some aspects of an association between the southern oscillation and Indian summer monsoon. *Arch. Meteorol. Geophys. Bioclimatol. B* **29**(3): 245–252. <https://doi.org/10.1007/BF02263246>.
- Parthasarathy B, Diaz H, Eischeid J. 1988. Prediction of all-India summer monsoon rainfall with regional and large-scale parameters. *J. Geophys. Res. Atmos.* **93**(D5): 5341–5350. <https://doi.org/10.1029/JD093iD05p05341>.
- Rasmusson EM, Carpenter TH. 1983. The relationship between eastern equatorial Pacific sea surface temperatures and rainfall over India and Sri Lanka. *Mon. Weather Rev.* **111**(3): 517–528. [https://doi.org/10.1175/1520-0493\(1983\)111;0517:TRBEEP;2.0.CO;2](https://doi.org/10.1175/1520-0493(1983)111;0517:TRBEEP;2.0.CO;2).
- Shrestha M. 2000. Interannual variation of summer monsoon rainfall over Nepal and its relation to Southern Oscillation Index. *Meteorol. Atmos. Phys.* **75**(1–2): 21–28. <https://doi.org/10.1007/s007030070012>.
- Shrestha KL. 2005. Global change impact assessment for Himalayan mountain regions for environmental management and sustainable development. *Global. Environ. Res.* **9**(1): 69–81.
- Shrestha AB, Wake CP, Mayewski PA, Dibb JE. 1999. Maximum temperature trends in the Himalaya and its vicinity: an analysis based on temperature records from nepal for the period 1971–94. *J. Clim.* **12**(9): 2775–2786. [https://doi.org/10.1175/1520-0442\(1999\)012;2775:MTTITH;2.0.CO;2](https://doi.org/10.1175/1520-0442(1999)012;2775:MTTITH;2.0.CO;2).
- Shrestha AB, Wake CP, Dibb JE, Mayewski PA. 2000. Precipitation fluctuations in the Nepal Himalaya and its vicinity and relationship

RAINFALL TRENDS IN NEPAL

- with some large scale climatological parameters. *Int. J. Climatol.* **20**(3): 317–327.
- Shrestha AB, Bajracharya SR, Sharma AR, Duo C, Kulkarni A. 2017. Observed trends and changes in daily temperature and precipitation extremes over the Koshi river basin 1975–2010. *Int. J. Climatol.* **37**: 1066–1083. <https://doi.org/10.1002/joc.4761>.
- Sigdel M, Ikeda M. 2013. Summer monsoon rainfall over Nepal related with large-scale atmospheric circulations. *J. Earth Sci. Clim. Change* **3**: 2012. <https://doi.org/10.4172/2157-7617.1000112>.
- Stephenson AG. June 2002. Evd: extreme value distributions. *R News* **2**(2). <http://CRAN.R-project.org/doc/Rnews/>
- Stocker T, Qin D, Plattner G, Tignor M, Allen S, Boschung J, Nauels A, Xia Y, Bex B, Midgley B. 2013. IPCC, 2013: Climate Change 2013: The Physical Science Basis. Contribution of Working Group I to the Fifth Assessment Report of the Intergovernmental Panel on Climate Change.
- Talchabhadel R, Karki R, Parajuli B. 2016. Intercomparison of precipitation measured between automatic and manual precipitation gauge in Nepal. *Measurement*. **106**: 264–273. <https://doi.org/10.1016/j.measurement.2016.06.047>.
- Tank AMGK, Peterson TC, Quadir DA, Dorji S, Zou X, Tang H, Santhosh K, Joshi UR, Jaswal AK, Kolli RK, Sikder AB, Deshpande NR, Revadekar JV, Yeleuova K, Vandashva S, Faleyeva M, Gomboludev P, Budhathoki KP, Hussain A, Afzaal M, Chandrapala L, Anvar H, Amanmurad D, Asanova VS, Jones PD, New MG, Spektorman T. 2006. Changes in daily temperature and precipitation extremes in central and South Asia. *J. Geophys. Res. Atmos. (1984–2012)* **111**: D16. <https://doi.org/10.1029/2005JD006316>.
- Trenberth KE. 1997. The definition of El Niño. *Bull. Am. Meteorol. Soc.* **78**(12): 2771.
- Wang XL. 2008a. Accounting for autocorrelation in detecting mean shifts in climate data series using the penalized maximal t or f test. *J. Appl. Meteorol. Climatol.* **47**(9): 2423–2444. <https://doi.org/10.1175/2008JAMC1741.1>.
- Wang XL. 2008b. Penalized maximal F test for detecting undocumented mean shift without trend change. *J. Atmos. Oceanic Technol.* **25**(3): 368–384. <https://doi.org/10.1175/2007JTECHA982.1>.
- Wang S-Y, Gillies RR. 2013. Influence of the Pacific quasi-decadal oscillation on the monsoon precipitation in Nepal. *Clim. Dyn.* **40**(1–2): 95–107. <https://doi.org/10.1007/s00382-012-1376-2>.

Paper II

7.3 Synoptic conditions and moisture sources actuating extreme precipitation in Nepal

Patrik Bohlinger, Asgeir Sorteberg, and Harald Sodemann

Journal of Geophysical Research: Atmospheres (accepted November 2017), doi: 10.1002/2017JD027543

Synoptic conditions and moisture sources actuating extreme precipitation in Nepal

Patrik Bohlinger^{1,2}, Asgeir Sorteberg^{1,2}, and Harald Sodemann^{1,2}

Patrik Bohlinger, patrik.bohlinger@uib.no

¹Geophysical Institute, University of

Bergen, Bergen, Norway

²Bjerknes Centre for Climate Research,

University of Bergen, Bergen, Norway

This article has been accepted for publication and undergone full peer review but has not been through the copyediting, typesetting, pagination and proofreading process, which may lead to differences between this version and the Version of Record. Please cite this article as doi: 10.1002/2017JD027543

Abstract. Despite the vast literature on heavy precipitation events in South Asia, synoptic conditions and moisture sources related to extreme precipitation in Nepal have not been addressed systematically. We investigate two types of synoptic conditions —low pressure systems and mid-level troughs—and moisture sources related to extreme precipitation events. To account for the high spatial variability in rainfall, we cluster station based daily precipitation measurements resulting in three well separated geographic regions: West, Central, and East Nepal. For each region, composite analysis of extreme events shows that atmospheric circulation is directed against the Himalayas during an extreme event. The direction of the flow is regulated by mid-tropospheric troughs and low pressure systems traveling toward the respective region. Extreme precipitation events feature anomalous high abundance of total column moisture. Quantitative Lagrangian moisture source diagnostic reveals that the largest direct contribution stems from land (ca. 75%), where in particular over the Indo-Gangetic Plain moisture uptake was increased. Precipitation events occurring in this region before the extreme event likely provided additional moisture.

Keypoints:

- Nepal can be divided into three regions of similar daily precipitation characteristics
- We identify synoptic conditions related to extreme precipitation in Nepal and pinpoint regions of additional moisture sources contributing to extreme events

- A conceptual sketch of the involved processes concludes our findings

Accepted Article

1. Introduction

Recent studies found considerable changes in extreme precipitation in Nepal over the last 40 years [Baidya *et al.*, 2008; Caesar *et al.*, 2011; Shrestha *et al.*, 2016]. Bohlinger and Sorteberg [2017] pointed to a statistically robust trend of increasing rainfall extremes in West Nepal, stressing the need to better understand the involved processes. However, despite vast literature on heavy precipitation events in South Asia, the role of synoptic conditions and moisture sources for extreme precipitation events in Nepal has not been addressed systematically. As described by Trenberth *et al.* [2003], three overarching constituents are crucial for generating precipitation. Ascending air tied to dynamics on different scales (from planetary scale to synoptic scale and mesoscale), microphysics which determine the condensation process, and the presence of moisture. We assess the role of synoptic conditions and moisture sources, and how they effect extreme precipitation in Nepal.

The spatial precipitation distribution in Nepal exhibits high spatial and temporal variability and is therefore of high socio-economic interest due to agriculture, natural hazards, and the use of hydro power. Precipitation in Nepal is heavily influenced by the Indian summer monsoon [Bohlinger and Sorteberg, 2017]. Based on meteorological stations, early studies estimated the average monsoon precipitation to approximately 80% of the annual precipitation across most of Nepal [Nayava, 1980]. In the far western part, the proportion reached only about 60%. Nepal exhibits a spatial pattern of rainfall climatologies according to its physiographic regions and main river systems [Kansakar *et al.*, 2004]. A

correlation between elevation and precipitation was found in West Nepal, whereas the middle and east show no clear dependency [Ichiyanagi *et al.*, 2007]. However, the rainfall distribution in Nepal is more complex and exhibits large differences on small scales, e.g. a difference by a factor of 8 in precipitation amounts was observed in the Marsyandi river basin in Nepal (factor of 4 on a scale of 10 km) [Lang and Barros, 2002; Barros and Lang, 2003]. A systematic approach should therefore take into account the spatial variability of precipitation when attributing synoptic conditions to extreme precipitation events.

Typical synoptic conditions leading to heavy precipitation in Nepal have been summarized to: monsoon low pressure systems, break monsoon conditions, western disturbances, and a change in the seasonal monsoon trough [Nandargi and Dhar, 2011]. This summary is largely based on studies of single events with impact along the Himalayas. The listed features can act on different regions along the Himalayas and are dominant in different months. For instance, in central Nepal, mesoscale systems are found to strongly interact with steep terrain at elevations of 1-2 km [Barros *et al.*, 2000] where during the monsoon onset, monsoon depressions from the Bay of Bengal (Fig. 1), can move close to the Himalayan mountain range and force air upslope causing precipitation [Lang and Barros, 2002]. However, implications of these studies for Nepal and where to expect which of the synoptic conditions are not clear.

Another approach in the literature was to relate the occurrence of different convective systems to synoptic anomalies for various regions along the Himalayas [Romatschke and Houze Jr, 2011]. Nepal was part of a larger region called central Himalayan foothills and

therefore not discussed in detail. For the central Himalayan foothills, trough conditions over the Tibetan Plateau and positive anomalies south of the Himalayas favored medium convective systems. *Houze Jr et al.* [2007] described various mechanisms triggering monsoon convection in the Himalayas, emphasizing a strong interaction with the complex terrain and regional differences between West, Central and East Himalayas. Over the West Himalayas a key feature was a cap of dry air flowing down from the Afghan Plateau (Fig. 1). This cap prevented premature triggering of convection of moist air coming from the Arabian Sea (first described by *Sawyer* [1947]). As the moist air masses approach the Himalayas they are orographically lifted, finally triggering convection. This was later confirmed by *Medina et al.* [2010] in numerical model experiments. Such a systematic assessment remain to be conducted for synoptic conditions related to extreme precipitation along the Nepalese Himalayas.

The second constituent for precipitation addressed in our study is the availability of precipitable water. This directly connects to the location and contribution of moisture sources raising the question: if there is more moisture precipitating, where does the additional moisture come from? However, various studies investigated the origin of moisture for the Indian subcontinent. *Ghosh et al.* [1978] derived water vapor flux from airborne measurements along different transects in the Arabian Sea concluding that evaporation along the Arabian Sea is a major moisture source. *Cadet and Reverdin* [1981] investigated surface water vapor transport for the 1975 summer monsoon season using a budget approach based on cross-sections. They state that during the monsoon season as much as 70% of the water vapor crossing the west coast of India could originate in the Southern

Hemisphere while the remaining 30% evaporate from the Arabian Sea. Moisture picked up by traversing air masses over the Indian Ocean in the Bay of Bengal would mainly contributes to the development of local weather phenomena. Later studies confirmed these findings and stress the importance of the Arabian Sea and the Southern Hemisphere as moisture sources [Cadet and Greco, 1987; Wang, 2005]. However, implications for moisture sources for Nepal are not clear and need to be addressed separately. To our knowledge there is no study assessing moisture sources for extreme precipitation in Nepal.

Research on single high impact events close to the Nepalese Himalayas hints to synoptic processes and moisture sources possibly applicable for Nepal. In particular, the city of Leh flood 2010 [Rasmussen and Houze Jr, 2012; Kumar et al., 2014] and floods in Pakistan [Medina et al., 2010; Houze Jr et al., 2011; Martius et al., 2013; Rasmussen et al., 2015] were explored. For the city of Leh flood 2010, moisture from the Arabian Sea and the Bay of Bengal was funneled to Leh and fed into mesoscale convective systems moving down from the Himalayan plateau [Rasmussen and Houze Jr, 2012]. For the Pakistan flood in 2010, Martius et al. [2013] found that orographical lifting and atmospheric flow directed against the Himalayan mountain chain was a main driver. Using the moisture source diagnostic from Sodemann et al. [2008], they found a considerable contribution from land, over India and Pakistan, and from the Arabian sea. The scope of their study did not include the mechanism by which a large amount of moisture could be taken up over an otherwise relatively dry land area like the Thar desert (Fig. 1). However, they proposed a possible intense coupling of precipitation and evapotranspiration. It is not known whether similar mechanisms prevail during extreme precipitation in Nepal. Therefore, we address

systematically regional aspects and explore the moisture sources in conjunction with the synoptic conditions leading to extreme precipitation over Nepal.

2. Data

We used data from meteorological stations provided by the Department of Hydrology and Meteorology (DHM) in Nepal measuring 24 h precipitations sums (from 9 am to 9 am local time). We picked 112 stations (Fig. 2) that remain after data availability control with constraints from *Bohlenger and Sorteberg* [2017]. The main criterion for choosing a station was that every month in the monsoon season June to September should have 75% of valid data for at least 30 years in the period 1971 to 2010. The 112 chosen stations are well distributed over the country and cover most of the climatic zones as defined in *Shrestha et al.* [2016]. The capital Kathmandu and the city Pokhara stand out from the otherwise sparsely covered country as more stations are located close-by (Fig. 2).

We used two additional datasets for our analysis: 6-hourly Era-Interim re-analysis [*Dee et al.*, 2011] at 0.75 degree horizontal resolution and a global particle trajectory dataset consisting of 5 million particles of equal mass representing the entire atmosphere (from 1979 to 2013) [*Läderach and Sodemann*, 2016]. This dataset was computed with the Lagrangian dispersion model FLEXPART [*Stohl et al.*, 2005] based on Era-Interim reanalysis fields.

3. Methods

3.1. Clustering of the rain gauge stations

We cluster our station based precipitation records to find groups of stations that behave similarly in terms of precipitation changes. As distance metric for the K-means algorithm with random seeding, we use correlation between the rain gauge stations based on daily precipitation amounts during 30 years of monsoon seasons. This distance metric is chosen since daily precipitation is not Gaussian distributed. A typical dilemma with cluster algorithms is that one has to know the number of clusters beforehand. There are different approaches to face this problem but the alleged objective methods still need subjective judgment. The methods we used to decide whether a chosen number of cluster was suitable were: comparison of silhouettes [Rousseeuw, 1987], aiming for high silhouette coefficients and applying gap statistics [Tibshirani *et al.*, 2001].

3.2. Identification of low pressure systems

We identified and tracked low pressure systems (LPS) using the Lagrangian-tracking algorithm [Hodges, 1994, 1995, 1999]. This algorithm is fed with relative vorticity from ERA-Interim [Dee *et al.*, 2011] on the Gaussian grid F128 and follows the relative vorticity maximum on 850 hPa. At this pressure level monsoon LPS are expected to exhibit a vorticity maximum [Tyagi *et al.*, 2012]. We further consider only systems that last longer than two days, travel more than 1000 km and exceed a vorticity threshold of $5 \cdot 10^{-6} s^{-1}$. This tracking algorithm has already been successfully applied for monsoon LPS in South Asia [Sørland and Sorteberg, 2015a].

3.3. Identification of moisture source regions

We assess moisture changes along each trajectory from [Läderach and Sodemann, 2016] with the moisture source diagnostic from *Sodemann et al.* [2008]. This diagnostic method allows the attribution of moisture sources by relating each moisture gain or loss along an air parcel trajectory to the current specific humidity of the same air parcel. In this methodology, moisture loss counts as precipitation. We follow the trajectory 10 days prior to the extreme event, which explains on average 91% of the moisture changes over Nepal. This means that on average 9% of the moisture in the air parcel were already present when starting the diagnostic and therefore cannot be attributed. The high fraction of explained moisture changes gives confidence in the applicability of the method in this area with limitations discussed in the next paragraph. We compute moisture sources only for trajectories that lose moisture ($> 0.1 \text{ mm}$) in the target region and by this only quantify sources relevant for precipitation.

The attribution of moisture uptake is divided into two vertical layers [*Sodemann et al.*, 2008]: contribution from the boundary layer and the free troposphere. Boundary layer contribution consists of all uptake below 1.5 times the boundary layer height in ERA-Interim. Consequently, everything above is defined as uptake in the free troposphere. This division is due to the assumption that within the boundary layer vertical mixing is much stronger than horizontal advection. The origin of the taken up moisture corresponds to the location of the parcel which is here defined as the moisture source region. This assumption is less obvious in the free troposphere where moisture can be advected from far away or introduced by plumes of convection and evaporating rain. For the moisture diagnostic we use 6 hourly steps for re-calculating the budget for the respective air par-

cel. During these 6 hours the parcel could cross a convective plume which would change its moisture content. In this study we only take into account the contribution from the planetary boundary layer to assess the contribution of regions over which moisture was picked up by an air parcel.

Winschall et al. [2014] compared the Lagrangian moisture source diagnostic against an Eulerian moisture source diagnostic using the limited area model COSMO with water vapor tracers. They focused on a heavy-precipitation event leading to the flood in eastern Europe in May 2010 and found that both approaches are generally consistent. They concluded that the Lagrangian moisture source diagnostic from *Sodemann et al. [2008]* is a computational efficient tool for determining moisture source regions. *Läderach [2016]* investigated the moisture transport to Kathmandu for a case study (22 days). He compared the Lagrangian diagnostic with Eulerian model results and concluded with a good agreement in this region, strengthening confidence in our approach.

To attribute moisture sources to extreme precipitation events we divided Nepal into West, Central, and East Nepal (Fig. 2). The area of Nepal was determined by the area within 26-31 N and 79-89 E. West Nepal was defined as 27.5-30.5 N and 80-83.5 E, Central Nepal as 26.5-29 N and 83-86 E, and East Nepal as 26-28.5 N and 85.5-88.5 E. For the discussion on moisture in the Thar desert, we chose an area in the Indian state Rajasthan defined as 25-28 N and 71-75 E. For all target regions we tracked air parcels back in time for 10 days to quantify their moisture sources. Only air parcels that enter through the above defined borders and lose moisture in the target region are tracked.

3.4. Definition of anomalies and extremes

The Indian summer monsoon is a transient feature with high variability in the onset date, the progression, and strength. Therefore, the mean state of the Indian summer monsoon is not representative as a reference field. Hence, anomalies are calculated as the difference between an event and a mean background state consisting of a 15 day average centered around the date of the event.

We focus on synoptic conditions related to precipitation events exceeding the threshold of the 99.5-percentile. We call these events for the rest of the study extreme events as they are far out in the tail of the distribution of daily precipitation. Fig. 3 illustrates that Nepal experiences most extremes simultaneously at multiple stations during the Indian summer monsoon. *Bohlenger and Sorteberg [2017]* found that the monsoon is the dominating season for the exceedence of high percentiles. They further point out that a relationship between the number of extreme events and the El Niño-Southern Oscillation (ENSO) have no significant linear correlation above the 99-percentile. Thus we do not need to treat extreme events in ENSO years in a special way. Exemplary time series of extreme events and the correlation with ENSO together with trends and climatology can be viewed in *Bohlenger and Sorteberg [2017]*. Choosing at least five stations indicating an extreme event should serve as division between very localized convective events and larger scale systems that trigger extreme precipitation at several stations simultaneously.

We pick a date whenever extreme precipitation is observed at minimum five stations on the same day (329 dates). Based on this constraint we select extreme dates for each

cluster (Section 4). We further exclude all extremes that occurred simultaneously at more than one cluster which leaves us 231 dates to obtain region specific characteristics. This means that roughly 70% of all extreme dates were confined to a single cluster. Additionally, we remove all dates prior to the start of Era-Interim in 1979 and use only dates between June and September. This results in 180 dates (cluster 1: 51, cluster 2: 77, cluster 3: 52) which despite the thinning process contain high impact events like 19/20 July 1993 and 30 August 1998 [*Chalise and Khanal, 2002*] in the second cluster. From the set of remaining dates we create composites of geopotential height to capture features of atmospheric dynamics (Section 6).

A limitation of this approach is that, due to the seasonal climate of Nepal, most of the extreme events fall within the monsoon season where also most of the annual precipitation falls [*Bohlenger and Sorteberg, 2017*]. This leads to an overrepresentation of dates with extreme events during the monsoon season. However, these are extreme events with considerable amounts of precipitation meaning that they are likely to be of greater importance to society. This and the fact that contemporaneous extreme events at multiple stations are concentrated in the monsoon seasons (Fig. 3) are reasons for us to focus on the monsoon season. Extremes relative to different seasons could be discussed separately in another study.

4. Regimes of daily precipitation in Nepal

Due to the large variety of processes leading to heavy precipitation events [*Nandargi and Dhar, 2011*] and the spatial variability discussed in the introduction, we divide Nepal

into subregions using clustering. By this, we can focus on the processes for each subregion with less probability of averaging out important features. Gap statistics suggest a best gain of information for two or three clusters. Due to the distribution of the silhouettes for two and three clusters we decide for the latter which leads to a division of Nepal into three well defined regions (Fig. 4).

The obtained clusters display a division into West, Central and East Nepal. This division is similar to results obtained by *Kansakar et al.* [2004] where precipitation regimes followed major drainage basins Karnali, Narayani, and Sapta Koshi. This is striking because their approach differs from ours in various significant points. They applied a hierarchical, agglomerative cluster analysis, to classify precipitation regimes in Nepal on a climate time scale. They clustered separately “shape” and “magnitude” as originally proposed by *Hannah et al.* [2000]. The classification using the stations “magnitude” was based on climatic time scale variables such as mean, min, max, etc., whereas clustering “shape” was based on monthly z-scores to produce an annual precipitation with values of similar magnitude for each station. *Kansakar et al.* (2004) first divided Nepal into physiographic regions and major drainage basins resulting in six regions and subsequently found the dominating precipitation type for this region. This differs substantially from our approach where we focus on classifying stations using daily precipitation amounts in order to cluster stations that react concurrently to a synoptic scale forcing. We further did not impose any constraints on the clustering and yet our study results in a similar division.

This robust result emerging from clustering station precipitation could be related to larger scale systems triggering precipitation in the respective region. When increasing the number of clusters, the stations divide into regions parallel to the Himalayas while mostly retaining the perpendicular division (not shown). Various studies [Barros *et al.*, 2000; Lang and Barros, 2002; Barros and Lang, 2003; Bookhagen and Burbank, 2006; Houze Jr *et al.*, 2007; Bookhagen and Burbank, 2010] illustrate a strong influence of topography on precipitation. The observed division of the clusters parallel to the mountain chain could mirror the influence of topography and how far weather systems are able to penetrate into the mountain chain. A more detailed discussion on the sensitivity of the results due to changes in the method or ingoing data can be read in the appendix. We investigate in the coming sections whether the synoptic conditions differ between extreme precipitation events occurring in the cluster regions.

5. Atmospheric circulation and moisture sources for Nepal during the monsoon

During the Indian summer monsoon, typically a surface low pressure area prevails over the Indo-Gangetic Plain covering North India and the Northern Bay of Bengal (e.g. Wang [2005]; Tyagi *et al.* [2012]). This is known as the Monsoon Trough. A band of high geopotential height with anticyclonic flow dominates the upper troposphere at 200 hPa (e.g. Houze Jr *et al.* [2007]; Romatschke *et al.* [2010]) reaching from the Arabian peninsula to Bangladesh along the Himalayas. This zone of low level convergence and upper level divergence represents the northward-shifted Intertropical Convergence Zone (ITCZ) during the Indian Summer Monsoon. In the mid-troposphere, a center of low geopotential

height resides over North-East India and the Bay of Bengal (Fig. 5a). Winds follow the geopotential height and veer toward north over the Bay of Bengal. Over Nepal, the low-level atmospheric flow changes direction from north-westerly to south-easterly and is consequently steered against the Himalayas (Fig. 5b). In the lower troposphere, an area of low geopotential height (Fig. 5b) extends from Pakistan to Bangladesh following the Indo-Gangetic Plain. This region of low geopotential height coincides with the location of LPS that form during the monsoon season and can influence the strength and direction of the moisture transport [Krishnamurthy and Ajayamohan, 2010; Sørland and Sorteberg, 2015b].

Averaged over the entire monsoon season the vertically integrated moisture transport is aligned with the surface winds and depicts a strong band from the region of the Somali Jet, crossing the Western Ghats in India (Fig. 1), and turning north in the Bay of Bengal (Fig. 6a). During the Indian summer monsoon the area with the strongest vertical integrated moisture transport is located over the Indian Ocean in the Southern Hemisphere close to the equator, over the Arabian Sea, over Sri Lanka, and in the Bay of Bengal. Moisture is steered toward the Himalayan mountain chain where the flow follows the topography and bifurcates, one branch to the northwest along the Nepal Himalayas and one to the northeast (Fig. 6a). Viewing the integrated moisture transport during the monsoon season in Figure 6a creates the notion that most of the moisture that precipitates along the Himalayas during the monsoon stems from the Bay of Bengal, the Arabian Sea or as far as south of the equator. Focusing on moisture sources for the Indian subcontinent, this has in fact been shown in multiple studies which describe the magnitude of the moisture

uptake over the ocean (*Ghosh et al.* [1978]; *Cadet and Reverdin* [1981]; *Cadet and Greco* [1987]; *Wang* [2005], Chapter 1 and 4). Their findings are based on a moisture budget approach investigating vertically integrated moisture fluxes or comparing evaporation with precipitation deducted from measurements. They find that during the monsoon season water vapor crossing the west coast of India stems mainly from the Southern Hemisphere (70%) and the Arabian Sea (30%).

With Figure 6a in mind, one could conclude that the moisture sources are similar for Nepal. Our results challenge this notion when exploring moisture sources computed using the Lagrangian moisture source diagnostic (Fig. 6b). The method reveals that most of the moisture precipitating over Nepal is taken up along a the Indo-Gangetic Plain north of the main branch of moisture transport in Era-Interim. We find that around 25% of all relevant uptake (solid black line) occurs over Nepal and the direct vicinity. Roughly 50% (stippled black line) stem from the Indo-Gangetic Plain. In total, 80% of the moisture is taken up over land and 20% over the ocean. Long range transport seems to be relevant for a large fraction of the 20% as it originates mainly from the Arabian Sea (15%) and off the coast of Somalia (details in Table 1).

We suggest that the reason for the difference between results from the budget approach and our results, obtained with the Lagrangian method, is that the budget approach cannot take into account recycling of moisture. The budget approach compares all evaporated moisture with all precipitation within certain borders or a volume. This can describe whether a region on average acts as a moisture source but cannot attribute moisture

sources contributing to a certain precipitation event. Specifically for Nepal, this could mean that originally the moisture had been taken up over sea but thereafter, due to multiple rain events on the way to Nepal, the moisture that stemmed from the Arabian Sea had left the air parcel and was gradually replaced by moisture taken up over land. Hence the direct source for the specific precipitation event over Nepal was over land. This chain of events would be masked in a budget approach. It becomes clear that the results of the two different approaches are not contradictory but rather complementary.

6. Synoptic conditions characterizing region specific extreme events

6.1. Composite analysis

After introducing the mean state of the Indian summer monsoon, regarding atmospheric circulation and moisture sources for Nepal, we continue to discuss the distinctive features characterizing extreme precipitation events. We test whether Era-Interim can qualitatively reproduce the extreme precipitation events over the respective cluster areas (Section 4). Fig. 7 depicts Era-Interim total precipitation composites for the dates of extreme precipitation for each cluster. For the dates of extreme precipitation Era-Interim produces a significant amount of rainfall over the cluster regions. Central Nepal receives substantial precipitation in all cases, consistent with the general precipitation distribution in Nepal [Bohlenger and Sorteberg, 2017]. We suggest that Era-Interim is capable of reproducing extreme precipitation events at the locations of the clusters. The result further indicates that mechanisms leading to extreme precipitation are governed by grid scale features and the synoptic conditions which we focus on are represented well enough for further investigations.

We identify synoptic flow patterns for each cluster connected to the extremes. The flow in the vicinity of the clusters is directed toward the respective cluster at the day of the extreme event throughout most of the troposphere, illustrated for 500 hPa and 850 hPa (Fig. 8). For cluster 1 the trough in mid-troposphere is steep and points toward the Himalayas (Fig. 8a). For cluster 2 and 3, the trough becomes more elongated and the flow turns gradually toward the cluster regions (Fig. 8b,c). Similarly, in the lower troposphere low geopotential height stretches from Pakistan southeast along the Himalayas toward Bangladesh. The shape and extent of this low geopotential height region changes from cluster 1 to 3 to become more aligned with the Himalayas (Fig. 8d-f).

Across the mid and lower troposphere, a dipole structure consisting of a center of high and low anomaly supports the direction of the flow to the respective cluster region (Fig. 8). For cluster 2 and 3 the flow needs to travel along the Himalayas and veer to the north farther east compared to cluster 1. This is reflected in the anomalies which support the respective flow patterns by their location, shape and strength. In the mid and upper troposphere at (500 hPa and 300 hPa) pronounced anomaly patterns help to guide the flow toward the respective cluster region (Fig. 9a-g) which is much like the trough structure in Figure 8a-c. The anomaly shows an increased north-south gradient with a negative anomaly trough at the location of cluster 1. Additionally, a positive anomaly region over north-east India forces the flow more northward and enhanced winds are directed toward the Himalayas. For cluster 2 and 3 an elongated band of positive geopotential anomaly extends from Pakistan across India to Myanmar and Thailand. The positive anomaly is more pronounced for cluster 3 than for cluster 2 supporting the flow to be parallel to

the mountains for a longer distance such that the flow does not turn north before east Nepal is reached. Our anomaly composites for Central and East Nepal are consistent with results from *Romatschke and Houze Jr* [2011] who found a negative geopotential height anomaly at 500 hPa across the Himalayas and south of the mountain chain a positive anomaly prevailing during the occurrence of medium convective systems over the central Himalayan foothills. While their findings include all of Nepal we resolve distinctive features characteristic for regions of Nepal revealing that the flow toward the Himalayas seems to be crucial for extreme precipitation events.

6.2. Variability within the cluster composites

The composite analysis indicates that synoptic conditions guide the atmospheric flow to the Himalayas and consequently drain the available moisture due to orographic uplifting. Based on the 180 considered cases, various weather features can be associated with extreme precipitation events recorded at the stations. Prominent synoptic conditions are: a trough over the Himalayas (Fig. 8, Fig. 11), a low pressure system from the Bay of Bengal (Fig. 10), and sometimes, although less common, a low pressure system from the Arabian Sea (Fig. 10c).

Monsoon LPS are known to mainly develop in the Bay of Bengal, travel to the north or north-west where some of them recurve to the east [*Krishnamurthy and Ajayamohan*, 2010; *Tyagi et al.*, 2012; *Sørland and Sorteberg*, 2015b]). We tracked all LPS (Section 3.2) that entered a target region around Nepal and were existing during an extreme event (Figure 10). Most LPS relevant for extreme precipitation events in Nepal develop in the

7.3 Synoptic conditions and moisture sources actuating extreme precipitation in Nepal

Bay of Bengal and move north-west where some recurve towards the north-east and east.

Despite the difference in the number of extreme precipitation events for each cluster, the number of LPS that were present varied only little: 9 LPS for cluster 1 (18%), 11 LPS for cluster 2 (14%), and 11 LPS for cluster 3 (21%). LPS being in the target region during extreme events in cluster 1 and 2 are characterized by a course farther west over India and end up close to West Nepal. For cluster 3, most are heading to the north, not undergoing the described recurring and end up close to the cluster region in East Nepal. We find that for our cases a trough structure with the accompanying wind field in the mid-troposphere contributed to guide the LPS to the north which we will elaborate on in the following.

An example of those interactions is the low pressure system that caused extreme precipitation in west Nepal on 25 September 2005 (Fig. 11). Originating in the Bay of Bengal a low pressure system reached the Indian west coast two days prior to the extreme event and was redirected to Nepal guided by a mid-level trough. Two days prior to the event, the system had weakened, however, when the trough and the low pressure system started to interact the storm shifted direction veering to the north and produced significant precipitation amounts, exceeding the 99.5 percentile at multiple rain gauges in western Nepal. We find that the interaction between troughs and monsoon LPS is closely connected to extreme precipitation events in Nepal.

6.3. Discussion of the synoptic conditions

The fact that mid-tropospheric troughs coincide with the extreme events in Nepal is consistent with other studies summarized in *Tyagi et al.* [2012]. They found that these

troughs considerably influence synoptic systems and rainfall during the Indian summer monsoon, e.g. by triggering and intensifying LPS and subsequently increasing rainfall.

Westerly troughs can also support guidance to LPS and can cause storms to recurve from their originally north-west course to the north or north-east (Section 4.4 in *Wang* [2005]; *Tyagi et al.* [2012]). *Martius et al.* [2013] described the effect of an upper level positive potential vorticity anomaly on the Pakistan flood of 2010, close to the area of cluster 1. Although the vorticity anomaly exerted quasi-geostrophic forcing on the affected region, its main effect was to orient the lower-troposphere windfield toward the Himalayas causing orographic uplift.

In our study, for all three cluster regions the orientation of the wind field and the orographic uplift seem to play a major role. We identified the orographic uplift along the air parcels retrieved from the trajectory dataset from *Läderach and Sodemann* [2016]. Entering the region of cluster 1 and 2, air parcels rise on average over 2000 m during their last two time steps (12 hours) prior to their respective extreme event. For cluster 3 an uplift of similar magnitude takes place more gradually, happening over the last 5-10 time steps (30 h-60 h). This is consistent with the orientation of the flow which is directed more perpendicular to the mountain chain for cluster 1 and 2, whereas for extreme events in cluster 3, the flow in the lower- and mid-troposphere is oriented almost parallel to the Himalayas (Fig. 8).

Besides features consistent with literature mentioned above, the meterological context of the described extreme events differ considerably from those accompanying the floods in

India and Pakistan [Rasmussen and Houze Jr, 2012; Martius et al., 2013; Kumar et al., 2014]. These studies consistently describe a blocking high over the Tibetan Plateau which together with monsoon LPS create an increased pressure gradient generating an easterly jet along the Himalayas which transports moist air from the Bay of Bengal to the precipitating regions. In our case, this feature appears to be reversed. The gradient across the Himalayan mountain barrier is increased in our cases as well. However, we observe the atmospheric flow not being easterly but westerly before turning north and rising up the Himalayas. This result stresses the spatial variations inherent in extreme precipitation events along the Himalayas.

Houze Jr et al. [2007] and *Medina et al.* [2010] find evidence for continental air coming down from the Afghan Plateau, capping low level moist air and consequently preventing premature convection. This is consistent with *Sawyer* [1947] who described this feature in a conceptual sketch. The composites in our study reveal a similar pattern where the flow in the high- and mid-troposphere emanates down from the Afghan Plateau when at the same time low level air travels from the Arabian Sea over the Indus valley and veers to the east. The strength and the covered distance of the mid-level flow coincides with the location of the extreme events (8a,b,c). Like in the conceptual sketch from *Sawyer* [1947], the continental air might contribute to prevent premature convection until the moisture is finally released at the location of the cluster. To assess this suggestion a separate study would be needed to investigate the existence of a causal link (beyond the scope of this manuscript).

7. Moisture flux and moisture sources

On days of extreme precipitation events, we find considerable positive total column moisture anomalies over the respective cluster regions (Fig. 12). This is consistent with *Barros and Lang* [2003] who measured a peak in total column moisture and atmospheric instability just before an event. Vertically integrated moisture flux anomalies are directed to our cluster regions (Fig. 12). For all cluster regions the moisture flux and its anomalies follow a similar path: coming from the Arabian Sea over Northwest India to Bangladesh along the Himalayas until they turn to the north at the cluster regions. For the first cluster the moisture flux anomaly is directed north toward the Himalayas (Fig. 12a). For cluster 2 and 3 the moisture flux anomaly is directed parallel to the Himalayas until it gradually veers to the north toward the respective cluster regions (Fig. 12b,c). The moisture flux is very similar to the anomalies (not shown).

The computed moisture sources for extreme precipitation events in the cluster regions mirror the pattern of moisture flux coming from the Arabian Sea and continuing along the Himalayas to the East. Moisture uptake occurs to a significant degree along the Indo-Gangetic plain (Fig. 13 and Fig. 1 for orientation). For cluster 1, the core area of moisture uptake (solid black line indicating 25%) includes the area of extreme precipitation in Nepal together with a filament along the Indo-Gangetic plain Fig. 13a. For cluster 2 and 3 (Fig. 13c,e) the 25-percentile is more concentrated around the cluster regions. For all clusters, roughly half of the moisture evaporated over the Indo-Gangetic plain (stippled line). The rest of the accounted moisture stems from as far as the equator region at the east coast of Africa. Moisture over India is the largest contributor supplying

half of moisture for extreme precipitation in Nepal while Nepal adds 5-10% (Tab. 1).

Although the magnitude of moisture uptake over Nepal is comparably large (blue colors in Fig. 13 a,c,d) the area is limited and cannot match the moisture supply from India and Pakistan. In total, moisture uptake over land accounts for ca. 75% which is just slightly lower than the climatological value (Fig. 6b, Tab. 1). The Bay of Bengal only plays a minor role while the long tail and the reddish colors spread over the Arabian Sea indicate some contribution from long range transport. However, the fraction of moisture contribution from the Southern Hemisphere is marginal which means that the budget derived results assessing moisture sources and sinks for the Indian subcontinent (*Cadet and Reverdin [1981]*, *Cadet and Greco [1987]*, and *Wang [2005]*) should be handled with caution when addressing precipitation and extreme precipitation in Nepal.

We computed moisture source anomalies, to test whether there are different source regions or increased moisture uptake involved in extreme precipitation events over Nepal. The anomaly figures (Fig. 13c,d,f) underline the above discussed results that a considerable fraction of the additional uptake occurs over the cluster region and the Indo-Gangetic plain. Interestingly, the region of cluster 1 is the only region where almost none of the additional moisture seems to stem from the cluster region itself (Fig. 13c). In this region the atmospheric flow might interact with the terrain as soon as it comes close to the border of Nepal. Through the ascend it might be lifted above the defined threshold of 1.5 times the boundary layer height (Section 3.3). In fact when combining the contribution of the free troposphere and the boundary layer a maximum over the cluster region appears (not shown). In complex terrain one should therefore be careful with interpreting the results

of this method.

The largest positive moisture uptake anomaly is located over the Indo-Gangetic plain.

We find no region with a coherent negative uptake anomaly, whereas a positive anomaly can be observed across all of the major uptake regions. Compared to the monsoon mean, there appears to be no specific region with an increase in moisture contribution but rather a uniform increase of moisture uptake prior to the extreme events. The magnitude of the increase is related to the magnitude of the absolute contribution meaning that regions that generally contributed more, e.g. the Indo-Gangetic Plain, also show the largest positive anomaly.

8. The shape of the moisture source patterns for Nepal

An important question that arises when exploring the moisture sources is: why is there moisture uptake over relatively dry regions like the Thar Desert in the Indus Plain (Fig. 1)? *Medina et al.* [2010] pointed to the possibility of moisture uptake over land for heavy precipitation over Pakistan if the soil was moistened by a previous precipitation event. *Martius et al.* [2013] detected a large moisture contribution from land for the Pakistan flood in July 2010. They suggested the possibility of an intense coupling of precipitation and evapotranspiration but did not further address this issue. However, even if moisture is abundant uptake will not be relevant for the extreme precipitation event if the air flow to the target region is not directed over the moist region.

The soil moisture depicts a considerable intra-seasonal cycle where the Indian subcontinent is moistened as the monsoon matures. We illustrate this for extreme events in June and August as an example on the progression of the monsoon (Fig. 14a,b). Northwest India, containing arid regions like the Thar desert, experiences an increase of soil moisture which makes moisture uptake possible later in the monsoon season. A similar pattern is visible in the precipitation field (not shown). *Romatschke et al.* [2010] present results using the TRMM 3A25 product consistent with our findings. They conclude that for the Indus Plain the predominant convective precipitation features are deep convective and wide convective cores. Examples for intense precipitation events in the comparably dry uptake region along the Indus valley are described for instance in *Houze Jr et al.* [2007], *Houze Jr et al.* [2015], and *Rasmussen et al.* [2015]. Due to a dry capping layer from the Afghan Plateau and Hindu Kush mountains convection is usually inhibited which is the reason for the prevalence of deep convective cores and wide convective cores in Northwest India. Broad stratiform precipitation regions are not able to break through the capping layer unless they are exposed to forced lifting e.g. onto the Himalayan mountain barrier where they can be activated. In the context of three consecutive years of floods in Pakistan, *Rasmussen et al.* [2015] described intense, wide convective cores causing heavy precipitation over the arid region along the eastern border of Pakistan and the Indian states Gujarat and Rajasthan (Fig. 1). Such intense convective events can moisten the otherwise dry region and might subsequently serve as moisture sources for extreme precipitation events in Nepal.

While the atmospheric flow changes throughout the season, extreme precipitation events depict considerable anomalies. To illustrate the seasonal changes we choose extreme events in cluster 1 (Fig. 14 c,d). During extreme events in June the air crosses India almost zonally to veer to the north and north-east when reaching the Himalayas. In August there is a strong northward component from the Arabian sea, crossing Northwest India and veering to the east along the Himalayas. The flow anomalies might be influenced by break periods (Section 9) resulting in the depicted pattern.

The progression of the soil moisture and the flow anomalies are reflected in the moisture sources (Fig. 15) which exhibit a similar pattern. While the moisture sources for extreme events in June are close to the Bay of Bengal, moisture can be taken up over the dryer areas later in the monsoon season when soil moisture had already increased e.g. by the above described precipitation events. Not only the uptake region changes but also the total amount of moisture that is taken up increases in August compared to June (Fig. 15). For instance, the minimum and maximum daily amounts of all moisture taken up prior to an event which contributes to the respective extreme precipitation event ranges from 26 mm to 205 mm for June and from 34 mm to 383 mm for August. In August, the Indian summer monsoon is in a more mature state compared to June and has progressed far into the Indian subcontinent where precipitation events continuously increase the soil moisture content.

The last discussed factor that could be partly responsible for the shape of the moisture source pattern is irrigation. The Indo-Gangetic plain is one of the strongest irrigated

regions in the world [Siebert *et al.*, 2005]. Era-Interim indirectly accounts for irrigation by using surface observations of humidity and temperature to subsequently correct soil moisture [Douville *et al.*, 2000; Wei *et al.*, 2013]. Wei *et al.* [2013] found that taking irrigation into account significantly changes evaporation over the Indo-Gangtic plain up to 200% or 500 mm annually. They further state that up to 25% of the annual precipitation in this region could stem from the increased evaporation. These are significant contributions to the moisture uptake and since Era-Interim supplies the boundary conditions for the used trajectories, the increased evaporation likely contributes to the increased uptake in our results and hence the shape of the moisture source pattern.

We quantify the moisture sources for the dryer regions to extend our chain of argument regarding the above mentioned preconditioning precipitation events. We choose an area in the state Rajasthan in Northwest India (Fig. 1) as an example for an arid region which cannot offer much moisture in general. Nonetheless, we see uptake of moisture in this region for precipitation and extreme precipitation events in Nepal, also described by Martius *et al.* [2013] for the Pakistan flood 2010. Figure 14 indicates that in the beginning of June only little moisture precipitates out over this region. From this moisture the largest contributors are the Arabian Sea with 50% (Tab. 2) and Southeast Pakistan together with the state Gujarat close to the Indus delta. Close to the delta, there are also lakes that could serve as moisture sources during the intense insolation in the Indian summer monsoon. The Southern Hemisphere only contributes with 8%. This is, however, double the fraction compared to regions in Nepal. The increased contribution from moisture sources in the Southern Hemisphere is consistent with the argument of residence time. Following the moisture path, Rajasthan is roughly 1000 km closer to the source regions

in the Southern Hemisphere than much of Nepal (Fig. 1). Hence, moisture taken up over the Southern Hemisphere needs to travel at least a day less assuming an average speed of 10 ms^{-1} which also increases the probability that it does not rain out along the way.

By the end of June more moisture has been transported over land and precipitated over the arid regions such that uptake can occur. The land fraction increases due to the increased moisture availability and India now contributes as much as the Arabian Sea with 37%. The occasional occurrence of precipitation in these dry regions is also present in Era-Interim (not shown). Era-Interim supplies the boundary data for the Lagrangian trajectories and makes our result in the presented framework physically consistent. Our result is also consistent with multiple studies which illustrated the occurrence of precipitation and intense rain storms in this region [Houze Jr *et al.*, 2007; Romatschke *et al.*, 2010; Romatschke and Houze Jr, 2011; Houze Jr *et al.*, 2015; Rasmussen *et al.*, 2015]. A large fraction of moisture contributing to the Pakistan flood in 2010 came from the Arabian Sea [Houze Jr *et al.*, 2011; Martius *et al.*, 2013].

9. Impact of break periods

A common feature often related to abnormal rainfall over the Himalays and India are monsoon break periods which are defined by less rainfall over most of central India but more in the north and south of the country [Tyagi *et al.*, 2012]. Break periods have also been tied to heavy precipitation along the Himalayas [Nandargi and Dhar, 2011]. A typical feature of monsoon break periods is a flow splitting west of India where the main branch curves around the southern edge of the subcontinent veering again to the north

in the Bay of Bengal [*Joseph and Sijkumar*, 2004]. A northern branch moves from the Arabian Sea to the north-west along the Himalayas. Our moisture source regions match the northern branch that prevails during monsoon break periods.

We test whether the dates of extreme precipitation in our study coincide with break periods based on the four studies compared in *Rajeevan et al.* [2010]. The compared break periods are only listed for the months July and August and do not always overlap. Therefore we count a date when it coincides with at least one of the defined periods. A noticeable fraction of the extreme events in July and August (cluster 1: 26%, cluster 2: 25%, cluster 3: 43%) occurs during break periods. If we ease the constraint and allow a deviation of ± 1 day, bearing in mind the temporal differences that come along with the different definitions, this fraction increases drastically (cluster 1: 44%, cluster 2: 35%, cluster 3: 57%). In total we count 7 hits and 12 close hits for cluster 1, 13 hits and 18 close hits for cluster 2, and 15 hits and 20 close hits for cluster 3. *Rajeevan et al.* [2010] found that with their definition there are on average 7 days (11%) during July and August defined as break period. However, counting all days in July and August which are considered break periods in at least one study compared in *Rajeevan et al.* [2010], we find that on average 15 days (24%) are defined as break period in July and August between 1951 and 1989. In *Rajeevan et al.* [2010], after 1989, there is only one study we can use for the identification of break periods which consequently leads to a lower hit rate. This means that the meaning of the break periods for the extreme events is likely underestimated. Hence, break periods during July and August appear to be related

to extreme precipitation in Nepal and may influence the displayed pattern of moisture sources (Fig. 13) and vertical integrated moisture transport (Fig. 12).

10. Conclusion

We systematically investigated and discussed synoptic conditions and moisture sources actuating extreme precipitation in Nepal for the time period from 1979 to 2010. The involved key processes are illustrated in Figure 16 which forms the basis for the following conclusion. Taking into account the high spatial variability in rainfall in Nepal through clustering, we revealed an interplay between different synoptic-scale features that act to direct the atmospheric flow against the Nepalese Himalayas at the location of the extreme event. Although there are likely more processes involved, we focused on LPS and mid-level troughs. The mid-level trough could force a low pressure system to change direction and ultimately lead it to Nepal where extreme precipitation occurred. This was illustrated for 25 September 2005, and is also evident in the composite analysis of the geopotential height and atmospheric flow together with the paths of the LPS. In average 14%-21% of the extreme events were accompanied by LPS. The result from this long-term, composite approach is consistent with existing studies that have described the influence of troughs on the path of LPS investigating single events. In a composite analysis we found further a low level flow from the Arabian Sea and mid-level flow from the Afghan Plateau. A resulting capping and retarded triggering of convection was described by *Sawyer* [1947], *Houze Jr et al.* [2007], and *Medina et al.* [2010]. We found indications that this process might be important for the location of extreme precipitation along the Nepalese Himalayas as well. Moisture uptake was increased prior to the extreme events explaining the origin of the emerging positive anomalies in moisture transport and total water vapor. We quantified

major moisture sources and detected the main moisture uptake over land (ca. 75%) where India, Pakistan and Nepal were major contributors. The most prominent uptake region was the Indo-Gangetic Plain where almost half of the precipitating moisture was taken up. The location of the moisture sources could be related to irrigation processes which are indirectly taken into account in ERA-Interim. Another reason for the increased moisture uptake is the progression of the monsoon preconditioning the soil moisture for increased moisture uptake during anomalies in the low level atmospheric flow. These anomalies were noticeably influenced by break period conditions in July and August. Between 35% and 57% of the events in July and August occurred close to, or during a break period where this fraction is likely underestimated. Half of the moisture taken up in our example region in Rajasthan, representing dryer regions along the main uptake path, stemmed from the Arabian Sea in the beginning of June. Once the monsoon had matured, by the end of June, more moisture came from land (62%). Further numerical studies might help to disentangle the involved processes and shed more light on the role of moisture sources and their implications for extreme precipitation in Nepal.

Appendix A: Method sensitivity

A challenge when dealing with observations is the presence of missing values. In terms of clustering there are two basic approaches: fill in missing values (imputation) or ignore them (marginalization). Since all stations used for the study have missing values in different time intervals there would be a substantial loss of information when applying marginalization. Although, in our case there is only 4% missing data, marginalization would result in a reduction of the dataset by approximately 43%. With the aim to minimize the loss of information we applied the imputation method. We acknowledge that

clustering with missing values using no imputation is possible which is described for instance in *Wagstaff* [2004]. However, from the findings of *Wagstaff* [2004] substituting with reasonable values, for example using the mean, should be no drawback when only few data is missing. Introducing artificial values into a dataset could distort the clustering results which is why we performed a brief sensitivity tests on this issue. We tested different values for imputation as mean, median, and an arbitrary value. However, changing the substituted values resulted in negligible changes in cluster membership at the rims of the clusters.

Another factor that can influence the outcome of clustering is the chosen distance metric. We find that the clusters are little sensitive to changes in distance measures, meaning that only stations at the cluster rims might switch cluster memberships. Additionally, the sensitivity to changing the amount of clustered stations is very low, e.g. clustering only the stations that have consistent records for all 40 years results in a very similar grouping of stations. Different distance measures like cosine or the city-block metric were tested with similar outcomes.

Acknowledgments. This work has been funded by the University of Bergen, Norway. The authors thank the Department of Hydrology and Meteorology (DHM) in Nepal for sharing their rain gauge dataset. ERA-Interim reanalyses were provided through the ECMWF data server. We would also like to thank Kevin Hodges, University of Reading, UK, for help with tracking the low pressure systems.

References

- Baidya, S., M. Shrestha, and M. Sheikh (2008), Trends in daily climatic extremes of temperature and precipitation in Nepal, *Journal of Hydrology and Meteorology*, 5(1), 38–51.
- Barros, A., M. Joshi, J. Putkonen, and D. Burbank (2000), A study of the 1999 monsoon rainfall in a mountainous region in central Nepal using TRMM products and rain gauge observations, *Geophysical Research Letters*, 27(22), 3683–3686.
- Barros, A. P., and T. J. Lang (2003), Monitoring the monsoon in the Himalayas: Observations in central Nepal, June 2001, *Monthly Weather Review*, 131(7), 1408–1427.
- Bohlenger, P., and A. Sorteberg (2017), A comprehensive view on trends in extreme precipitation in Nepal and their spatial distribution, *International Journal of Climatology, Early View*, doi: 10.1002/joc.5299.
- Bookhagen, B., and D. W. Burbank (2006), Topography, relief, and TRMM-derived rainfall variations along the Himalaya, *Geophysical Research Letters*, 33(8).
- Bookhagen, B., and D. W. Burbank (2010), Toward a complete Himalayan hydrological budget: Spatiotemporal distribution of snowmelt and rainfall and their impact on river discharge, *Journal of Geophysical Research: Earth Surface (2003–2012)*, 115(F3).
- Cadet, D., and G. Reverdin (1981), Water vapour transport over the Indian Ocean during summer 1975, *Tellus*, 33(5), 476–487.
- Cadet, D. L., and S. Greco (1987), Water vapor transport over the Indian ocean during the 1979 summer monsoon. Part II: water vapor budgets, *Monthly weather review*, 115(10), 2358–2366, doi: 10.1175/1520-0493(1987)115;2358:WVTOTI;2.0.CO;2.

Caesar, J., L. Alexander, B. Trewin, K. Tse-ring, L. Sorany, V. Vuniyayawa, N. Keosavang,

A. Shimana, M. Htay, J. Karmacharya, et al. (2011), Changes in temperature and precipitation extremes over the Indo-Pacific region from 1971 to 2005, *International Journal of Climatology*, 31(6), 791–801, doi: 10.1002/joc.2118, doi:10.1002/joc.2118.

Chalise, S., and N. Khanal (2002), Recent extreme weather events in the Nepal Himalayas, *The extremes of the extremes: extraordinary floods*, 271, 141–146, IHAS Publ. no. 271.

Dee, D., S. Uppala, A. Simmons, P. Berrisford, P. Poli, S. Kobayashi, U. Andrae, M. Balmaseda, G. Balsamo, P. Bauer, et al. (2011), The ERA-Interim reanalysis: configuration and performance of the data assimilation system, *Quarterly Journal of the royal meteorological society*, 137(656), 553–597.

Douville, H., P. Viterbo, J.-F. Mahfouf, and A. C. Beljaars (2000), Evaluation of the optimum interpolation and nudging techniques for soil moisture analysis using fife data, *Monthly Weather Review*, 128(6), 1733–1756, doi: 10.1175/1520-0493(2000)128;1733:EOTOIA;2.0.CO;2.

Ghosh, S., M. Pant, and B. Dewan (1978), Influence of the Arabian Sea on the Indian summer monsoon, *Tellus*, 30(2), 117–125.

Hannah, D. M., B. P. Smith, A. M. Gurnell, G. R. McGregor, et al. (2000), An approach to hydrograph classification, *Hydrological processes*, 14(2), 317–338.

Hodges, K. (1995), Feature tracking on the unit sphere, *Monthly Weather Review*, 123(12), 3458–3465.

Hodges, K. (1999), Adaptive constraints for feature tracking, *Monthly Weather Review*, 127(6), 1362–1373.

Hodges, K. I. (1994), A general method for tracking analysis and its application to meteorological data, *Monthly Weather Review*, 122(11), 2573–2586.

Houze Jr, R. A., D. C. Wilton, and B. F. Smull (2007), Monsoon convection in the Himalayan region as seen by the TRMM Precipitation Radar, *Quarterly Journal of the Royal Meteorological Society*, 133(627), 1389–1411, doi: 10.1002/qj.106.

Houze Jr, R. A., K. Rasmussen, S. Medina, S. Brodzik, and U. Romatschke (2011), Anomalous atmospheric events leading to the summer 2010 floods in Pakistan, *Bulletin of the American Meteorological Society*, 92(3), 291–298, doi: 0.1175 / 2010 BAM S3173.1.

Houze Jr, R. A., K. L. Rasmussen, M. D. Zuluaga, and S. R. Brodzik (2015), The variable nature of convection in the tropics and subtropics: A legacy of 16 years of the Tropical Rainfall Measuring Mission satellite, *Reviews of Geophysics*, 53(3), 994–1021, doi: 10.1002/2015RG000488.

Ichiyanagi, K., M. D. Yamanaka, Y. Muraji, and B. K. Vaidya (2007), Precipitation in Nepal between 1987 and 1996, *International Journal of Climatology*, 27(13), 1753–1762, doi: 10.1002/joc.1492.

Joseph, P., and S. Sijikumar (2004), Intraseasonal variability of the low-level jet stream of the asian summer monsoon, *Journal of Climate*, 17(7), 1449–1458, doi: 10.1175/1520-0442(2004)017j1449:IVOTLJ;2.0.CO;2.

Kansakar, S. R., D. M. Hannah, J. Gerrard, and G. Rees (2004), Spatial pattern in the precipitation regime of Nepal, *International Journal of Climatology*, 24(13), 1645–1659.

Krishnamurthy, V., and R. Ajayamohan (2010), Composite structure of monsoon low pressure systems and its relation to Indian rainfall, *Journal of Climate*, 23(16), 4285–

4305, doi: 10.1175/2010JCLI2953.1.

Kumar, A., R. A. Houze Jr, K. L. Rasmussen, and C. Peters-Lidard (2014), Simulation of a flash flooding storm at the steep edge of the Himalayas, *Journal of Hydrometeorology*, 15(1), 212–228, doi: 10.1175/JHM-D-12-0155.1.

Läderach, A. (2016), CHARACTERISTIC SCALES OF ATMOSPHERIC MOISTURE TRANSPORT, Ph.D. thesis, ETH Zurich.

Läderach, A., and H. Sodemann (2016), A revised picture of the atmospheric moisture residence time, *Geophysical Research Letters*, 43(2), 924–933, doi:10.1002/2015GL067449, 2015GL067449.

Lang, T. J., and A. P. Barros (2002), An investigation of the onsets of the 1999 and 2000 monsoons in central Nepal, *Monthly Weather Review*, 130(5), 1299–1316, doi: 10.1175/1520-0493(2002)130;1299:AIOTOO;2.0.CO;2.

Martius, O., H. Sodemann, H. Joos, S. Pfahl, A. Winschall, M. Croci-Maspoli, M. Graf, E. Madonna, B. Mueller, S. Schemm, et al. (2013), The role of upper-level dynamics and surface processes for the Pakistan flood of July 2010, *Quarterly Journal of the Royal Meteorological Society*, 139(676), 1780–1797, doi: 10.1002/qj.2082.

Medina, S., R. A. Houze, A. Kumar, and D. Niyogi (2010), Summer monsoon convection in the Himalayan region: Terrain and land cover effects, *Quarterly Journal of the Royal Meteorological Society*, 136(648), 593–616, doi: 10.1002/qj.601.

Nandargi, S., and O. Dhar (2011), Extreme rainfall events over the Himalayas between 1871 and 2007, *Hydrological Sciences Journal*, 56(6), 930–945, doi: 10.1080/02626,667.2011.595,373.

Nayava, J. L. (1980), Rainfall in nepal, *Himalayan Review*, 12, 1–18.

Rajeevan, M., S. Gadgil, and J. Bhate (2010), Active and break spells of the Indian summer monsoon, *Journal of earth system science*, 119(3), 229–247.

Rasmussen, K., A. Hill, V. Toma, M. Zuluaga, P. Webster, and R. Houze (2015), Multi-scale analysis of three consecutive years of anomalous flooding in Pakistan, *Quarterly Journal of the Royal Meteorological Society*, 141(689), 1259–1276, doi: 10.1002/qj.2433.

Rasmussen, K. L., and R. A. Houze Jr (2012), A flash-flooding storm at the steep edge of high terrain: disaster in the Himalayas, *Bulletin of the American Meteorological Society*, 93(11), 1713–1724, doi: 10.1175/BAMS-D-11-00236.1.

Romatschke, U., and R. A. Houze Jr (2011), Characteristics of precipitating convective systems in the South Asian monsoon, *Journal of Hydrometeorology*, 12(1), 3–26.

Romatschke, U., S. Medina, and R. A. Houze Jr (2010), Regional, seasonal, and diurnal variations of extreme convection in the South Asian region, *Journal of climate*, 23(2), 419–439.

Rousseeuw, P. J. (1987), Silhouettes: a graphical aid to the interpretation and validation of cluster analysis, *Journal of computational and applied mathematics*, 20, 53–65.

Sawyer, J. (1947), The structure of the intertropical front over NW India during the SW monsoon, *Quarterly Journal of the Royal Meteorological Society*, 73(317-318), 346–369, doi: 10.1002/qj.49707331,709.

Shrestha, A. B., S. R. Bajracharya, A. R. Sharma, C. Duo, and A. Kulkarni (2016), Observed trends and changes in daily temperature and precipitation extremes over the koshi river basin 1975–2010, *International Journal of Climatology*, doi: 10.1002/joc.4761, doi:10.1002/joc.4761.

Siebert, S., P. Döll, J. Hoogeveen, J.-M. Faures, K. Frenken, and S. Feick (2005), Development and validation of the global map of irrigation areas, *Hydrology and Earth System Sciences Discussions*, 2(4), 1299–1327.

Sodemann, H., C. Schwierz, and H. Wernli (2008), Interannual variability of Greenland winter precipitation sources: Lagrangian moisture diagnostic and North Atlantic Oscillation influence, *Journal of Geophysical Research: Atmospheres*, 113(D3), doi: 10.1029/2007JD008503.

Sørland, S. L., and A. Sorteberg (2015a), The dynamic and thermodynamic structure of monsoon low-pressure systems during extreme rainfall events, *Tellus A*, 67, doi: 10.3402/tellusa.v67.27039.

Sørland, S. L., and A. Sorteberg (2015b), Low-pressure systems and extreme precipitation in central india: sensitivity to temperature changes, *Climate Dynamics*, 47(1-2), 465–480, doi: 10.1007/s00382-015-2850-4.

Stohl, A., C. Forster, A. Frank, P. Seibert, and G. Wotawa (2005), Technical note: The Lagrangian particle dispersion model FLEXPART version 6.2, *Atmospheric Chemistry and Physics*, 5(9), 2461–2474, doi:10.5194/acp-5-2461-2005.

Tibshirani, R., G. Walther, and T. Hastie (2001), Estimating the number of clusters in a data set via the gap statistic, *Journal of the Royal Statistical Society: Series B (Statistical Methodology)*, 63(2), 411–423.

Trenberth, K. E., A. Dai, R. M. Rasmussen, and D. B. Parsons (2003), The changing character of precipitation, *Bulletin of the American Meteorological Society*, 84(9), 1205–1217, doi: doi: 10.1175/BAMS-84-9-1205.

- Tyagi, A., P. Asnani, U. De, H. Hatwar, and A. Mazumdar (2012), The monsoon monograph, vols. 1 and 2, *Indian Meteorological Department*.
- Wagstaff, K. (2004), *Clustering with missing values: No imputation required*, Springer.
- Wang, E. B. (2005), *The Asian Monsoon*, Springer/Praxis Publishing Co., New York.
- Wei, J., P. A. Dirmeyer, D. Wisser, M. G. Bosilovich, and D. M. Mocko (2013), Where does the irrigation water go? an estimate of the contribution of irrigation to precipitation using merra, *Journal of Hydrometeorology*, 14(1), 275–289, doi: 10.1175/JHM-D-12-079.1.
- Winschall, A., S. Pfahl, H. Sodemann, and H. Wernli (2014), Comparison of Eulerian and Lagrangian moisture source diagnostics—the flood event in eastern Europe in May 2010, *Atmospheric Chemistry and Physics*, 14(13), 6605–6619, doi:10.5194/acp-14-6605-2014.

Accepted

Table 1. Contribution to the total moisture supply and, in parenthesis, the positive moisture anomaly in [%] for selected countries on the moisture pathway for extreme precipitation events.

country/region	Nepal	cluster 1	cluster 2	cluster 3
Nepal	12	6 (0)	10 (5)	5 (3)
Pakistan	4	11 (14)	5 (6)	5 (6)
India	38	49 (52)	48 (56)	49 (57)
Over land	80	77 (75)	76 (76)	73 (74)
Bay of Bengal	5	3 (2)	4 (2)	5 (3)
Arabian Sea	15	20 (22)	20 (22)	22 (24)
Southern hemisphere	3	4 (5)	4 (4)	4 (4)

Accepted Article

Table 2. Contribution to the total moisture supply for Rajasthan in [%] for each country that exceeds a contribution of 5%. To illustrate the temporal change two periods are contrasted, 1-10 June and 21-30 June. Values for the chosen periods are averaged from 1979 to 2010.

Rajasthan	1-10 June	21-31 June
Pakistan	9	13
India	28	37
Over land	49	62
Arabian Sea	50	37
Southern hemisphere	8	7

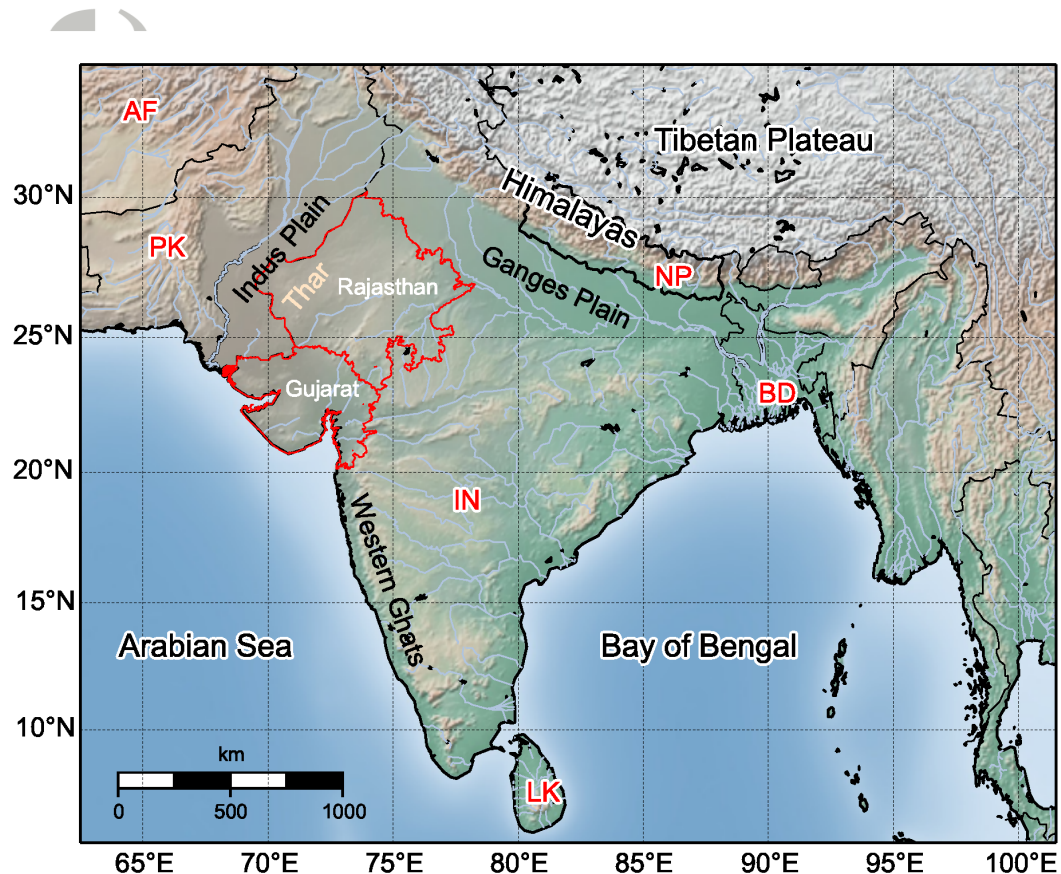


Figure 1. Overview map for South Asia including India (IN), Pakistan (PK), Afghanistan (AF), Bangladesh (BD), and Sri Lanka (LK). Nepal (NP) is located at the rim of the Himalayas and marked with thicker borders. The Indian states Rajasthan and Gujarat are indicated in red for further discussion. Main rivers are colored blue and follow the main basins, Indus Plain and Ganges Plain (together called Indo-Gangetic Plain). The location of the Thar Desert is indicated with light brown font, the Western Ghats are indicated in black font.

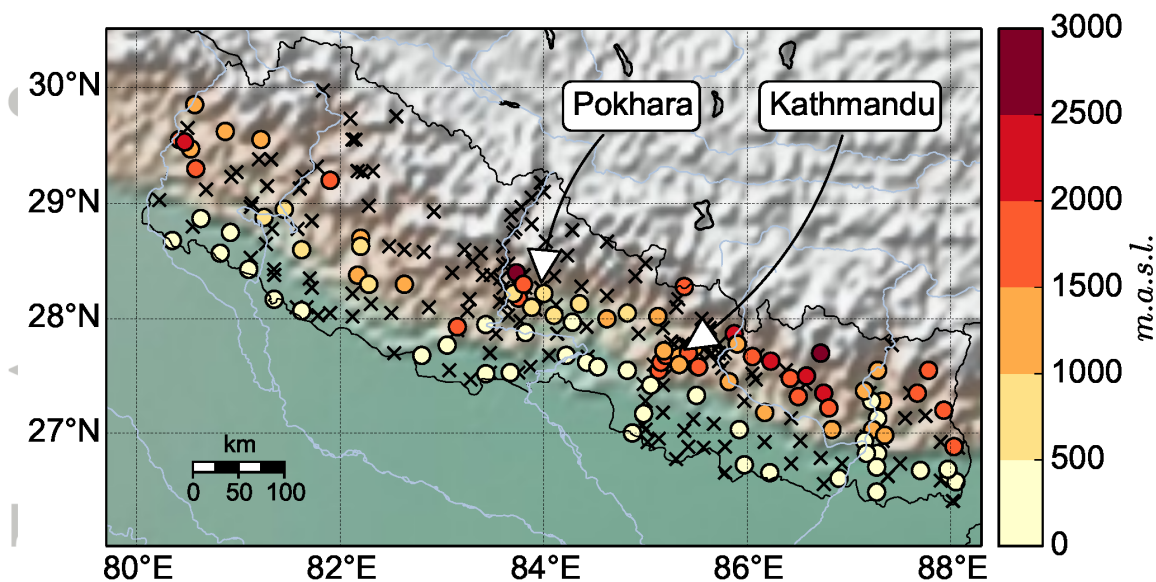


Figure 2. The location of 278 meteorological stations from the Department Of Hydrology and Meteorology (DHM) in Nepal. Stations we use for our analysis are displayed with circles and their elevation is given in meters above sea level [m.a.s.l.]. Disregarded stations in our study are marked with a cross. Regions with comparable high density population, Pokhara and the capital Kathmandu, have also a higher station density. Rivers are colored blue.

Accepted Article

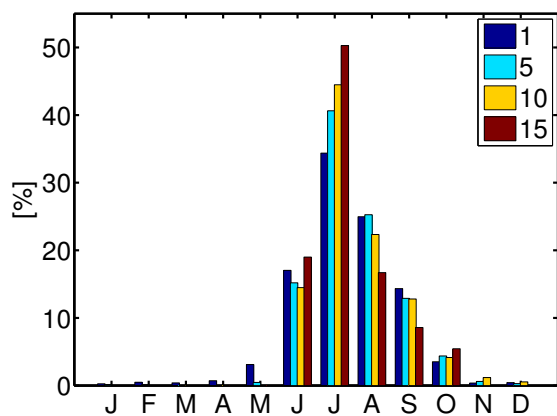


Figure 3. Monthly contribution to annual number of extreme events in [%] for a minimum of 1, 5, 10, or 15 stations indicating extreme precipitation at the same day.

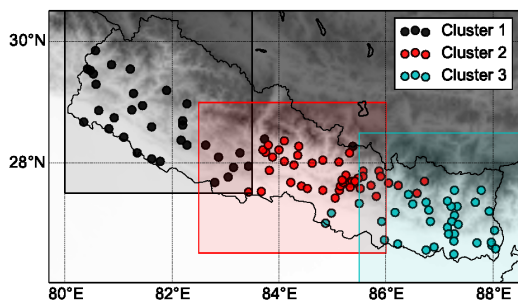


Figure 4. Result of K-means clustering with the distance metric correlation on precipitation raw data. Regions for the clusters used for moisture sources are filled in the respective colors. Topography is shaded in gray for orientation.

article
Accepted
Manuscript

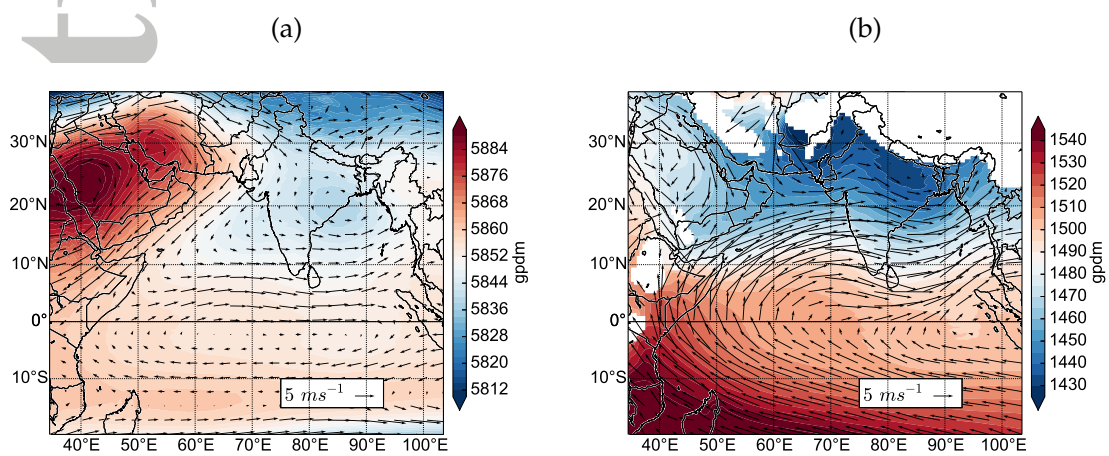


Figure 5. Geopotential height from Era-Interim averaged for June to September from 1979–2010 at a) 500 hPa and b) 850 hPa. The geopotential height contours are in geopotential decameters [gpdm] and arrows depict the wind at the respective levels.

Article

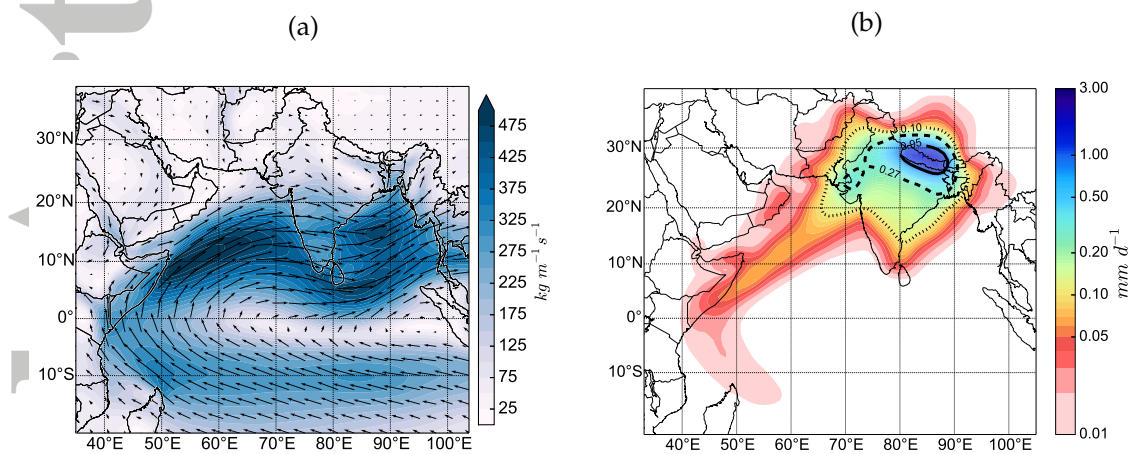


Figure 6. a) Vertically integrated moisture flux from Era-Interim (1979-2010) averaged from June to September. b) Moisture uptake for air parcels raining out over Nepal. The solid line encloses 25%, the stippled line 50% and the dotted line 75%. Note that the colorbar is logarithmic.

Accepted Article

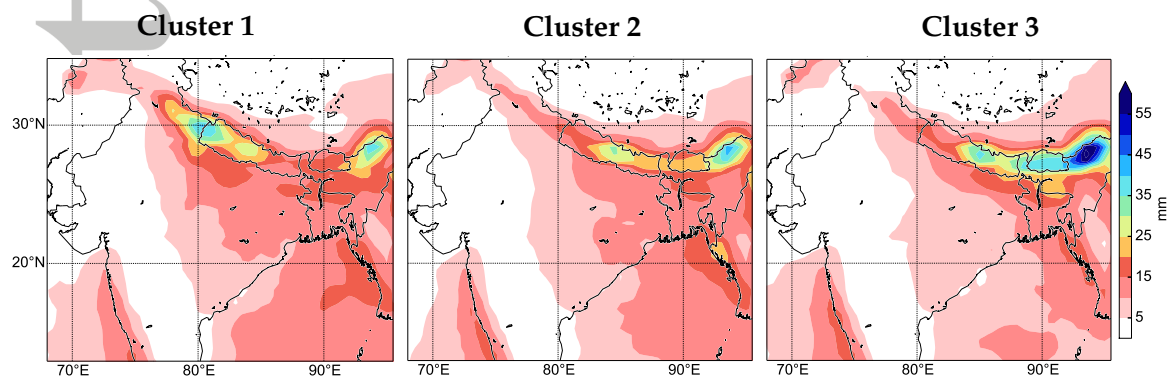


Figure 7. Composites of total precipitation from Era-Interim for all dates of extreme precipitation for cluster 1, cluster 2 and cluster 3. Daily amounts are displayed where the average is taken from 6 am of the day before to 6 am when the event is recorded. This adjustment was done to account for the time zone of Nepal.

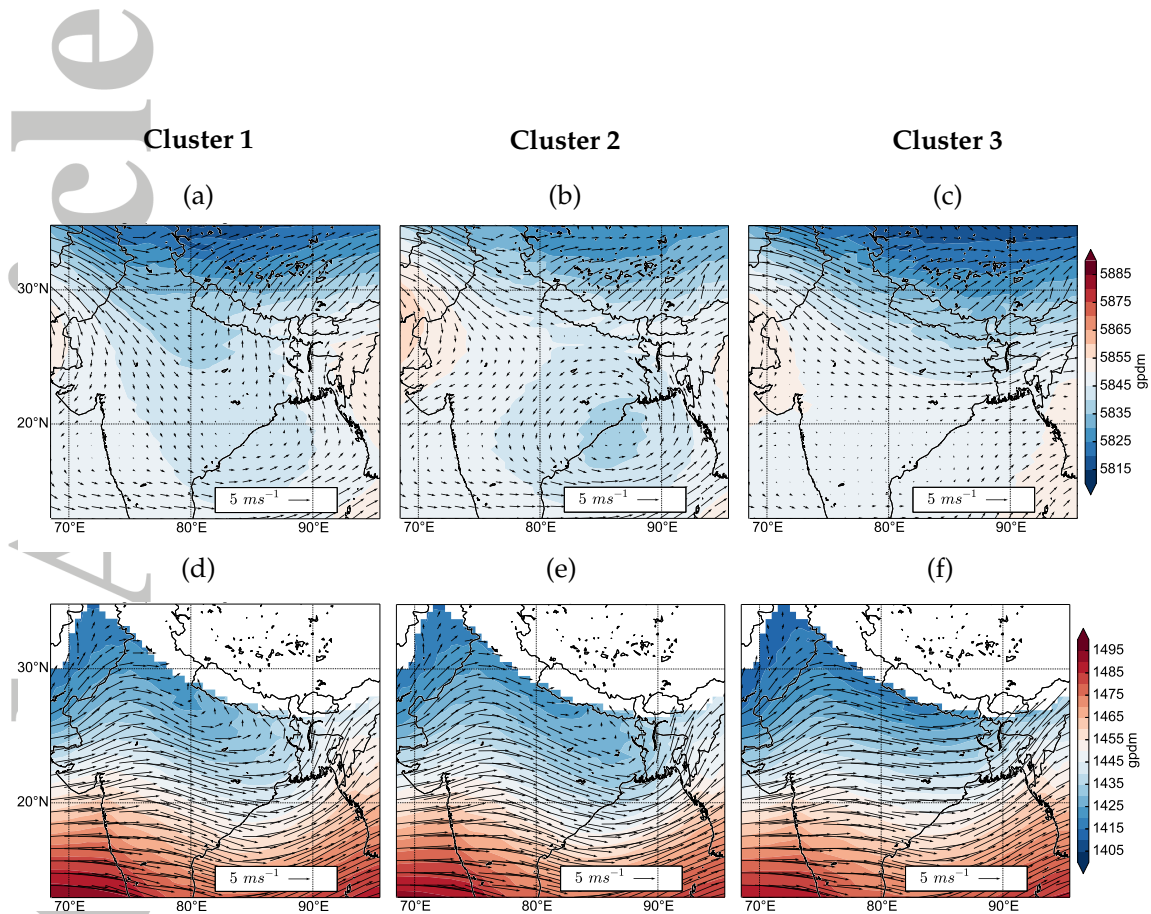


Figure 8. Era-Interim geopotential height at 500 hPa averaged over all extreme precipitation events for the period 1979-2010 from June to September a) for cluster 1 b) cluster 2 and c) cluster 3. The same for d), e), f) but at 850 hPa. The arrows indicate the wind at the corresponding height.

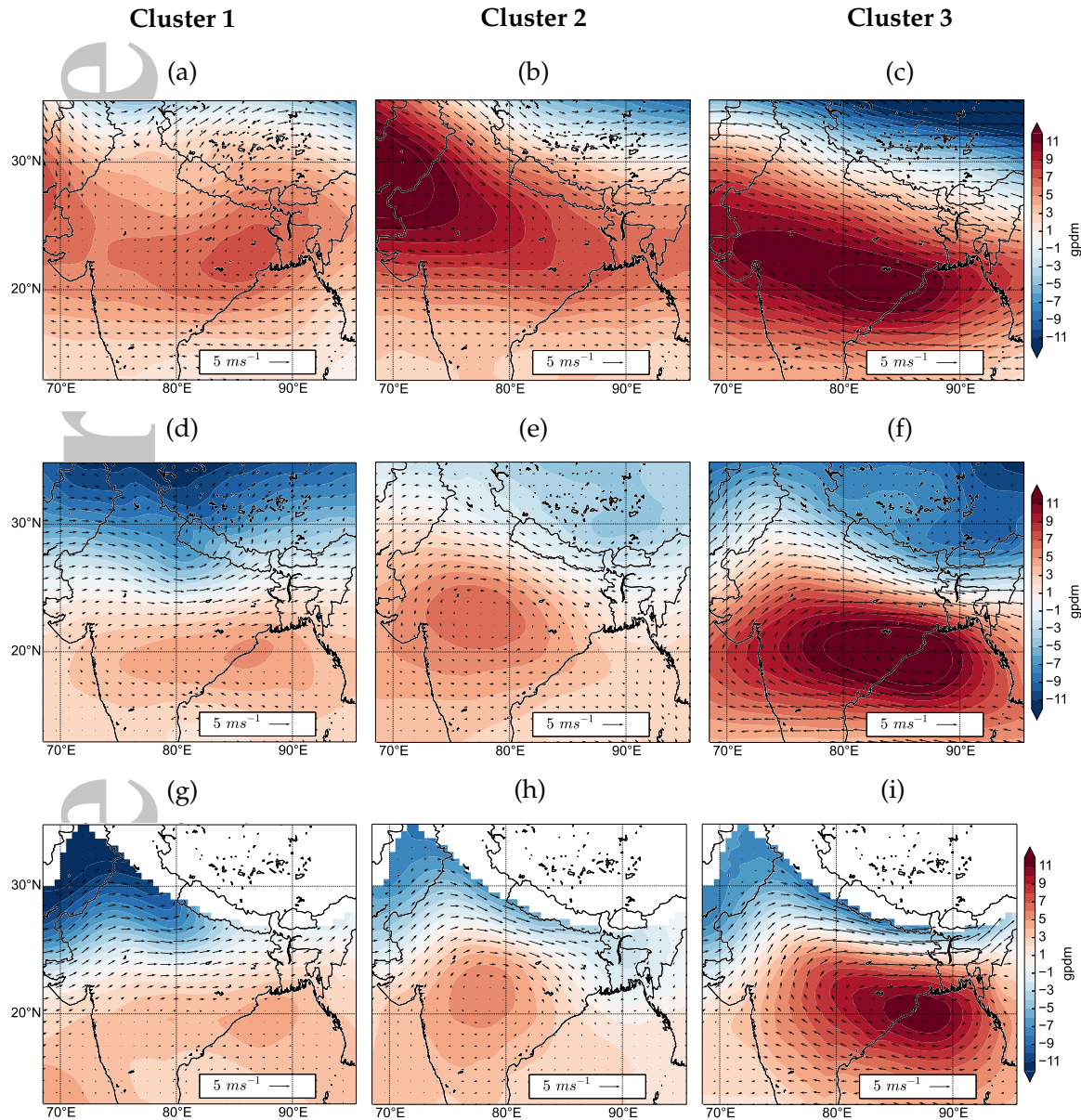


Figure 9. Geopotential height anomalies at 300 hPa from Era-Interim averaged for the period 1979-2010 from June to September a) for cluster 1 b) cluster 2 and c) cluster 3. The same for 500 hPa in d), e), and f) and 850 hPa in g), h), and i). The arrows indicate the wind anomalies at the corresponding height.

©2017 American Geophysical Union. All Rights Reserved.

Article

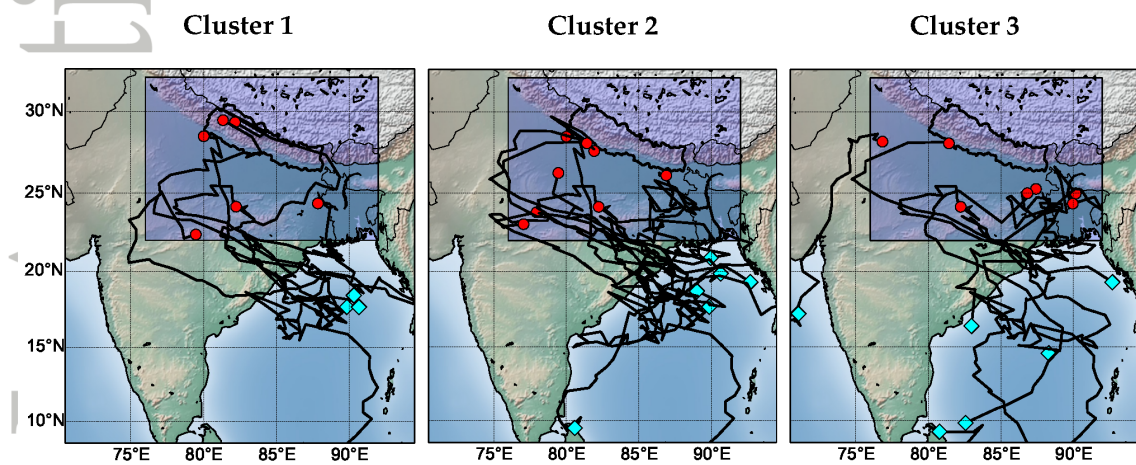


Figure 10. Trajectories of monsoon LPS that come close to Nepal during an extreme event. The blue boxes represent the target region for the LPS. Only LPS residing in this target region during an extreme event are tracked. Blue diamond represents the starting point and the red dot the end. Cluster 1: 9 LPS, Cluster 2: 11 LPS, Cluster 3: 11 LPS

Accepted Article

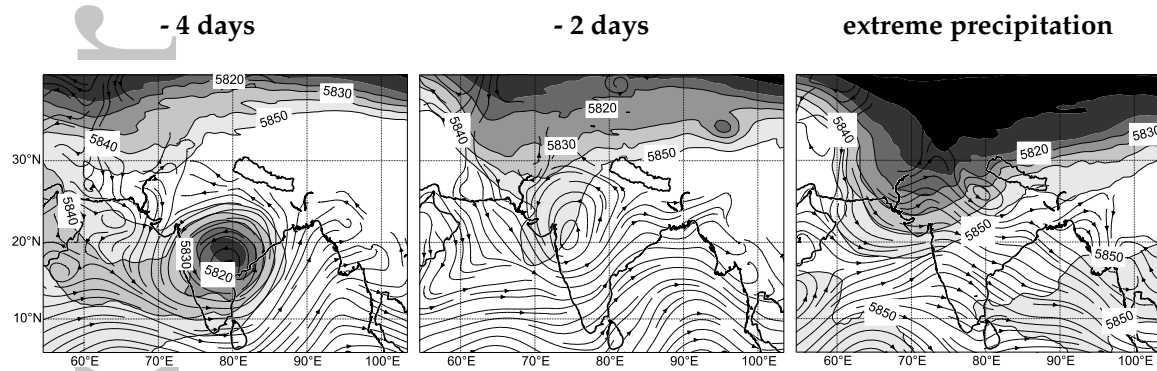


Figure 11. Streamlines illustrating the atmospheric flow field on 850 hPa prior to an extreme precipitation event in West Nepal on 25 September 2005. Contours represent the geopotential height at 500 hPa.

Accepted Article

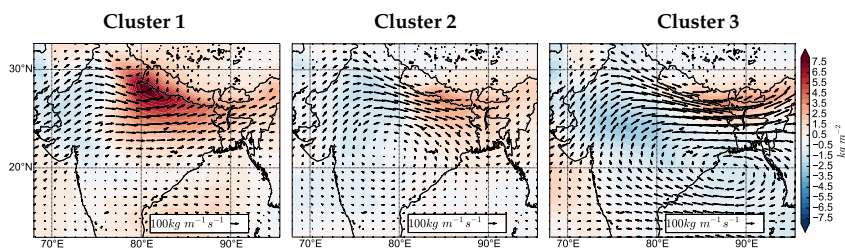


Figure 12. Vertically integrated moisture flux anomaly (arrows) composites for all extremes in the respective clusters. Total column moisture anomalies are displayed in contours.

Accepted Article

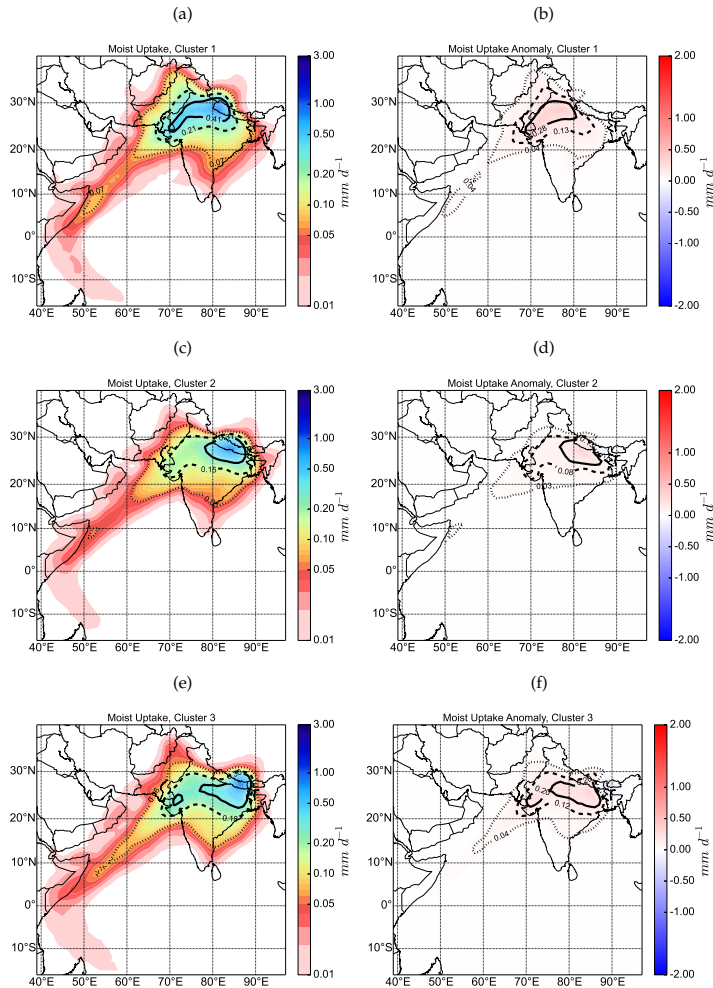


Figure 13. Composites of moisture uptake for extreme events in each cluster, a) cluster 1, c) cluster 2, and e) cluster 3. b), d), and f) depict the anomalies for these composites. The solid line encloses 25%, the stippled line 50% and the dotted line 75% of the total uptake. For the anomalies, these lines enclose only positive contributions. Note that the colorbars are logarithmic for a), c), e).

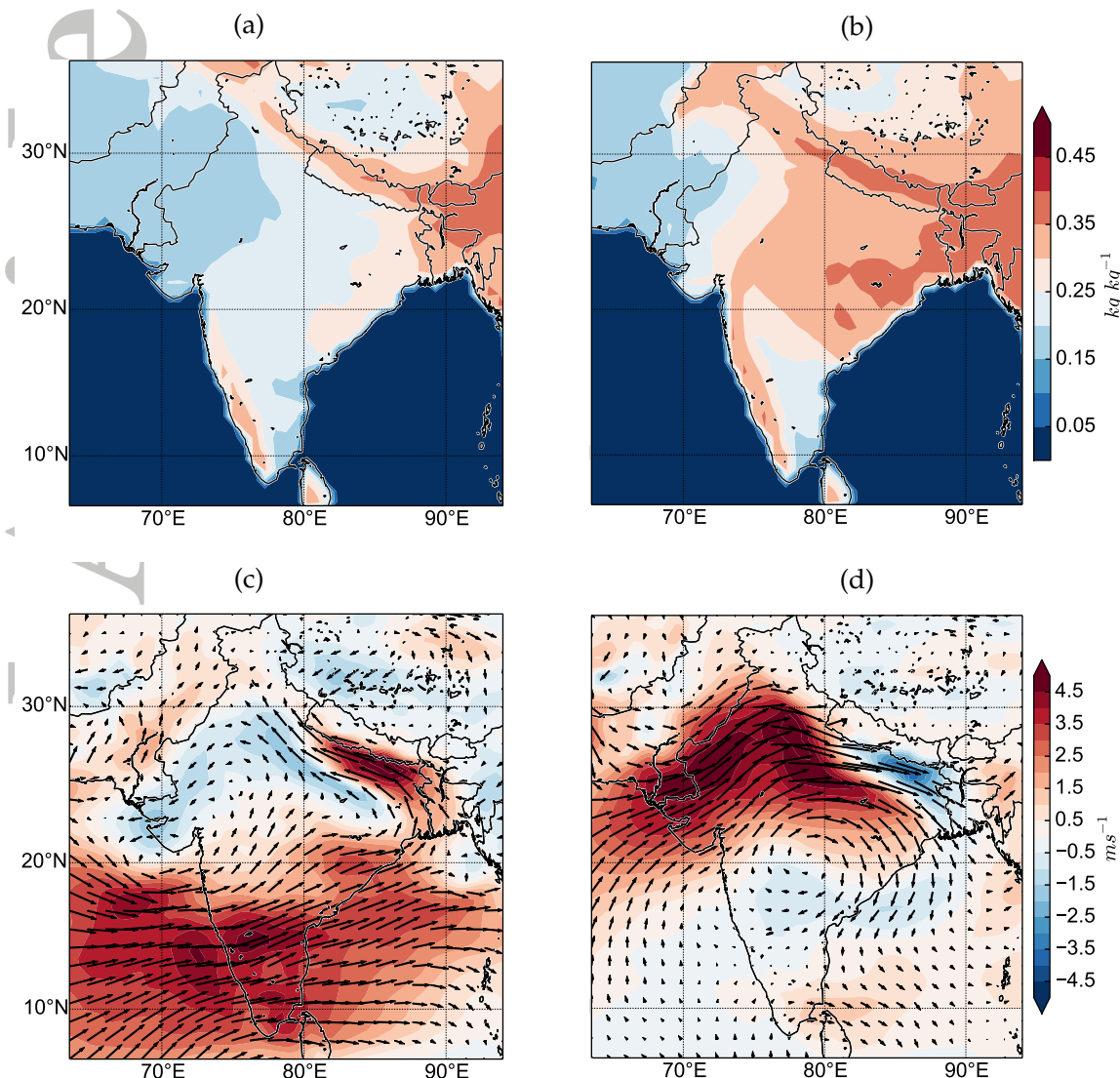


Figure 14. Monthly Mean (1979–2010) Era-Interim soil moisture for June a) and August b), and wind anomalies on 850 hPa for extreme events occurring in June c) and August d).

Accepted Article

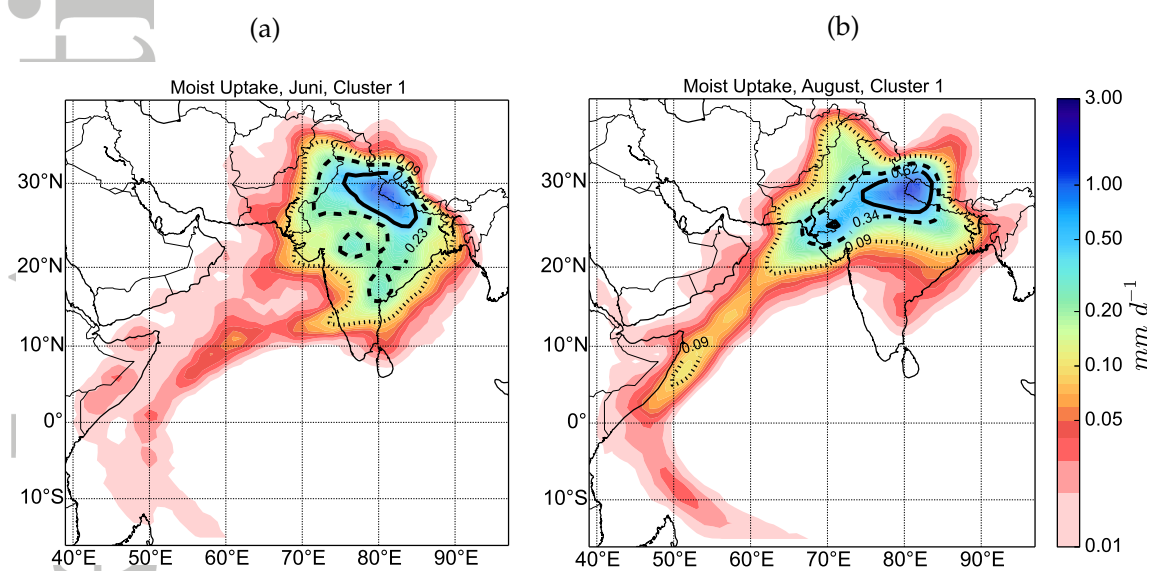


Figure 15. Moisture uptake for all extreme events at cluster 1 in June a) and b) in August. The solid line encloses 25%, the stippled line 50% and the dotted line 75%. Note that the colorbar is logarithmic.

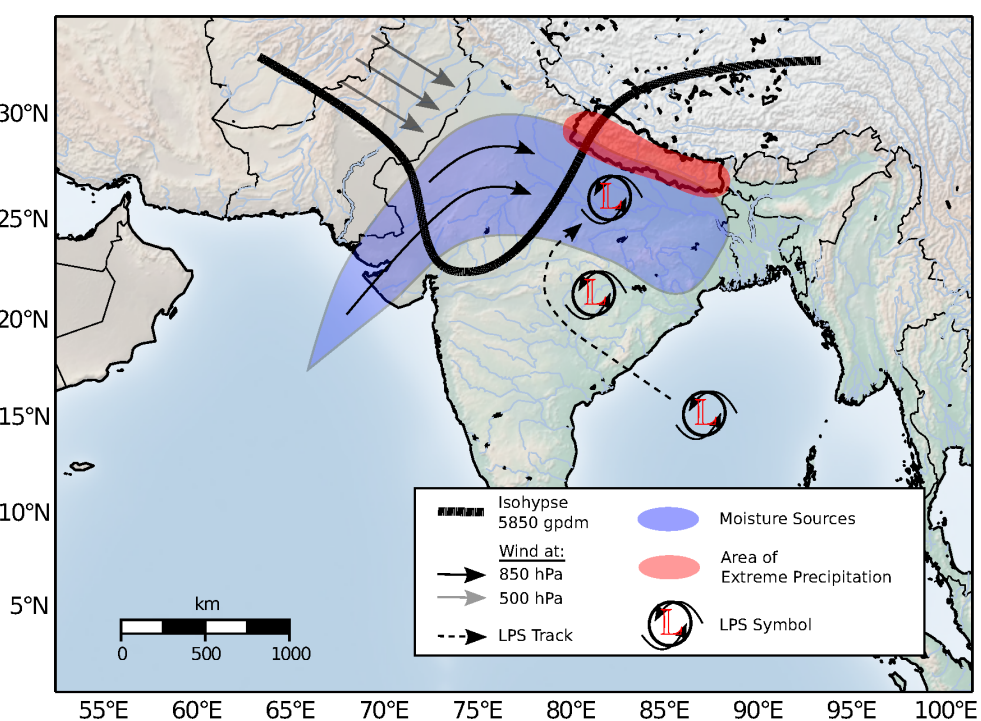


Figure 16. Conceptual sketch of processes leading to extreme precipitation in Nepal.

Paper III

7.4 Multiscale characteristics of an extreme precipitation event over Nepal

Patrik Bohlinger, Asgeir Sorteberg, Changhai Liu, Roy Rasmussen, Harald Sodemann and Fumiaki Ogawa

submitted to Quarterly Journal of the Royal Meteorological Society

Multiscale characteristics of an extreme precipitation event over Nepal

1

Multiscale characteristics of an extreme precipitation event over Nepal

Patrik Bohlinger^{*a}, Asgeir Sorteberg^a, Changhai Liu^b, Roy Rasmussen^b, Harald Sodemann^a, and Fumiaki Ogawa^a

^a Geophysical Institute, University of Bergen and Bjerknes Centre for Climate Research, Bergen, Norway

^b Research Applications Laboratory, Hydrometeorological Applications Program, NCAR/UCAR, Boulder, US

*Correspondence to: University of Bergen, Geophysical Institute, Allégaten 70, Box 7803, 5020 Bergen. E-mail:
patrik.bohlinger@gsi.uib.no

This study focuses on the analysis of the extreme precipitation event in Central Nepal on 19 July 2007 which was part of a sequence of rain events leading to the devastating South Asia flood 2007. We investigate synoptic scale conditions using reanalysis and attribute moisture sources with a Lagrangian moisture source diagnostic. Further, we characterize the mesoscale precipitation event with a high resolution numerical simulation. The simulation reveals an intense wide convective event with a simulated 40 dBZ echo core of considerable horizontal extent (1550 km^2) exceeding a height of 12 km. Initially small convective cells were invigorated by high CAPE and a potentially unstable layer at mid-tropospheric levels. This layer reached conditional instability adding latent energy to the system. Isolated convective cells organized upscale into a wide intense convective system, fueled with moist low-level inflow. The result was torrential rain with over 250 mm within 24 hours. Several synoptic scale conditions contributed to the intense development: 1) supply of moist air with the help of a typical monsoon break condition flow pattern, 2) anomalously pronounced moisture sources along this path due to prior precipitation events, 3) an upper tropospheric trough orienting the atmospheric flow against the Himalayas with associated quasi-geostrophic forcing creating a favorable environment for convection, and 4) destabilized stratification due to an upslope flow. This analysis encompasses multiple scales and shows how a wide intense convective system, not unusual for this region, can be intensified by distinct synoptic constituents.

Key Words: extreme precipitation, Nepal, South Asian monsoon, convective system, moisture sources, dynamical downscaling, Lagrangian trajectories, quasi-geostrophic forcing

Prepared using qjrms4.cls

1. Introduction

In the summer of 2007, South Asia (Fig. 1) experienced unprecedented amounts of monsoon precipitation leading to one of the worst floods during the past few decades (CNN 2007). By 4 August 2007, 20 million people were affected (CNN 2007). From 10 July until the end of July, the Nepal Red Cross Society counted 69 casualties and stated that flood and landslides affected over 262000 people in 29 districts in Nepal (Nepal Red Cross Society 2007; reliefweb 2007). During this period a sequence of precipitation events struck the country, in which one was of particularly severe magnitude. On 19 July, precipitation amounts exceeded the 99 percentile at nine stations simultaneously. The Syangja station (S0805) recorded the highest ever daily rainfall amount of 257 mm since it was installed in 1973. This paper characterizes the responsible convective event and describes the multi-scale meteorological conditions that contributed to the intense convective development. The conditions are subsequently contrasted to previous work on conditions leading to heavy precipitation events in Pakistan and Northwest India.

The occurrence of convective events over Pakistan and Northwest India have been related to distinct meteorological conditions by multiple studies. Sawyer (1947) and Houze Jr *et al.* (2007) noticed that westerly warm dry flow at mid-tropospheric levels from the Hindu Kush overran southerly low-level moist flow from the Arabian Sea and created an inversion preventing premature convection. Convection developed preferably at the rim of this inversion layer. Deep intense convection formed when the inversion was penetrated e.g. by orographic lifting of air at the foothills of the Himalayas. The low-level moist air subsequently released latent energy hurtling through the dry inversion layer and contributed to an intense convective development. Houze Jr *et al.* (2007) pointed to the high lightning frequency in the regions of a concave indent in the Himalays in Northwest India as evidence for the presence of deep convective systems.

This mechanism was confirmed in a numerical modelling study of a deep intense convective system over Pakistan (Medina *et al.* 2010). Two lids of warm and dry air had to be overcome

by the triggering mechanism in order to develop deep convection. Medina *et al.* (2010) described topographic lifting as the primary cause of convection initiation. Heating over the Thar desert and forced synoptic scale lifting on the other hand was presumably not enough to break through the capping layers. Once topographic ascent caused condensation a potentially unstable mid-level layer became conditionally unstable and could contribute to the development of a deep intense convective echo.

The described conceptual model on the occurrence of convection was followed by the question: what mechanisms contribute to the intense development of various high impact events in Pakistan and Northwest India? Enhanced moisture transport to the affected regions caused by synoptic scale features was a key ingredient (Houze Jr *et al.* 2011; Rasmussen and Houze Jr 2012; Martius *et al.* 2013; Kumar *et al.* 2014; Rasmussen *et al.* 2015). A mesoscale convective storm system leading to the flood in Leh 2010 in Northwest India was invigorated by moisture inflow from the Arabian Sea and the Bay of Bengal (Rasmussen and Houze Jr 2012; Kumar *et al.* 2014). Flooding events in Pakistan were accompanied by quasi-stationary synoptic conditions featuring an anomalous, easterly, mid-level flow transporting moisture from the Bay of Bengal to Pakistan (Houze Jr *et al.* 2011; Martius *et al.* 2013; Rasmussen *et al.* 2015). In 2010, in addition to the occurrence of wide convective systems, highly unusual stratiform systems developed in this region, moistening a broad region and contributing to large runoff (Houze Jr *et al.* 2011).

Due to the described importance of synoptic conditions, Rasmussen *et al.* (2015) investigated reasons for the quasi-stationary blocking conditions prevailing during the Pakistan flood 2010. They found signs of a Rossby wave train over Eurasia preceding the blocking and concluded that the Rossby wave train as a flood precursor could be exploited to gain skill in predictability. However, they did not investigate whether the Rossby wave was directly connected to the blocking situation and contributed to the intensification of the high pressure system. How this could be assessed was shown in Takaya and Nakamura (2005) who used the wave activity flux formulation from Takaya

Multiscale characteristics of an extreme precipitation event over Nepal

3

and Nakamura (2001). Bohlinger *et al.* (2017) demonstrated that large-scale anomalies were related to extreme precipitation in Nepal. For predictability, it would be interesting to explore a possible connection between a Rossby wave and the here investigated extreme precipitation event.

Quasi-geostrophically forced ascent, resulting from the described synoptic conditions, and orographically forced ascent, have been linked to triggering and intensification of deep convective systems in Pakistan (Medina *et al.* 2010; Martius *et al.* 2013). The forced ascent resulted in a destabilization of the air column and created a favourable environment for convection. For instance, for the Pakistan flood 2010, orographically forced ascent was assumed to have contributed to destabilization of the air column and finally triggering of the heavy precipitation events (Martius *et al.* 2013). Martius *et al.* (2013) further found a weak quasi-geostrophic forcing component which impacted the organization and initiation of precipitation.

In a composite study for Nepal, Bohlinger *et al.* (2017) considered precipitation events that contemporaneously exceeded the 99.5th percentile at multiple stations from 1979 to 2010. On average, these events were accompanied by a trough over the Himalayas and anomalously high moisture sources along the Indo-Gangetic plain. Approximately 75% of the moisture in the planetary boundary layer was picked up over land. Bohlinger *et al.* (2017) found evidence for precipitation systems preconditioning the soil moisture along the major uptake region helping to explain the unusually high moisture abundance. In addition, a noticeable influence from low pressure systems (LPS) and monsoon break periods was detected and quantified. The case study from (Houze Jr *et al.* 2017) for a flood event in Northwest India exhibits similar atmospheric flow characteristics as described in Bohlinger *et al.* (2017) for extreme precipitation events in Nepal.

The high variability among the precipitation systems investigated in the composite study of Bohlinger *et al.* (2017) does not allow to see the interaction of the involved processes for a single case. Moreover, the different nature of high impact

precipitation systems investigated close to Nepal, and the high spatial variability of rainfall and the occurrence of different precipitation systems (Houze Jr *et al.* 2007; Romatschke *et al.* 2010; Romatschke and Houze Jr 2011) along the Himalayas, makes it difficult to draw conclusions for Nepal.

In this study, we investigate a single extreme precipitation event that exceeded high percentiles at multiple stations and contributed to a devastating flooding period in Nepal and South Asia. We focus on meteorological conditions accompanying the event, in particular synoptic scale forcing, moisture sources, and model derived high resolution characteristics of the precipitating system. It will be shown how mechanisms on these multiple meteorological scales could foster an intense wide convective event. We will start with the synoptic scale context and subsequently delve into the mesoscale characteristics of the storm.

2. Data and methods

Our analysis is based on five different datasets: 1) 3-hourly precipitation from the Tropical Rainfall Measuring Mission (TRMM 3B42) (Huffman *et al.* 2007) at a quarter degree horizontal resolution, 2) 6-hourly ERA-Interim reanalysis (Dee *et al.* 2011) at 0.75 degree horizontal resolution, 3) a global trajectory dataset (Läderach and Sodemann 2016) with trajectories from the Lagrangian dispersion model FLEXPART (Stohl *et al.* 2005), 4) the output of a high resolution numerical simulation (Section 2.1), 5) and rainfall measurements from meteorological stations. The station dataset contained 273 rain gauge stations from the Department of Hydrology and Meteorology (DHM) in Nepal (Fig. 1a). The stations recorded daily precipitation sums from 9 am to 9 am local time. Nepal time is defined as UTC/GMT +05:45 hours meaning that stations recorded from 03:15 UTC to 03:15 UTC (Bohlinger and Sorteberg 2017). We used the subset of 112 stations that remained after quality control (Bohlinger and Sorteberg 2017).

2.1. WRF model setup

We conducted numerical simulations with the Weather Research & Forecasting (WRF-ARW) model (Skamarock and Klemp 2008; Skamarock *et al.* 2008) v.3.8.1 to dynamically downscale

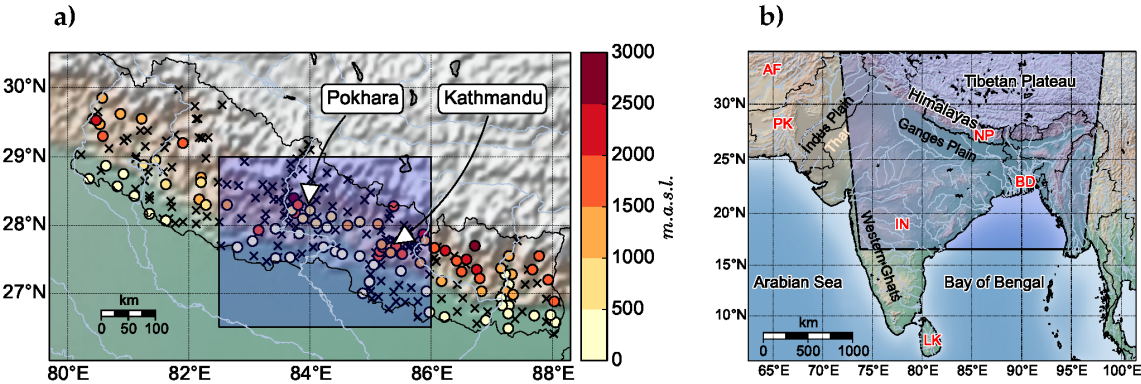


Figure 1. a) Nepal with the high density population areas Pokhara and the capital Kathmandu and the location of 278 meteorological stations from the Department of Hydrology and Meteorology (DHM) in Nepal. We use 112 stations for our analysis, displayed with circles with their elevation given in meters above sea level [m.a.s.l.]. Disregarded stations in our study are marked with a cross. The target region for moisture source diagnostic (Section 3.3) is marked with a blue rectangle. Rivers are colored blue. b) South Asia overview map displaying countries, regions, deserts, basins, and mountain chains used for orientation when discussed in the results. The blue region indicates the WRF-ARW domain for the numerical simulation of the extreme precipitation event.

Table 1. Model setup for WRF-ARW v.3.8.1.

Horizontal Resolution	4 km
Horizontal grid	612 × 502 grid boxes
Number of Vertical Levels	50
Microphysics	Thompson graupel scheme (2-moment scheme)
Planetary Boundary Layer Scheme	MYNN 2.5 level TKE
Surface Layer Scheme	MYNN
Land Surface Scheme	unified Noah LSM

ERA-Interim reanalysis. WRF has been successfully applied in comparable studies e.g. in Kumar *et al.* (2014) and Medina *et al.* (2010) to assess precipitating systems in Pakistan and Northwest India. The horizontal resolution was set to 4 km in order to resolve the mesoscale topographical features and the main features of deep convective systems which are common in the considered domain (Houze Jr *et al.* 2007; Romatschke *et al.* 2010; Romatschke and Houze Jr 2011). Due to highly complex topography, slope dependent radiation was activated. In total we simulated the period from 17 July 2007 to 22 July 2007. The precipitating system could be reproduced well using spectral nudging. Spectral nudging was only applied to the wavenumber-1 horizontal wind field above the 12th model level (roughly corresponding to 850 hPa over the ocean). Further details of the model setup are summarized in Table 1, the chosen model domain is displayed in Figure 1b.

2.2. Moisture source diagnostic

We applied the quantitative moisture source diagnostic from Sodemann *et al.* (2008) and tracked changes in moisture along FLEXPART parcels from the dataset of Läderach and Sodemann (2016) for 10 days back in time as described in Bohlinger *et al.* (2017). All parcels which entered the target region in Central Nepal defined from 26.5–29N and 83–86E (Fig. 1a) and lost moisture in the target region were tracked. Moisture source anomalies for the event were computed against a 15 days mean centered around the date of interest and averaged across the entire period (1979 to 2010).

This Lagrangian method was successfully used for Nepal in Bohlinger *et al.* (2017) and evaluated against an Eulerian model simulation by Winschall *et al.* (2014) with consistent results. The moisture source diagnostic can attribute direct moisture sources. This means that it takes into account changes of moisture along the trajectory of an air parcel. Bohlinger *et al.* (2017) demonstrated that moisture sources for Nepal obtained with this method differ significantly from previous findings contributing with additional information.

2.3. Evaluation of quasi-geostrophic forcing

As mentioned in the introduction, quasi-geostrophic forcing was found to accompany other high impact events in neighbouring

Multiscale characteristics of an extreme precipitation event over Nepal

5

countries and is therefore computed for our study. Räisänen (1995) assessed the quasi-geostrophic forcing effect on synoptic scale vertical motion across all latitudes and noticed considerable contribution to all regions but the tropics ($15^{\circ}N$ to $15^{\circ}S$). Nepal is located between $25^{\circ}N$ and $30^{\circ}N$ and could therefore experience a noticeable forcing contribution from quasi-geostrophic motion. We estimated the theoretical quasi-geostrophic forcing using the Q-vector form (Eq. 1 and Eq. 2) of the quasi-geostrophic ω -equation (Bluestein 1992).

$$\left(\nabla_p^2 + \frac{f_0^2}{\sigma} \frac{\partial^2}{\partial p^2} \right) \omega = -2\vec{\nabla}_p \cdot \vec{Q} - \frac{R_d}{\sigma p} \beta \frac{\partial T}{\partial x} \quad (1)$$

$$\vec{Q} = -\frac{R_d}{\sigma p} \begin{pmatrix} \frac{\partial v_g}{\partial x} \nabla_p T \\ \frac{\partial v_g}{\partial y} \nabla_p T \end{pmatrix} = \begin{pmatrix} Q_1 \\ Q_2 \end{pmatrix} \quad (2)$$

σ is the static stability parameter $\sigma = -T (\partial \ln \theta) (\partial p)^{-1}$ which is set to a fixed positive value of $\sigma = 2 \cdot 10^{-6}$. The geostrophic wind v_g is computed on an f-plane ($f_0 \sim \mathcal{O}(10^{-4})$) from the geopotential height. Using an β -plane assumption does not change the result. The temperature field from ERA-Interim is denoted with T . p is the pressure, ∇_p the ∇ -operator on a pressure surface, and R_d the gas constant for dry air.

Applying scale analysis, we neglected the second term on the left-hand side in Equation 1 because it is at least an order of magnitude smaller than ω due to $\frac{f_0^2}{\sigma} = \mathcal{O}(10^{-2})$. The second term on the right hand side is also neglected resulting from scale analysis. This is reasonable for mid-latitudes where the β contribution is of the order of $\mathcal{O}(10^{-11})$. Both neglected terms could contribute to effectively dampen the computed omega in either direction meaning that the quasi-geostrophic forcing effect might be slightly overestimated. Diabatic processes and forced ascent due to orographic lifting are not included such that only the destabilizing component of the trough at a specified pressure level is evaluated. Nonetheless, the main processes, divergence of Q-vectors (Eq. 3), are included to assess the effect of quasi-geostrophic forcing.

$$\nabla_p^2 \omega = -2\vec{\nabla}_p \cdot \vec{Q} \quad (3)$$

After the above-described simplifications the resulting elliptic equation (Eq. 3) for the vertical pressure tendency ω takes the form of a Poisson's equation and could be solved iteratively applying the Successive over relaxation (Press 2007) with Dirichlet boundary conditions (boundary values = 0) and a relaxation parameter of 1.5. We chose an error tolerance of $\epsilon = 10^{-4}$ as exit condition for the iterative field relaxation which is reached within 436 steps. For the transformation of the vertical pressure tendency ω to the vertical velocity w we assume hydrostatic conditions which, considering the height of the trough and the horizontal resolution of ERA-Interim, is a reasonable assumption. We further assume that at this altitude, no noteworthy amount of moisture is present and use the gas constant for dry air R_d , and the Earth's gravitational acceleration is set to $g = 9.81 \text{ ms}^{-1}$. These assumptions yield the equation for the vertical velocity (Eq. 4).

$$w = \frac{\omega R_d T}{pg} \quad (4)$$

2.4. Computing wave activity flux for a quasi-stationary Rossby wave

The value of a variable can be understood as a superposition of its mean state and a perturbation. This allows us to compute the wave activity flux as formulated in Takaya and Nakamura (2001). We use only the horizontal component in the upper troposphere and assume stationarity which yields a simplified formulation for the horizontal wave activity flux W_h (Eq. 5).

$$W_h = \frac{p \cos(\phi)}{2|U|} \begin{pmatrix} \frac{U}{a^2 \cos^2(\phi)} \cdot \left[\left(\frac{\partial \psi'}{\partial \lambda} \right)^2 - \psi' \frac{\partial^2 \psi'}{\partial \lambda^2} \right] + \\ \frac{V}{a^2 \cos(\phi)} \cdot \left[\left(\frac{\partial \psi'}{\partial \lambda} \frac{\partial \psi'}{\partial \phi} \right) - \psi' \frac{\partial^2 \psi'}{\partial \lambda \partial \phi} \right] \\ \frac{U}{a^2 \cos(\phi)} \cdot \left[\left(\frac{\partial \psi'}{\partial \lambda} \frac{\partial \psi'}{\partial \phi} \right) - \psi' \frac{\partial^2 \psi'}{\partial \lambda \partial \phi} \right] + \\ \frac{V}{a^2} \cdot \left[\left(\frac{\partial \psi'}{\partial \phi} \right)^2 - \psi' \frac{\partial^2 \psi'}{\partial \phi^2} \right] \end{pmatrix} \quad (5)$$

ϕ and λ represent latitude and longitude, a is the earth's radius, ψ' is the anomaly of the stream function defined as $\psi' = \frac{g}{f} Z'$ where f is the Coriolis parameter and Z' the geopotential height anomaly. $|U|$ represents the magnitude of the zonal wind, U the zonal wind and V is the meridional wind component at each grid point.

6

P. Bohlinger

With this equation we can explore the impact of quasi-stationary Rossby waves on the studied extreme event. Following Takaya and Nakamura (2005), we apply a low pass filter (5 day running mean) to the geopotential height field and compute the geopotential height anomaly. The anomaly is defined as the difference between a 5 day mean centered around the date of interest and a 31 day mean centered around the date of interest and averaged across the ERA-Interim years 1979 to 2010. A 31 day mean is assumed to embody the background flow. By computing the 5 day mean, we attempt to remove high frequency migratory eddies from the energy spectra and by subtracting a 31 day average, we removed the low frequency peak representing the annual cycle. The residual should then mainly stem from Rossby waves.

3. Synoptic conditions encompassing the extreme event

Prior to the precipitation event a trough in the upper troposphere (300 hPa) approached Nepal (Fig. 2a). On 19 July 2007, the day of the extreme event, this trough traversed Nepal and in the evening (12:00 UTC) it was situated over Central Nepal at the location of the extreme event (Fig. 2b). The day after, the subsequent ridge gained influence over Nepal (Fig. 2c). The trough structure oriented the flow in the upper troposphere against the Himalayas. Farther west, air was flowing down from the Hindu Kush following the isohypsides. In the lower troposphere (850 hPa) a monsoon low pressure system closed in on Nepal two days prior to the event, was redirected towards the east along the Himalayas and finally dissipated close to Bangladesh (not shown). On the day of the event the north-westerly flow, coming from the Arabian Sea, was oriented parallel to the Himalayas until it turned toward a center of low geopotential at the location of the extreme precipitation event. According to ERA-Interim and the WRF simulation (Section 4), this center of low geopotential at 850 hPa on 19 July formed after the low pressure system had turned to East Nepal and weakened. The low geopotential height on the day of the extreme event was thus the extreme event itself, mostly independent but possibly influenced by the prior existing low pressure system. Bohlinger *et al.* (2017) quantified that for 14% of the considered extreme events in Central Nepal a low pressure systems was detected in the vicinity of the extreme

precipitation event. For the present case, we note that the low pressure system was at least not directly involved in producing the recorded rainfall.

The day prior to the day of the extreme event, low tropospheric flow was blocked by the Western Ghats and developed a flow splitting over Central India which prevailed during the extreme precipitation event, lasting until 22 July (Fig. 3a). The influence of the flow blocking at 850 hPa is illustrated with the inverse Froude number (Eq. 6, red line in Fig. 3a).

$$\frac{1}{Fr} = \frac{N \cdot H}{U} \quad (6)$$

N is the Brunt-Vaisala frequency, H the height and U the wind speed. Based on the constituents of the Froude number, wind speed and stability, blocking was probably caused by reduction of the zonal wind speed over the Arabian Sea. The exact cause of the wind speed reduction is beyond the scope of this study. The low-level flow bifurcated into a southern branch curving around the southern edge of India while the northern branch coming from the Arabian Sea regorged onto the Indo-Gangetic plain and veered to the east (Fig. 3a). As the flow reached the Himalayas it was blocked and directed along the mountain range. The described flow splitting is characteristic of monsoon break periods (Joseph and Sijikumar 2004) which are connected to less rain in Central India and excess rainfall along the Himalayas. Rajeevan *et al.* (2010) defined a break period lasting from 18 July to 22 July affirming that the extreme precipitation event occurred in fact during a break period. Bohlinger *et al.* (2017) quantified that during July and August at least 26% of the extreme events in Central Nepal occurred during break conditions. Our result illustrates this connection for a single event where the characteristic low-level flow was a consequence of a flow blocking by the Western Ghats due to a reduction of the zonal wind.

In the middle (500 hPa) and upper (300 hPa) troposphere, air emanated from the Hindu Kush onto the Indus plain (Fig. 3b,c). Over Nepal the flow was directed partly along the Himalayas and partly directed toward them as dictated by the geopotential

Multiscale characteristics of an extreme precipitation event over Nepal

7

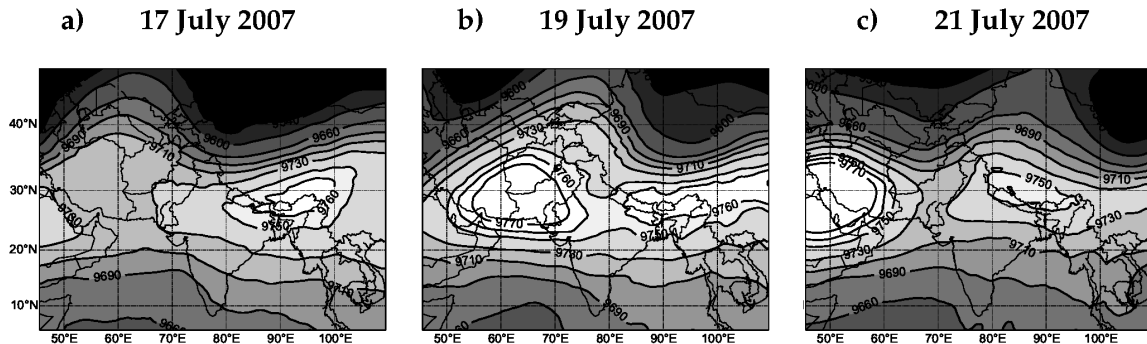


Figure 2. Geopotential height over South Asia at 300 hPa for 17 July 2007, 19 July 2007 (day of extreme event), and 21 July 2007.

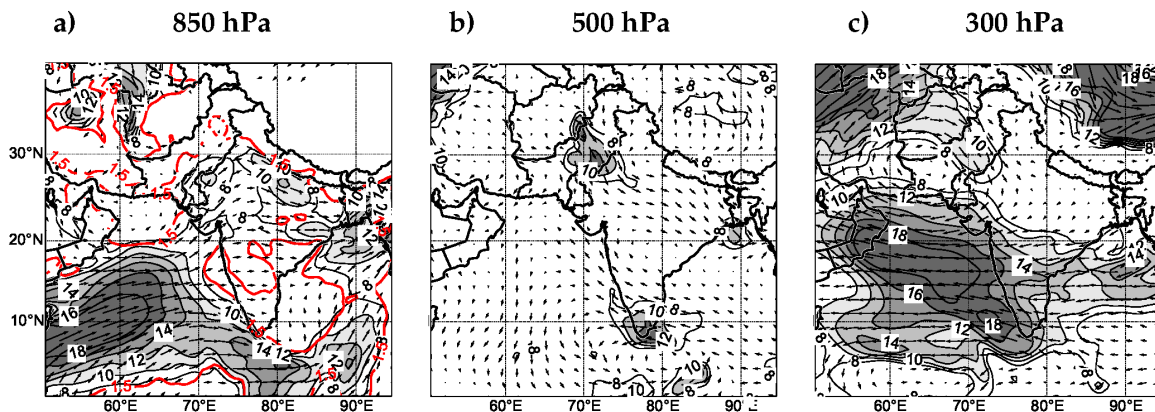


Figure 3. ERA-Interim fields for 19 July 2007. Wind at 850 hPa (a), 500 hPa (b), and 300 hPa (c). Isotaches are labeled with wind speed in m s^{-1} . The wind direction is illustrated with arrows. The isoline of the inverse Froude number at 850 hPa $h=1.5$ is depicted in red (a).

height pattern (Fig. 2b). This further illustrates that there was a considerable vertical shear over the Indus plain where the air flowed with a wind speed up to a strong breeze ($> 10 \text{ m s}^{-1}$) in opposite directions on different levels. However, over Central Nepal, where the here considered precipitation system developed, the shear was comparably low. Such an environment is characteristic of the development of deep and wide intense echoes in this region (Houze Jr *et al.* 2007).

In our study, we have synoptic conditions reminiscent of the findings in Houze Jr *et al.* (2007). We identified a moist low-level inflow from the Arabian Sea and in mid- and upper-levels dry and warm air flowing from the Hindu Kush to the southeast overrunning the moist low-level flow. This is indicated in Figure 3 and is supported by radiosonde soundings from stations in Jodhpur and New Delhi (<http://weather.uwyo.edu/upperair/sounding.html>,

not shown). Especially in the mid-troposphere the direction of the flow from the Hindu Kush is directed to the east, parallel to the Himalayas (Fig. 3b). Following the findings from Sawyer (1947), Houze Jr *et al.* (2007) and Medina *et al.* (2010), the fact that the moist low-level air was capped might have prevented premature convection and by this aided the transport of moisture further to Nepal. The specific thermodynamic environment at the site of the extreme event is investigated in Section 4.2. There, it will be shown, that the dry continental air reached all the way to Nepal accommodating a favourable environment for the extreme event.

3.1. The role of quasi-geostrophic forcing

To investigate the influence of the above described upper tropospheric trough (Fig. 2b), we estimated the theoretical quasi-geostrophic forcing on the day of the extreme event. Forced large-scale ascent was present ahead of the trough (Fig. 4a) which

is in agreement with quasi-geostrophic theory. The estimated magnitude of the forced ascent constituted 0.5 to 3 cm s^{-1} over Nepal which results in a rise of roughly 100 m to 600 m within the 6 hourly time step in the ERA-Interim output. This makes quasi-geostrophic forcing a possible contributor for destabilizing the air columns and by that preparing a favourable environment for subsequent triggering of convection. Given that we neglected the β -term and the second term on the left-hand side, our computed vertical velocity might be slightly overestimated. Entrainment processes during the ascent will also deteriorate the net forcing effect.

The pattern of the vertical velocity field in ERA-Interim and WRF (not shown) is similar to the precipitation field (Fig. 4 b) and hence seemed to be governed by the related diabatic heat release which is not taken into account in the here applied Q-vector formulation. Nonetheless, the alignment of precipitation anomalies in ERA-Interim and precipitation in TRMM with the upper tropospheric trough is striking (Fig. 4). The quasi-geostrophic forcing was weak in our case but might still have prepared a suitable environment for the development of the considered precipitation event.

During the Indian summer monsoon there is generally significant precipitation along the Himalayas and in the Bay of Bengal, visible in rainfall climatologies, e.g. Houze Jr *et al.* (2015) and Bohlinger and Sorteberg (2017). Nonetheless, for our case, not only absolute precipitation but also considerable positive precipitation anomalies are aligned along the trough suggesting that a destabilizing component from quasi-geostrophic forcing was present. The lack of precipitation over large parts of the Tibetan Plateau despite quasi-geostrophic forcing might be related to deficient moisture over this region (Wang and Gaffen 2001). Another hint that large-scale forcing played a role in triggering the extreme event is that we could not simulate the event without applying spectral nudging.

Our results are consistent with Martius *et al.* (2013) who investigated the influence of upper-level dynamics on the Pakistan flood in 2010. They found an upper-level potential vorticity (PV)

anomaly with the presumed main effect of orienting the lower-tropospheric flow against the mountains, forcing orographic uplift. The related quasi-geostrophic forcing over Pakistan was estimated applying a PV-inversion technique together with the evaluation of the quasi-geostrophic omega equation. The forced large-scale ascent was estimated up to 1 cm s^{-1} over Pakistan. Martius *et al.* (2013) stated that the upper-level forcing contributed in particular to the alignment of the low-level flow against the mountains. The upper-level forcing further impacted the spatial organization and initiation of precipitation consistent with our findings.

3.2. Rossby wave train from Europe

We dwell on the quasi-geostrophic theory and explore in the following whether the trough structure was associated with a quasi-stationary Rossby wave train and where it was excited. As mentioned in the introduction, a connection between the extreme event and a Rossby wave could add predictive skill.

Geopotential height anomalies depict the structure of a Rossby wave train across Eurasia with anomaly maxima propagating toward east (Fig. 5a,b,c) similar to Rasmussen *et al.* (2015). A week prior to the extreme event this pattern had not yet established (not shown). Two days prior to the extreme event a negative anomaly west of the British Islands represented a strong source emitting wave activity flux to the east (Fig. 5a). The positive anomaly to the east over central Europe was followed by two negative anomalies farther east which subsequently amplified (Fig. 5b). A positive anomaly over Russia started to amplify on the day of the extreme. The wave activity fluxes in Figure 6 (a-b) indicate the maintenance of a negative anomaly over Nepal as part of the Rossby wave train. The negative anomaly over Nepal already existed prior to receiving wave activity flux and therefore did probably not originate west of the British Islands. Rather, the Rossby wave train may have enhanced the persistency of the anomaly over Nepal through the period of the extreme precipitation event (Figure 6a-c).

A measure for the propagation path of the quasi-stationary Rossby wave (so called the Rossby-wave guide) is the axis of the zonal westerly background wind (Fig. 5d). The described splitting

Multiscale characteristics of an extreme precipitation event over Nepal

9

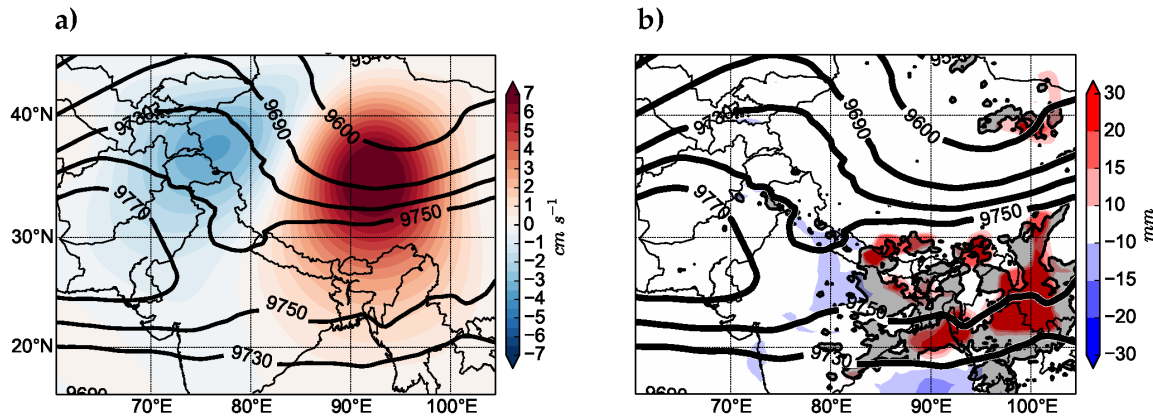


Figure 4. a) Quasi-geostrophic forcing with a maximum of 7.7 cm s^{-1} (filled contours) and contour lines depicting geopotential height at 300 hPa on 19 July 2007 12:00 UTC. b) Precipitation anomalies (color coded) in ERA-Interim are averaged from 06:00 UTC to 06:00 UTC to obtain a daily mean and adjust for the time zone of Nepal. TRMM 3B42 (03:00 UTC to 03:00 UTC) precipitation larger than 10 mm is shaded in grey.

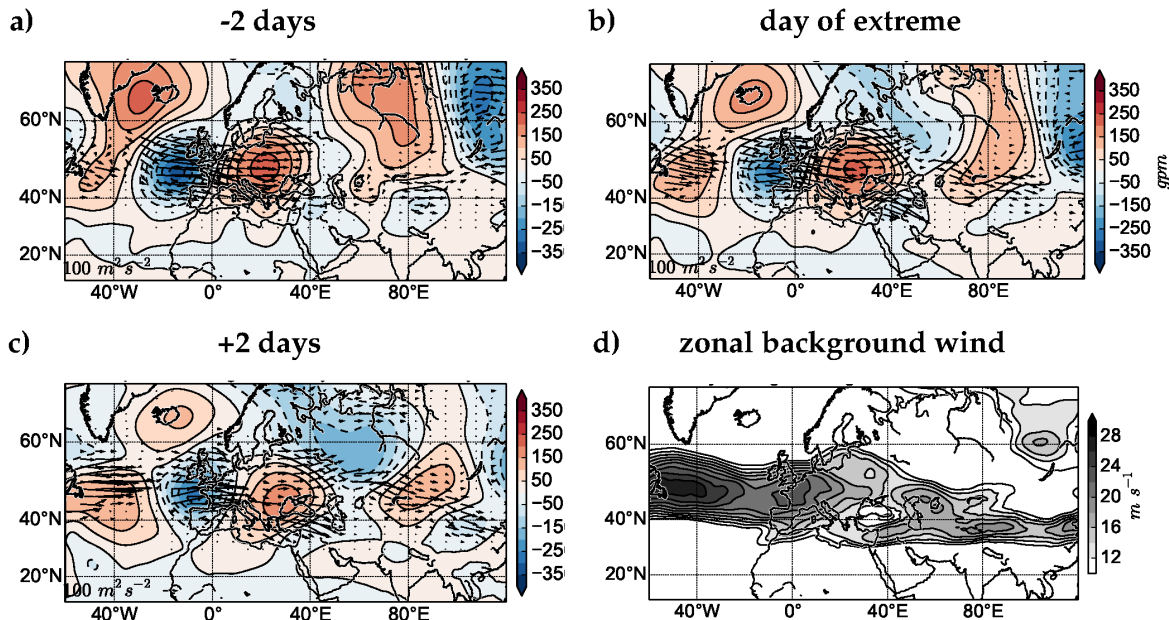


Figure 5. 300 hPa geopotential height anomalies (filled contours), wave activity flux (arrows), and the zonal background wind (shaded grey). 2 days prior to the extreme event (a), for the date of the extreme event (b) and for 2 days after (c). Coastlines and Nepal are plotted with black lines.

of the wave activity flux to a northern and southern negative anomaly coincides with the background flow which exhibits a split at the same location.

filtered by the 5-day running mean. This is because splitting of the continuous atmospheric energy spectrum into bins of frequencies is not unambiguous.

3.3. Moisture flux and moisture sources

3.4. Moisture flux

We find considerable total column integrated moisture flux along the Himalayas on the date of the extreme event (Fig. 6). The shape of the moisture flux resembles the low-level flow shown in

10

P. Bohlinger

(Fig. 3), which is characteristic of break periods (Rajeevan *et al.* 2010). The division into a southern and northern branch enabled high moisture fluxes to reach the Himalaya mountain barrier and thus supplied moisture for the observed excess precipitation along the Himalayas. A large moisture transport along the northern branch might be a generic mechanism during break periods which could help to explain the relationship between break periods and extreme precipitation along the Nepal Himalayas found by Bohlinger *et al.* (2017). The precipitation system that developed on the day of the extreme event could consequently tap into moist air coming from the Arabian Sea contributing to the intensity of the event.

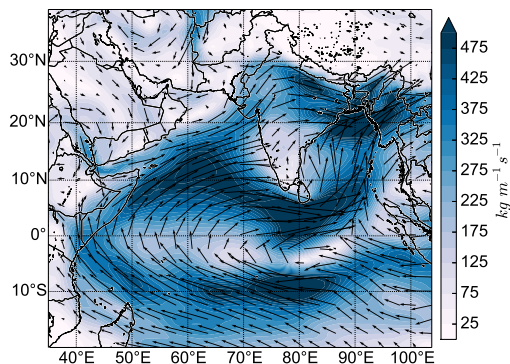


Figure 6. Vertically integrated moisture flux over South Asia from ERA-Interim, averaged over 19 July 2007 06:00 UTC to 20 July 2007 06:00 UTC.

3.5. Moisture sources

The observed high moisture abundance raises the question where the moisture originated. Direct moisture sources for precipitation (Fig. 7a) in Nepal two days prior to the extreme event mirror the location of the low pressure system described in Section 3. Moisture sources depict a pathway from the Arabian Sea across Central and North India to the Bay of Bengal turning north to Nepal (Fig. 7a). The main weight of moisture sources is situated around the position of the low pressure system at that stage. In this phase the low-level flow clearly had not yet fully developed the splitting characteristics as the pathway of moisture sources was still crossing Central India. Most of the moisture was picked up over land (70%) with India (29%) as main contributor (Tab. 2). Although the low pressure system originated over the Bay of Bengal, the Arabian Sea is a larger moisture source (24%) than

the Bay of Bengal (6%). This indicates that the original moisture in the low pressure system, possibly from the Bay of Bengal, had already rained out and was replaced by moisture taken up over land. The positive anomalies of moisture sources support this conclusion (Fig. 7c). The anomaly values are weak in absolute numbers which is matching an ordinary rainy day in Nepal. The additional moisture sources were located mainly over India (52%) and the Bangladesh (7%).

As the low pressure system moved east and weakened, the flow direction shifted and the flow splitting fully developed (Fig. 3a). The direct moisture sources for the extreme precipitation event (Fig. 7b) were located along the northern branch of moisture transport (Fig. 6) over the Indo-Gangetic plain. Most of the moisture stemmed from the countries India (53%), Pakistan (17%), and Nepal (13%) which also depicted the largest positive anomalies (Tab. 2). Almost all of the additional moisture was taken up over land (97%). The anomalies are more pronounced and depict a distinct area of high positive values along the Indo-Gangetic plain. There was only little additional uptake in the Bay of Bengal, over Bangladesh, and Northeast India for precipitation (Fig. 7d). These are regions where, during the monsoon, the air is very moist in general. On the other hand, the moisture sources over comparably dry regions, such as the Thar desert, exhibited a strong positive anomaly. How can such an anomaly develop in these dry regions?

3.6. Preconditioning the soil for moisture uptake

Bohlinger *et al.* (2017) presented evidence that the soil in the moisture source region might have been moistened by previous precipitation events prior to the moisture uptake that was directly related to extreme events. Medina *et al.* (2010) and Martius *et al.* (2013) discussed the possibility that soil moisture from previous events might have contributed to heavy precipitation events over Pakistan. Martius *et al.* (2013) noticed significant moisture uptake over land together with wet soil moisture anomalies, possibly from precipitation events prior to the moisture uptake. In our case, there was considerable precipitation along the moisture source region within 15 days before the extreme precipitation event (Fig. 8). ERA-Interim (Fig. 8a) and TRMM (Fig. 8b) depict a long area

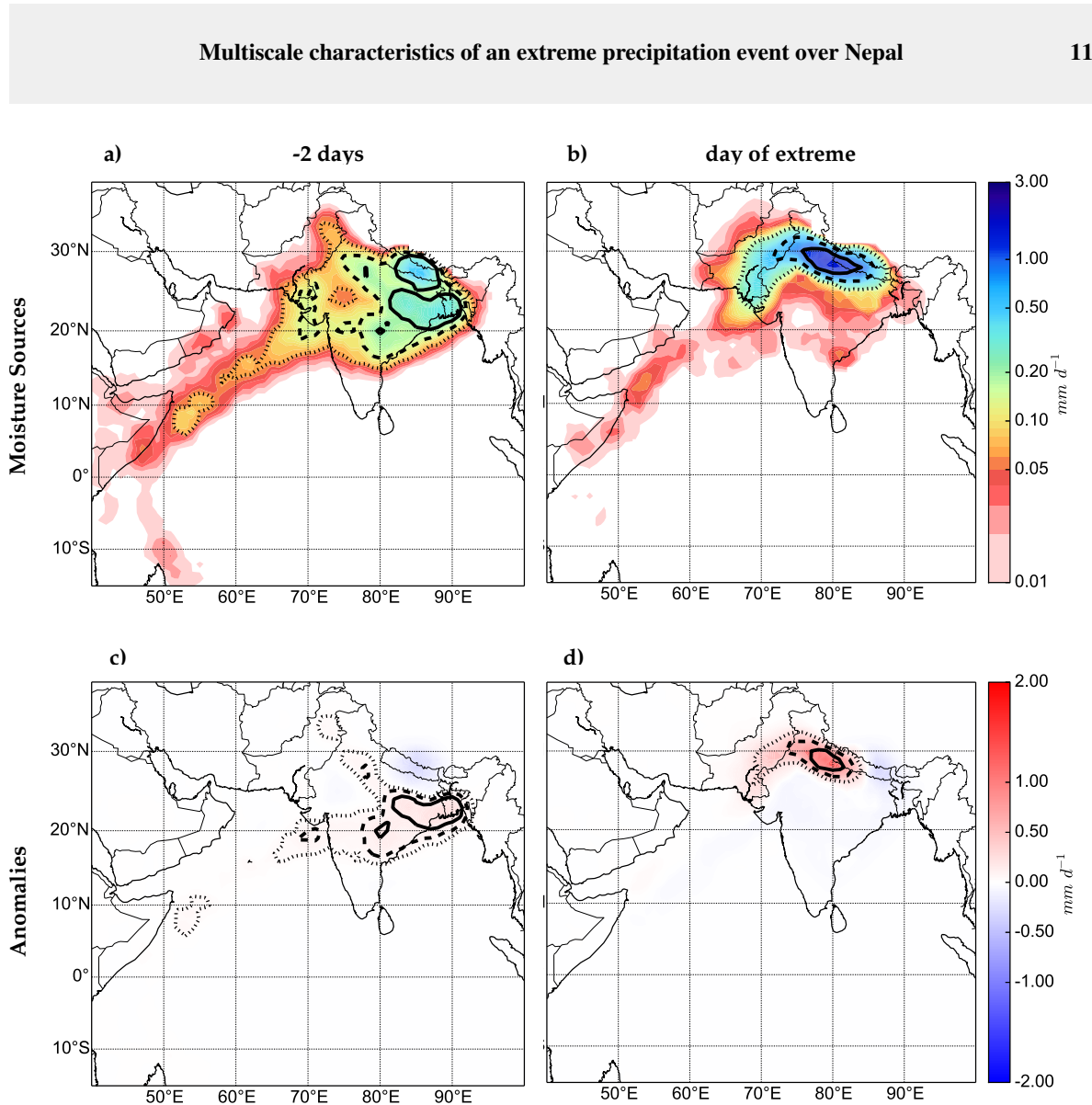


Figure 7. Moisture sources (a,b) and moisture source anomalies (c,d) for FLEXPART parcels entering the domain depicted in Figure 1 for 2 days prior to the event (a,c) and for the event (b,d). Moisture sources were averaged over 24 hours from 6 UTC to 6 UTC. The 75, 50, and 25 percentiles are marked with a solid, dashed, and dotted line. Anomalies were calculated against a 15 days climatological mean over 1979–2010 centered around the single event. In the anomaly panels the percentiles are computed only for the positive anomaly. Note that the colourbar for moisture sources is logarithmic and that for the anomalies linear.

Table 2. Contribution to the total moisture supply and, in parenthesis, the positive moisture anomaly in [%] for selected countries and regions along the moisture pathway for the extreme precipitation event. Regions are abbreviated in the table below as follows: AS = Arabian Sea, BoB = Bay of Bengal, SH = Southern Hemisphere.

Country/Region	Nepal	Pakistan	India	Bangladesh	Land	AS	BoB	SH
2007-07-18								
Moisture Sources	4	3	29	4	70	24	6	4
Anomalies	0	3	52	7	66	24	10	3
2007-07-20								
Moisture Sources	13	17	53	0	91	9	0	1
Anomalies	10	24	61	0	97	3	0	0

of precipitation stretching along the Himalayas and the region of increased moisture uptake. TRMM exhibits a pronounced local precipitation maximum just where the low pressure system

closes in on Central Nepal. The spatial precipitation pattern in ERA-Interim agrees generally well with TRMM 3B42 data although ERA-Interim underestimates the highly regional rainfall

amounts. In particular, the precipitation related to the low pressure system is underestimated in ERA-Interim. The lower resolution in ERA-Interim might be responsible for the underestimation and smoothed precipitation field.

We assess the connection between previous rainfall events and moisture sources by comparing the location of the Lagrangian particles with the surface latent heat flux in ERA-Interim. Two days prior to the precipitation event, the air parcels arriving at Central Nepal, were located over a region with considerable surface latent heat flux (Fig. 9a). While they resided or traveled over the region with pronounced surface fluxes their moisture content increased. This indicates a moisture source in the applied method (Section 2.2). As the parcels moved, also the surface fluxes increased along their way, such that there were constantly high surface fluxes underneath (Fig. 9b). This co-location of air parcels and high surface latent heat flux illustrates that the moisture increase along the FLEXPART trajectories is physically consistent with ERA-Interim.

To further verify the connection between the surface latent heat flux and the moisture sources, we test whether the moisture was taken up close to the ground. On 18 July, 12 UTC, 44% of the parcels were below 1000 m and 76% were below 2000 m. On 17 July 12 UTC, 39% of the parcels were below 1000 m and 76% were below 2000 m. Not only were most parcels close to the ground, but also most of the moisture was taken up at low elevation. For instance, on 17 July between 06:00 UTC and 12:00 UTC 82% of the moisture uptake could be assigned to parcels residing below 1000 m. This supports the assumption that the moisture evaporated from the surface. Hence, not horizontal advection in the free troposphere but rather the availability of soil moisture, established by preconditioning precipitation events, was crucial for feeding the extreme precipitation event with this large amount of moisture. The strong surface fluxes are consistently present in our WRF simulation (not shown) passing on the information on soil moisture to the high resolution simulation.

4. High resolution characteristics of the extreme event

Although ERA-Interim exhibits a precipitation pattern qualitatively similar to TRMM it does not develop the same magnitude of precipitation and underestimates the daily precipitation recorded by the stations at least by a factor of four. This might be due to the low horizontal resolution. To overcome this problem and to gain more insights into the nature of the simulated precipitation system and its thermodynamic environment, we simulated the extreme precipitation event with the WRF model. In the WRF simulation the main precipitating system was initiated between 09:00 UTC and 12:00 UTC. Smaller convective cells started to develop and organized upscale such that at 12:00 UTC a deep and wide convective system was clearly visible over Central Nepal (Fig. 10). This high convective cloud top is visible in an Meteo 7 satellite IR image (Fig. 10a) at 18:00 UTC just at the rim of the Himalayas as a round white area in the middle of Figure 10a. At 12:00 UTC the system was not yet visible in Meteo 7 images indicating an early initiation in WRF. In the TRMM 3B42 data this time-lag can be better assessed. Smaller precipitating systems start to form around 12:00 UTC and develop into the full size event until 15:00 UTC depicting considerable precipitation over Central Nepal. This implies a time-lag in WRF of up to 3 hours.

The daily rain amount is depicted in Figure 11 to show the similarities between TRMM 3B42 (Fig. 11a), WRF (Fig. 11b), and rain gauges. WRF simulates an intense rainfall event close to the region indicated by TRMM and the rain gauges. The simulated daily rainfall amounts match well with the magnitude of the measured rain and the horizontal extent is comparable between TRMM and WRF. There is a slight spatial and temporal offset in the simulation compared to TRMM. Both TRMM and the simulation deviate from the station data. TRMM seems to overlook precipitation amounts up to 50 mm at some single stations scattered across Nepal (Fig. 11a). WRF overestimates precipitation in the east of the country where multiple convective cells were triggered in the simulation (Fig. 11b). Unfortunately, there was no overpass of the TRMM satellite during the event such that we could not compare the simulation results with TRMM

Multiscale characteristics of an extreme precipitation event over Nepal

13

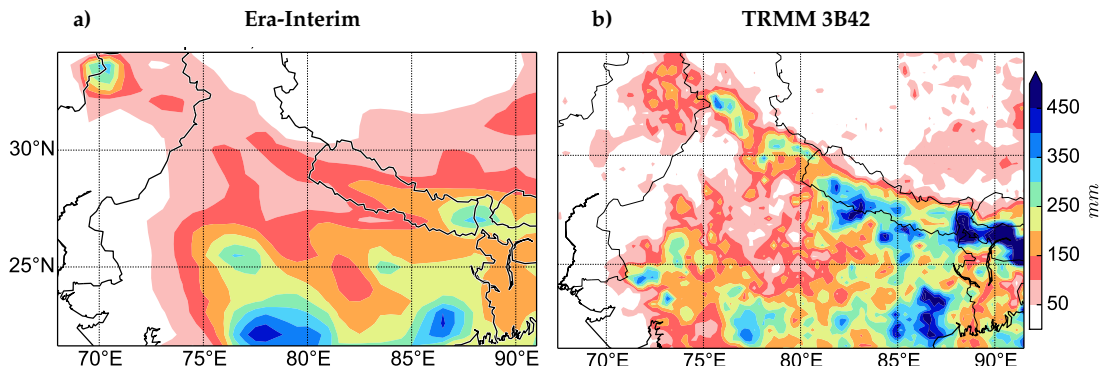


Figure 8. Total precipitation in ERA-Interim (a) and TRMM 3B42 (b) for the period of 15 days prior to the event on the 19 July 2007.

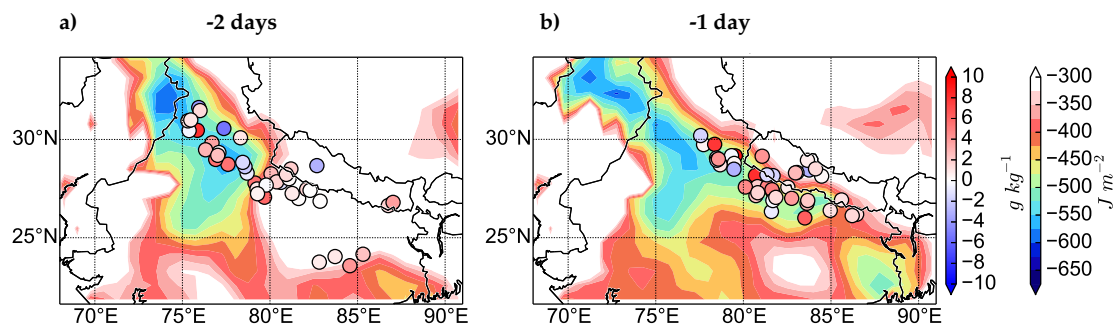


Figure 9. FLEXPART parcels with their moisture change during the last 6 hours for 2 days prior (a) and 1 day prior (b) to the considered precipitation event. Surface latent heat flux from Era-Interim is depicted in filled contours.

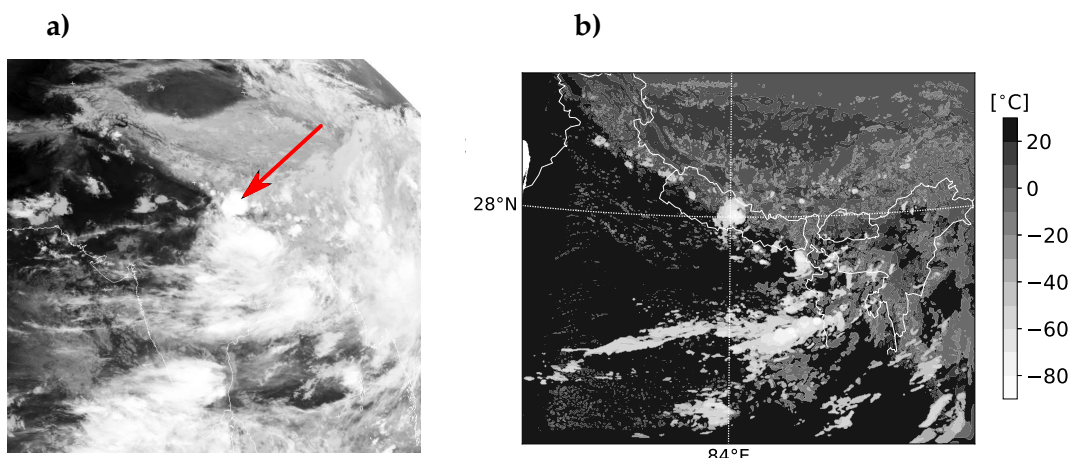


Figure 10. a) Meteosat 7 IR image 18:00 UTC from <http://www.sat.dundee.ac.uk/> without available scaling. b) WRF simulated cloud top temperature 12:00 UTC. The red arrow shows the location of the convective event.

high resolution 3D data. However, given the described similarities and the fact that WRF could simulate an intense rainfall event, we continue analyzing our WRF simulation.

4.1. Rainstorm characteristics and evolution

The simulated rain storm developed during the afternoon when single convective cells were initiated (Fig. 12). The main

14

P. Bohlinger

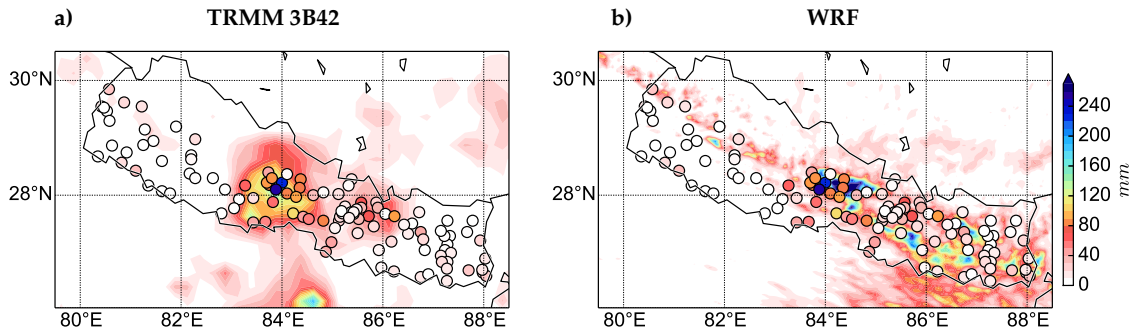


Figure 11. Daily precipitation from meteorological stations (filled circles), TRMM 3B42 (a), and WRF 4 km (b). Daily precipitation is defined here from 03:00 UTC to 03:00 UTC to adjust for the measurement period of the stations and time zone in Nepal.

precipitation system reached its maximum in the evening around 12:00 UTC (17:45 Nepal time). Despite the mentioned time-lag also in TRMM the initiation of the main convective system occurred in the evening which is consistent with findings from Romatschke *et al.* (2010) who investigated the diurnal cycle of precipitation from deep and wide convective cores over land in South Asia. They conclude that deep convective cores exhibit almost exclusively a maximum between noon and midnight. Wide convective cores were found to have a maximum in the evening together with a second maximum between midnight and early morning. Both in the WRF simulation and in TRMM we find a continuation of precipitation possibly forming a second local maximum before dawn. However, neither the simulated reflectivity and cloud top temperature, nor the precipitation intensity in WRF and TRMM compare with the magnitude of the first convective system. We will therefore focus on the initial convective event in the following detailed analysis, continuing to carve out what processes led to the intense development.

Before noon small convective cells start to develop along the slope over Nepal as a result of the exposure to the intense summertime insolation and the moist flow running toward and along the Himalayas over the Himalayan foothills (Fig. 12). These individual cells are scattered and not yet connected. As time progresses they grow and their life cycle depicts a pulsing pattern rather than a migratory character. While they reside roughly over the location where they originally developed, they grow and decline. This was characteristic throughout the event and probably stemmed from the low-level flow that pushed

against the mountains trapping the convective cells at their location of origin. The negligible vertical shear and weak winds could not organize the convective echoes, e.g. in a squall line structure. In the afternoon and evening (between 09:00 UTC and 12:00 UTC) convective echoes close to the location of the extreme event became more intense and organized upscale into a large contiguous, simulated echo region of 40 dBZ at ca. 12:00 UTC. Later, this intense echo region collapsed into multiple separated cores as the development of the cells continued (visible in the panels for 12:00 UTC and 15:00 UTC). Later during the evening and night more convective cells developed but did not reach the same magnitude or intensity (not shown).

The simulated convective echoes are vertically erect and do not tilt after forming the wide convective echo, visible in the reflectivity cross section of the fully developed convective system (Fig. 12, 12:00 UTC). This is consistent with Houze Jr *et al.* (2007) who investigated a wide and deep intense echo consisting of multiple vertically erect cells forming an amorphous structure, a structure of no particular shape. The here considered system was amorphous and did not show signs of a squall-line. This structure is consistent with the weak shear environment described in Section 3 and Houze Jr *et al.* (2007).

The horizontal extent exhibits characteristics of a deep and wide intense convective system (Houze Jr *et al.* 2007). The core of 40 dBZ exceeds an altitude of 12 km and has a width of approximately 40 km at the surface along the depicted cross section (Fig. 12). Houze Jr *et al.* (2007) defined a contiguous

Multiscale characteristics of an extreme precipitation event over Nepal

15

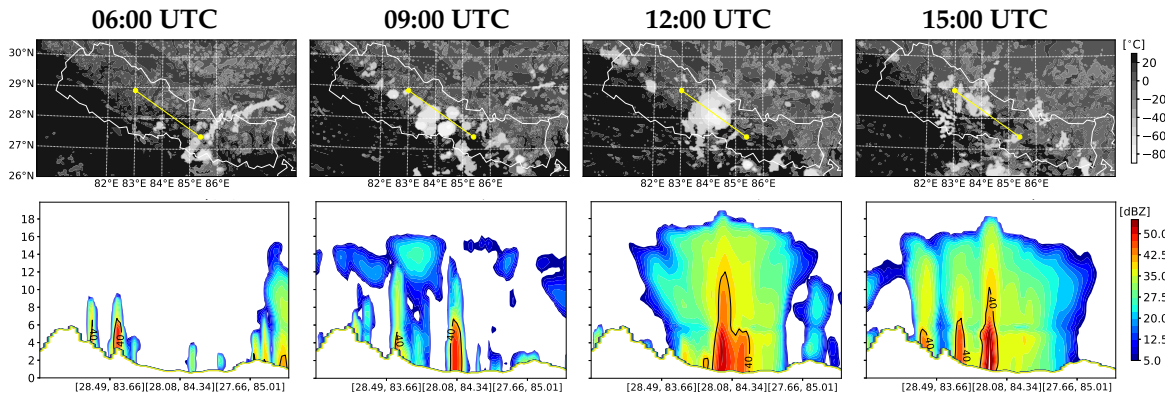


Figure 12. Simulated cloud top temperature (upper panels) and simulated reflectivity (lower panels) for the development of the main convective system. The x-axis in the lower panels describes coordinates along the transection in latitude and longitude.

region of 40 dBZ over a horizontal extent of more than 1000 km² as a wide convective system. Counting all grid cells on a model level that exceed 40 dBZ on the same level yields a maximum horizontal extent of our system of ca. 1550 km², hence it qualifies for the category of a wide convective system. Wide intense convective systems preferably develop along the central Himalayas according to climatologies of occurrence of different convective systems (Houze Jr *et al.* 2007; Romatschke *et al.* 2010; Romatschke and Houze Jr 2011). The system that formed is thus not very unusual in the region where it occurred, but did reach a considerable intensity. The simulated convective system depicted an echo maximum of 62 dBZ at an altitude of ca. 2900 m.a.s.l. (2200 m above ground) which was below the melting level at approximately 6 km (Fig. 16). The vertical location of the reflectivity maximum and the altitude of the zero degree line is similar to findings from Houze Jr *et al.* (2007) for deep convective events. The maximum vertical velocity of 26 ms⁻¹ is reached at an altitude of 13800 m.a.s.l. (13200 m above ground). The altitude of the maximum wind speed is consistent with measurements of mature convective systems over Gadanki (India) described in Uma and Rao (2009).

The wind field in the WRF-simulation suggests that northwesterly, moist, low-level flow was directed along the Himalayas, curving to the north and pushing onto the Siwalik Hills with an elevation of over 1000 m.a.s.l. (Fig. 13). The flow consequently underwent a significant lifting, which might have contributed

to destabilize the atmospheric column and thus to triggering and intensifying the convective system (see also Section 4.2). Moisture accumulated in the concave shaped topographic indentation close to Pokhara (Fig. 13). The accumulation of moisture created an environment where the convective system was able to tap into moist air, supplying more latent energy. A similar mechanism on a larger scale was suggested by Houze Jr *et al.* (2007) who argued that the concave indent in Northwest India leads to moisture accumulation from the low-level moist inflow which could feed deep convection.

Moreover, the low-level moist inflow is warmer than its surrounding, in particular compared to the low-level monsoon air from the Bay of Bengal and over Northeast India (not shown). The low-level monsoon air from the east has been cooled by frequent monsoon precipitation (Fig. 8) while moving onto the Indian subcontinent. This feature was also described in Sivall (1977). The westerly flow has probably gained heat while traveling across the hot regions in Pakistan and Northwest India. Not only surface latent heat fluxes were large but also surface sensible heat fluxes were considerable (up to 180 Wm⁻¹) compensating for cooling due to moisture uptake.

4.2. Thermodynamic environment

To obtain further insights into reasons for the intense development of the convective system, we assess the thermodynamic conditions using the parcel theory. On the day of the extreme event, just before the initiation, the environment is statically unstable

16

P. Bohlinger

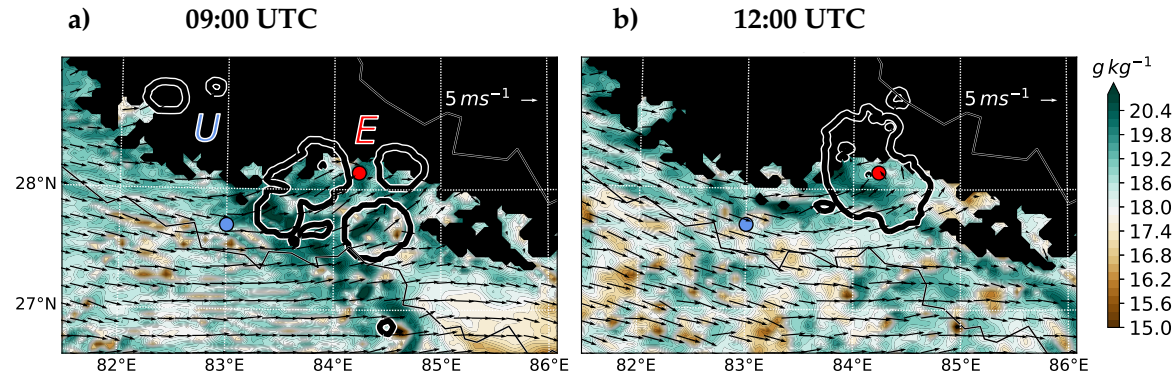


Figure 13. Specific humidity (filled contours) and wind at 850 hPa for 09:00 UTC (a) and 12:00 UTC (b). The considered convective system is indicated with the -60°C cloud top temperature isotherm and is displayed as black contour. Thermodynamic soundings are taken at the location of the event (E) and upstream (U) evaluated in Section 4.2.

with a large amount of convective available potential energy ($\text{CAPE} = 2335 \text{ J kg}^{-1}$) at the location of the main convective echo (Fig. 14a). When convection is triggered, CAPE is used up (Fig. 14b), but the convective cell is constantly supplied with energy from inflow with large CAPE (2431 J kg^{-1}). This can be seen in the sounding from the point upstream of the event indicated with the letter U (Fig. 13b and Fig. 14c). When convection occurs moisture is vertically redistributed. The vertical redistribution becomes visible in the skew-T diagrams when comparing the sounding of the inflow with the sounding at the location of the event. The dryer upper-level indent, at 300 hPa, and the mid-level indent, at 600 hPa, are removed by convective moistening (Fig. 14).

Medina *et al.* (2010) show a sounding structure depicting two layers of dry airmasses below 4 km and above 6 km. Similar to their study we can relate the dry layer between 700 hPa and 600 hPa to continental air emanating from the Hindu Kush. At 600 hPa, ERA-Interim depicts a maximum of westerly flow just downstream of the maximum at 500 hPa representing the slight descent of the continental dry air (not shown). The upper dry indent in the profile can be related to the planetary westerly flow (Fig. 3b,c) described in Sivall (1977) and also visible in Medina *et al.* (2010).

The question remains, why is there a moist bulge at around 500 hPa? In ERA-Interim, the air at 500 hPa is clearly dryer

than its surroundings as it flows down from the Hindu Kush meaning that this cannot be the origin of the moisture (not shown). Just before the flow passes Nepal, the air becomes moist at the mid-levels. The same can be seen along the Himalayas. The air is more moist suggesting that not horizontal advection but other processes were moistening this atmospheric layer. Medina *et al.* (2010) suggested that the moist layer in mid-levels might have been caused by previous convective events injecting moist monsoonal air into layers at higher altitude. This might be partly true for our case as well since there are various smaller convective events developing prior and upstream of the extreme event primarily along the Himalayas. Another source for the moisture at the mid-levels could stem from evaporation of cloud droplets. WRF simulates clouds at that altitude on the day of the extreme and previous days especially along the Himalayas.

The destabilizing effect of the orographic forcing discussed in Section 4.1 can be illustrated when comparing the inflow sounding upstream of the extreme event (marked with the letter U in Fig. 13) with the sounding at the location of the extreme event (marked with the letter E). In the lowermost pressure levels, the sounding depicts static stability indicated by a small amount of convective inhibition ($\text{CIN} = 56 \text{ J kg}^{-1}$). In order to release the large CAPE that is brought along with the flow, the CIN had to be removed. We described in Section 4.1 that the low-level flow pushed onto the Himalayan foothills of over 1000 m.a.s.l.. Such a lift could have removed the low-level stability and led to the

Multiscale characteristics of an extreme precipitation event over Nepal

17

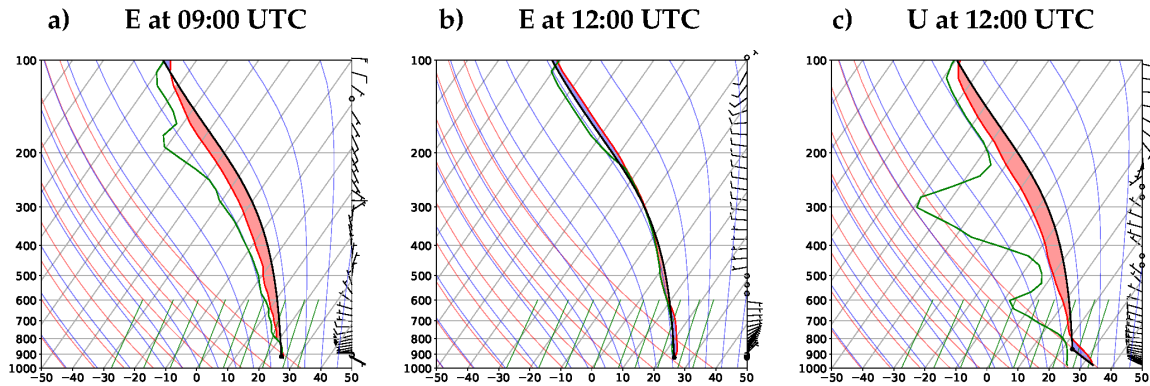


Figure 14. Skew-t Log-p diagrams for soundings taken at the location of the main convective event (E) and just upstream (U) as indicated in Figure 13 b). CAPE is filled with red and CIN with blue. For calculations of the CAPE and CIN we used the NCAR wrf-python library <http://wrf-python.readthedocs.io/en/latest/index.html>. The temperature sounding is depicted in red, the dewpoint temperature (Td) in green and the path of the considered air parcel in black. Dry adiabats are displayed as thin red lines and moist adiabats as thin blue lines. Wind barbs indicate wind direction and strength at all model levels.

unstable profile at the location of the extreme event. Additionally, quasi-geostrophic forcing might have contributed to further destabilize the air column (Section 3.1).

Medina *et al.* (2010) described a potentially unstable layer that was released for a deep convective system in Pakistan. In our case, the moist inflow at low-levels and a dry mid-level flow that is topped with a moist layer in the mid-troposphere create a potentially unstable environment (Fig. 14). The moisture profile reveals thus another reason for the severe development of the system. A thick layer of potentially unstable air, illustrated with the equivalent potential temperature θ_e (Fig. 15b), resides in the low to mid-troposphere. Near the ground θ_e is higher which means that if the moist air reaches condensation the air will become conditionally unstable and will continue to rise following the moist adiabat. Extra energy from latent heating is added to the convective system. At the location of the main event the potential instability is removed and the vertical extend of the updraft becomes visible represented by a tall chimney-like structure where the highly active 40 dBZ echo is simulated. Also the potential instability is supplied by the large-scale flow advecting dry airmasses in the mid-troposphere while supplying moist inflow at lower levels.

At the location of the extreme event there is only little vertical shear, consistent with the upright structure of the simulated echo

(Section 4.1). However, at the particular location of the chosen sounding the moist low-level inflow changes direction from 09:00 UTC to 12:00 UTC (compare Fig. 14a and 14b), which is probably due to two reasons. The incoming flow was trapped in the concave indentation and circles back out creating a northerly and north-easterly component (Fig. 13a,b). Another reason could be the convergence zone close to the thermal low created by the convective cell. Airmasses are consequently arriving from various directions depending on the location of the main updraft region. Once the convergence zone is established air could be sucked in from different directions. The wind barbs indicate only weak flow in the low-levels meaning that fine scale orographic features could be superimposed on the two mentioned mechanisms. Shifting the position of the sounding affects the direction of the wind barbs in the lower layers after initiation of the main convective system while it remains the same during the hours prior to the initiation (Fig. 13a,b). This supports the above explanation indicating that the two mechanisms were not yet in place before the initiation of the main convective system.

4.3. Simulated hydrometeors

A glance on the hydrometeors can reveal the reason for the simulated convective echo and helps when comparing our results with other case studies. The mixing ratio of three species simulated with the Thompson microphysics scheme are plotted in Figure 16a, graupel, snow, and rain. The graupel core together

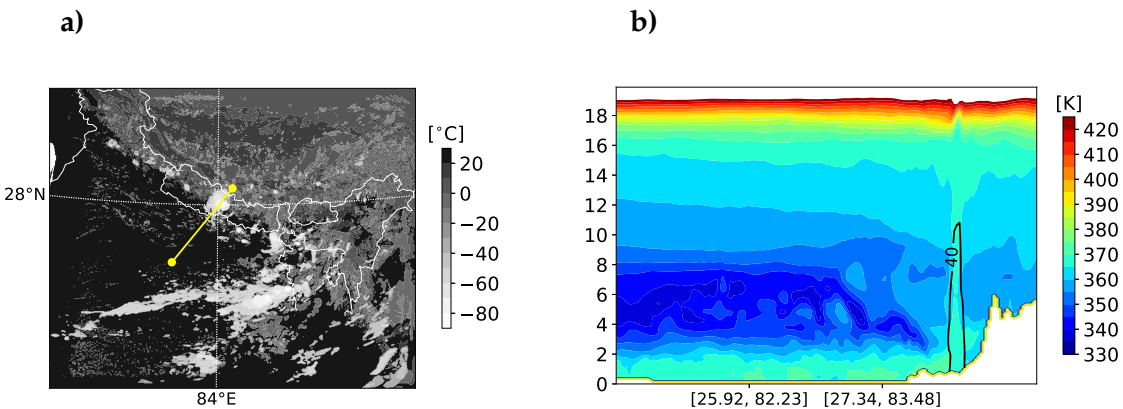


Figure 15. a) Simulated cloud top temperature and b) equivalent potential temperature in filled contours for 19 July 2007, 12:00UTC. The main convective system is indicated with the 40 dBZ reflectivity contour. Coordinates for the transection are displayed in b) as latitude and longitude for orientation.

with the strong updraft (Fig. 16b) is consistent with the described deep wide convective system and the high reflectivity (Section 4.1). The graupel core was probably accompanied by lightning. Houze Jr *et al.* (2007) showed that the frequency of lightning was connected to the frequency of deep and wide convective systems along the Himalayas with a maximum in Northwest India and northern Pakistan. Above the melting level a wide area of snow hydrometeors is present. Below, there is a distinct and strong rain core.

The vertical velocity core of values greater than 10 ms^{-1} has a large vertical extent reaching from 8 km to 16 km close to the tropopause. Vertical velocities exceed 20 ms^{-1} with a maximum of 26 ms^{-1} . The high vertical wind speed can elevate graupel particles to high altitudes with the 1 gkg^{-1} isoline reaching 17 km. Medina *et al.* (2010) and Kumar *et al.* (2014) reported similar updraft and graupel values for a convective event in Pakistan and Northwest India, respectively.

5. Discussion of similarities and differences to other findings

Given the various scales and diversity of the analyzed mechanisms, we summarize the main similarities and differences to other findings and discuss them in a larger context. The convective type of the extreme precipitation event in Nepal was classified as a deep and wide convective system which is not an unusual type of convective system for the considered region (Houze Jr *et al.* 2007). Moreover, the system developed in a region

prone to rain events as can be seen in rainfall climatologies from (Houze Jr *et al.* 2007; Bohlinger and Sorteberg 2017). However, the convective cell developed an unusual intensity due to the described supporting conditions across meteorological scales which, additional to the discussed results, are worth contrasting with existing findings.

On the large scales, similarities but also differences to high impact events over Pakistan and Northwest India became visible indicating the complex nature and high spatial variability of these events. Rasmussen *et al.* (2015) described a blocking situation over the Tibetan Plateau forcing quasi-stationary conditions. The long duration enabled a large amount of the moisture being funneled from the Bay of Bengal across India to Pakistan. This branch of moisture, additional to moist air from the Arabian Sea, could fuel convective systems causing floods in Pakistan. A Rossby wave train over Eurasia was suggested to be associated with this blocking high. During the extreme event over Nepal, there was no blocking high pressure system over the Tibetan Plateau. Instead, an upper-level trough was situated over Nepal imposing quasi-geostrophic forcing and inducing large-scale ascent. We detect a weak contribution from a quasi-stationary Rossby wave possibly sustaining the trough. The Rossby wave, however, was presumably not the origin of the upper-level trough.

In our case, low-level moist air did not flow from the Bay of Bengal to the west as described in Rasmussen *et al.* (2015) but

Multiscale characteristics of an extreme precipitation event over Nepal

19

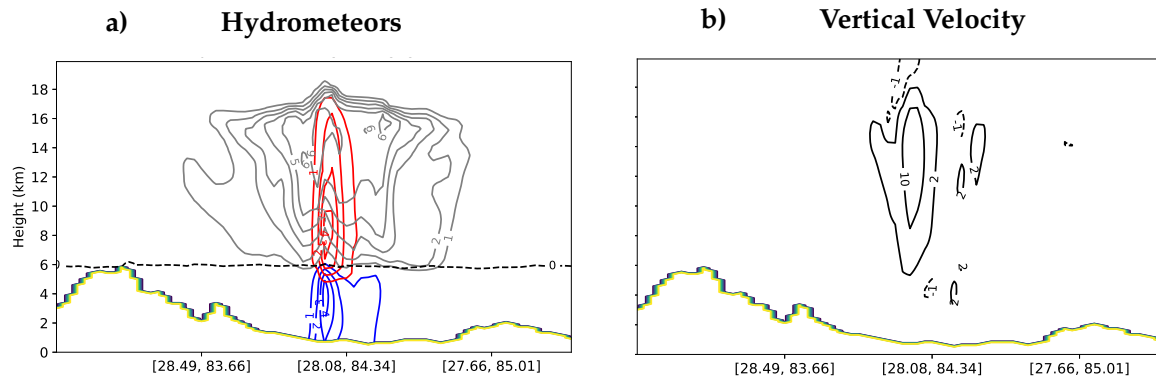


Figure 16. Simulated hydrometeors in g kg^{-1} (a) and vertical velocity in m s^{-1} (b) along the transect in Figure 12 with latitude and longitude on the x-axis for 19 July 2007, 12:00UTC. Graupel is plotted in red, snow in gray, and rain in blue contours. The melting level is marked as dashed black line.

was instead directed the opposite way, from Northwest India along the Himalayas toward the Bay of Bengal. This came about as a result of split flow conditions characteristic of break periods. Despite the described differences, it seems that the conditions in the contrasted cases met the same target: enabling high moisture amounts to be transported to the location of a deep convective system which could consequently develop a high intensity.

Moisture sources were consistent with Bohlinger *et al.* (2017) partly contrasting findings from Houze Jr *et al.* (2007), Medina *et al.* (2010), Martius *et al.* (2013), and Rasmussen *et al.* (2015). While Houze Jr *et al.* (2007) and Medina *et al.* (2010) discussed incoming moist airmasses that gain buoyancy over dry and heated land, we find evidence that for the discussed extreme event almost all direct moisture sources are located over land. Medina *et al.* (2010) and Martius *et al.* (2013) already suggested the possibility of preconditioning precipitation events moistening the soil prior to the main convective event. In fact, for one period of heavy rain in Pakistan, Martius *et al.* (2013) determined a major contribution from moisture sources over land. However, for another period, the moisture fraction from land was considerably reduced and a large contribution from the Arabian Sea was detected. For extreme precipitation events in Nepal, the high moisture contribution from land seems to be a generic feature as presented in Bohlinger *et al.* (2017). Based on a composite study they suggest that moisture sources were mainly located over land moistened by foregone precipitation events. This could be shown now for the

here discussed single case supporting their results.

The large-scale flow conditions enabling the build up of instability are similar to the findings in Houze Jr *et al.* (2007) and Medina *et al.* (2010). Dry and warm continental air emanated from the Hindu Kush region overrunning the low level flow from the Arabian Sea as suggested in Sawyer (1947). This leads to a capping inversion and prevents premature convection enabling the moisture to arrive and converge in the concave indent in Northwest India. A forced ascent e.g. by orography could help to break through the lid resulting in deep convective echoes. In our case, the moisture reached even farther to the east, namely to Nepal. Once the air column was destabilized by quasi-geostrophic forcing and orographic lifting, the continental air finally contributed to creating a potentially unstable environment and allowed for the intense development of the convective system.

6. Conclusions

We investigated conditions on multiple meteorological scales facilitating the extreme precipitation event in Central Nepal on 19 July 2007. This event was part of a series of heavy precipitation events leading to the devastating South Asia flood 2007. The involved processes are listed in the following:

1. Quasi-geostrophic forcing, imposed by an upper-tropospheric trough, prepared a favourable environment for the development of deep convection. The trough may have been supported by a Rossby wave train from Europe.

20

P. Bohlinger

2. The flow was orographically lifted onto the Siwalik hills reducing column static stability and possibly triggering the extreme event.
3. Monsoon break period low-level flow conditions directed the flow over the preconditioned moisture sources and supplied the convective system with an unusual warm and moist inflow. Moreover, the inflow was loaded with a large amount of CAPE fueling the convective system.

There was not a single dominating process responsible for the extreme event but the specific interplay and co-existence of the enumerated meteorological conditions that facilitated the formation of a deep and wide intense convective system of significant strength. The sequence of events and how they together create a favourable environment for the extreme precipitation event to happen is outlined in the following.

Break period low-level flow conditions and the approach of an upper tropospheric trough preluded the event. The low-level flow coming from the Arabian Sea was blocked by the Western Ghats and bifurcated, where the northern branch reached the Himalayas and turned east to continue along slope traversing Nepal. On the way to Nepal, moisture that stemmed from recent precipitation events allowed for anomalously high moisture uptake along the path, creating an unusual high moisture flux toward Nepal. Meanwhile, the upper-level trough exerted quasi-geostrophic forcing, contributing to destabilize the atmospheric column. A propagating stationary Rossby wave might have contributed to sustain the negative geopotential height anomaly. In Central Nepal, the moist low-level flow turned north, converging in an concave indent close to Pokhara where moisture could accumulate. Consequently, air was forced upslope destabilizing the stratification through orographic lifting. Convective systems were triggered organizing upscale into a deep and wide, intense convective system exhibiting an amorphous structure. Triggering was likely fostered by orographic lifting onto the Siwalik range in a favourable environment created by weak quasi-geostrophic forcing. The convective system was fed with potentially unstable air containing significant levels of CAPE facilitating the intense development and leading to precipitation amounts exceeding

250 mm d^{-1} . The main moisture sources were located along the Himalayas where the flow splitting during a break period might have been crucial for creating these conditions. The large-scale flow was mainly westerly during the entire lifetime of the convective event supplying moist low-level air. Rather dry air advected from the Hindu Kush mountains contributed to creating potentially unstable airmasses beneficial for the convective development.

While this case is interesting to study by itself, differences and similarities with other findings also reveal large spatial variability of extreme precipitation events and thus the value of an approach that appreciates regional differences. This case study further explains how a not unusual type of convective system can develop into an extreme precipitation event, and is hopefully valuable for the ultimate goal to better predict these events. Further research could focus on disentangling more the trigger mechanisms under different synoptic conditions as well as on the sensitivity of moisture abundance on the precipitation event.

Acknowledgement

This work has been funded by the University of Bergen, Norway. We thank the Department of Hydrology and Meteorology (DHM) in Nepal for sharing their rain gauge dataset. ERA-Interim reanalyses were provided by the ECMWF data server.

References

- Bluestein H. 1992. *Synoptic-dynamic meteorology in midlatitudes: Volume 1, principles of kinematics and dynamics*. New York, NY (United States); Oxford Univ. Press.
- Bohlanger P, Sorteberg A. 2017. A comprehensive view on trends in extreme precipitation in Nepal and their spatial distribution. *International Journal of Climatology* : doi: 10.1002/joc.5299.
- Bohlanger P, Sorteberg A, Sodemann H. 2017. Synoptic conditions and moisture sources actuating extreme precipitation in Nepal. *Journal of Geophysical Research: Atmosphere*, (status: accepted) : doi: 10.1002/2017JD027543.
- CNN. 2007. Millions flee 'worst ever' floods. <http://edition.cnn.com/2007/WORLD/asiapcf/08/03/soasia.floods/index.html>. Accessed: 2017-08-17.
- Dee D, Uppala S, Simmons A, Berrisford P, Poli P, Kobayashi S, Andrae U, Balmaseda M, Balsamo G, Bauer P, et al. 2011. The ERA-Interim

Multiscale characteristics of an extreme precipitation event over Nepal

21

- reanalysis: configuration and performance of the data assimilation system. *Quarterly Journal of the royal meteorological society* **137**(656): 553–597.
- Houze Jr R, McMurdie L, Rasmussen K, Kumar A, Chaplin M. 2017. Multiscale Aspects of the Storm Producing the June 2013 Flooding in Uttarakhand, India. *Monthly Weather Review* **145**(11): 4447–4466, doi: 10.1175/MWR-D-17-0004.1.
- Houze Jr RA, Rasmussen K, Medina S, Brodzik S, Romatschke U. 2011. Anomalous atmospheric events leading to the summer 2010 floods in Pakistan. *Bulletin of the American Meteorological Society* **92**(3): 291–298, doi: 0.1175 / 2010 BAM S3173.1.
- Houze Jr RA, Rasmussen KL, Zuluaga MD, Brodzik SR. 2015. The variable nature of convection in the tropics and subtropics: A legacy of 16 years of the Tropical Rainfall Measuring Mission satellite. *Reviews of Geophysics* **53**(3): 994–1021, doi: 10.1002/2015RG000488.
- Houze Jr RA, Wilton DC, Smull BF. 2007. Monsoon convection in the Himalayan region as seen by the TRMM Precipitation Radar. *Quarterly Journal of the Royal Meteorological Society* **133**(627): 1389–1411, doi: 10.1002/qj.106.
- Huffman GJ, Bolvin DT, Nelkin EJ, Wolff DB, Adler RF, Gu G, Hong Y, Bowman KP, Stocker EF. 2007. The TRMM multisatellite precipitation analysis (TMPA): Quasi-global, multiyear, combined-sensor precipitation estimates at fine scales. *Journal of Hydrometeorology* **8**(1): 38–55, doi: 10.1175/JHM560.1.
- Joseph P, Sijikumar S. 2004. Intraseasonal variability of the low-level jet stream of the asian summer monsoon. *Journal of Climate* **17**(7): 1449–1458, doi: 10.1175/1520-0442(2004)017;1449:IVOTLJ;2.0.CO;2.
- Kumar A, Houze Jr RA, Rasmussen KL, Peters-Lidard C. 2014. Simulation of a flash flooding storm at the steep edge of the Himalayas. *Journal of Hydrometeorology* **15**(1): 212–228, doi: 10.1175/JHM-D-12-0155.1.
- Läderach A, Sodemann H. 2016. A revised picture of the atmospheric moisture residence time. *Geophysical Research Letters* **43**(2): 924–933, doi:10.1002/2015GL067449, URL <http://dx.doi.org/10.1002/2015GL067449>.
- Martius O, Sodemann H, Joos H, Pfahl S, Winschall A, Croci-Maspoli M, Graf M, Madonna E, Mueller B, Schemm S, et al. 2013. The role of upper-level dynamics and surface processes for the Pakistan flood of July 2010. *Quarterly Journal of the Royal Meteorological Society* **139**(676): 1780–1797, doi: 10.1002/qj.2082.
- Medina S, Houze RA, Kumar A, Niyogi D. 2010. Summer monsoon convection in the Himalayan region: Terrain and land cover effects. *Quarterly Journal of the Royal Meteorological Society* **136**(648): 593–616, doi: 10.1002/qj.601.
- Nepal Red Cross Society. 2007. Flood and Land slide information bulletin. http://reliefweb.int/sites/reliefweb.int/files/resources/48504C007E08F66F4925732A0026986F-Full_Report.pdf. Accessed: 2017-08-17.
- Press WH. 2007. *Numerical recipes 3rd edition: The art of scientific computing*. Cambridge university press.
- Räisänen J. 1995. Factors affecting synoptic-scale vertical motions: A statistical study using a generalized omega equation. *Monthly weather review* **123**(8): 2447–2460, doi: 10.1175/1520-0493(1995)123;2447:FASSVM;2.0.CO;2.
- Rajeevan M, Gadgil S, Bhate J. 2010. Active and break spells of the Indian summer monsoon. *Journal of earth system science* **119**(3): 229–247.
- Rasmussen K, Hill A, Toma V, Zuluaga M, Webster P, Houze R. 2015. Multiscale analysis of three consecutive years of anomalous flooding in Pakistan. *Quarterly Journal of the Royal Meteorological Society* **141**(689): 1259–1276, doi: 10.1002/qj.2433.
- Rasmussen KL, Houze Jr RA. 2012. A flash-flooding storm at the steep edge of high terrain: disaster in the Himalayas. *Bulletin of the American Meteorological Society* **93**(11): 1713–1724, doi: 10.1175/BAMS-D-11-00236.1.
- reliefweb. 2007. Nepal: Disaster Situation of Landslides, Floods and Epidemics 2007. <http://reliefweb.int/map/nepal/nepal-disaster-situation-landslides-floods-and-epidemics-2007>. Accessed: 2017-08-17.
- Romatschke U, Houze Jr RA. 2011. Characteristics of precipitating convective systems in the South Asian monsoon. *Journal of Hydrometeorology* **12**(1): 3–26, doi: 10.1175/2010JHM1289.1.
- Romatschke U, Medina S, Houze Jr RA. 2010. Regional, seasonal, and diurnal variations of extreme convection in the South Asian region. *Journal of climate* **23**(2): 419–439, doi: 10.1175/2009JCLI3140.1.
- Sawyer J. 1947. The structure of the intertropical front over NW India during the SW monsoon. *Quarterly Journal of the Royal Meteorological Society* **73**(317-318): 346–369, doi: 10.1002/qj.49707331709.
- Sivall TR. 1977. Synoptic-climatological study of the Asian Summer monsoon in Afghanistan. *Geografiska Annaler. Series A. Physical Geography* : 67–87.
- Skamarock WC, Klemp JB. 2008. A time-split nonhydrostatic atmospheric model for weather research and forecasting applications. *Journal of Computational Physics* **227**(7): 3465–3485, doi: 10.1016/j.jcp.2007.01.037.
- Skamarock WC, Klemp JB, Dudhia J, Gill DO, Barker DM, Duda MG, Huang XY, Wang W, Powers JG. 2008. A description of the Advanced Research WRF version 3. NCAR Tech. Note NCAR/TN-475ISTR. http://www.mmm.ucar.edu/wrf/users/docs/arw_v3.pdf.
- Sodemann H, Schwierz C, Wernli H. 2008. Interannual variability of Greenland winter precipitation sources: Lagrangian moisture diagnostic and North Atlantic Oscillation influence. *Journal of Geophysical Research: Atmospheres* **113**(D3), doi:10.1029/2007JD008503.
- Stohl A, Forster C, Frank A, Seibert P, Wotawa G. 2005. Technical note: The Lagrangian particle dispersion model FLEXPART version 6.2. *Atmospheric Chemistry and Physics* **5**(9): 2461–2474, doi:10.5194/acp-5-2461-2005.

22

P. Bohliger

- Takaya K, Nakamura H. 2001. A formulation of a phase-independent wave-activity flux for stationary and migratory quasigeostrophic eddies on a zonally varying basic flow. *Journal of the atmospheric sciences* **58**(6): 608–627, doi: 10.1175/1520-0469(2001)058;0608:AFOAPI;2.0.CO;2.
- Takaya K, Nakamura H. 2005. Mechanisms of intraseasonal amplification of the cold Siberian high. *Journal of the atmospheric sciences* **62**(12): 4423–4440, doi: 10.1175/JAS3629.1.
- Uma K, Rao TN. 2009. Characteristics of vertical velocity cores in different convective systems observed over Gadanki, India. *Monthly Weather Review* **137**(3): 954–975, doi: 10.1175/2008MWR2677.1.
- Wang JX, Gaffen DJ. 2001. Late-twentieth-century climatology and trends of surface humidity and temperature in China. *Journal of Climate* **14**(13): 2833–2845, doi: 10.1175/1520-0442(2001)014;2833:LTCCAT;2.0.CO;2.
- Winschall A, Pfahl S, Sodemann H, Wernli H. 2014. Comparison of Eulerian and Lagrangian moisture source diagnostics—the flood event in eastern Europe in May 2010. *Atmospheric Chemistry and Physics* **14**(13): 6605–6619, doi:10.5194/acp-14–6605–2014.

Bibliography

- Ashok, K., Z. Guan, and T. Yamagata (2001), Impact of the Indian Ocean dipole on the relationship between the Indian monsoon rainfall and ENSO, *Geophysical Research Letters*, 28(23), 4499–4502, doi: 10.1029/2001GL013,294. [2.3.2](#)
- Baidya, S., M. Shrestha, and M. Sheikh (2008), Trends in daily climatic extremes of temperature and precipitation in Nepal, *Journal of Hydrology and Meteorology*, 5(1), 38–51. [1.1](#)
- Barros, A., M. Joshi, J. Putkonen, and D. Burbank (2000), A study of the 1999 monsoon rainfall in a mountainous region in central Nepal using TRMM products and rain gauge observations, *Geophysical Research Letters*, 27(22), 3683–3686, doi: 10.1029/2000GL011,827. [6.1](#)
- Barros, A. P., and T. J. Lang (2003), Monitoring the monsoon in the Himalayas: Observations in central Nepal, June 2001, *Monthly Weather Review*, 131(7), 1408–1427, doi: 10.1175/1520–0493(2003)131<1408:MTMITH>2.0.CO;2. [2.2](#)
- Blahak, U. (2008, updated June 2012), RADAR_MIE_LM and RADAR_MIELIB - Calculation of Radar Reflectivity from model output., *Tech. rep.*, Institute of Meteorology and Climate Research, University Karlsruhe, Research Center Karlsruhe. [6.2.2](#)
- Bluestein, H. (1992), *Synoptic-dynamic meteorology in midlatitudes: Volume 1, principles of kinematics and dynamics*, New York, NY (United States); Oxford Univ. Press. [6.2.2](#), [6.2.2](#), [6.2.2](#)
- Bolstad, W. M. (2007), *Introduction to Bayesian Statistics (Second Edition)*, John Wiley & Sons, Inc, Hoboken, New Jersey. [6.2.1](#)
- Bookhagen, B. (2010), Appearance of extreme monsoonal rainfall events and their impact on erosion in the Himalaya, *Geomorphics, Natural Hazards and Risk*, 1(1), 37–50, doi: 10.1080/19475701003625,737. [1.2](#), [2.2](#)
- Bookhagen, B., and D. W. Burbank (2006), Topography, relief, and TRMM-derived rainfall variations along the Himalaya, *Geophysical Research Letters*, 33(8), doi: 10.1029/2006GL026037. [1.2](#), [2.2](#)
- Bookhagen, B., and D. W. Burbank (2010), Toward a complete Himalayan hydrological budget: Spatiotemporal distribution of snowmelt and rainfall and their impact on river discharge, *Journal of Geophysical Research: Earth Surface (2003–2012)*, 115(F3), doi:10.1029/2009JF001426. [1.2](#), [2.2](#)

- Boos, W. R., and Z. Kuang (2010), Dominant control of the South Asian monsoon by orographic insulation versus plateau heating, *Nature*, 463(7278), 218–222, doi: 10.1038/nature08,707. [2.3.1](#)
- Cadet, D., and G. Reverdin (1981), Water vapour transport over the Indian Ocean during summer 1975, *Tellus*, 33(5), 476–487, doi: 10.3402/tellusa.v33i5.10,737. [2.3.1](#), [5](#)
- Cadet, D. L., and S. Greco (1987a), Water vapor transport over the Indian Ocean during the 1979 summer monsoon. Part I: Water vapor fluxes, *Monthly weather review*, 115(3), 653–663, doi: 10.1175/1520–0493(1987)115<0653:WVTOTI>2.0.CO;2. [2.3.1](#)
- Cadet, D. L., and S. Greco (1987b), Water vapor transport over the Indian ocean during the 1979 summer monsoon. Part II: water vapor budgets, *Monthly weather review*, 115(10), 2358–2366, doi: 10.1175/1520–0493(1987)115<2358:WVTOTI>2.0.CO;2. [2.3.1](#)
- Caesar, J., et al. (2011), Changes in temperature and precipitation extremes over the Indo-Pacific region from 1971 to 2005, *International Journal of Climatology*, 31(6), 791–801, doi: 10.1002/joc.2118. [1.1](#)
- Chalise, S., and N. Khanal (2002), Recent extreme weather events in the Nepal Himalayas, *The extremes of the extremes: extraordinary floods*, 271, 141–146, IHAS Publ. no. 271. [1.1](#)
- Coles, S., J. Bawa, L. Trenner, and P. Dorazio (2001), *An Introduction to Statistical Modeling of Extreme Values*, vol. 208, Springer, London. [6.2.1](#)
- Dee, D., et al. (2011), The ERA-Interim reanalysis: configuration and performance of the data assimilation system, *Quarterly Journal of the royal meteorological society*, 137(656), 553–597, doi: 10.1002/qj.828. [6.1](#), [6.2.2](#)
- Field, C., et al. (Eds.) (2012), *IPCC, 2012: Managing the Risks of Extreme Events and Disasters to Advance Climate Change Adaptation: Special Report of Working Groups I and II of the Intergovernmental Panel on Climate Change*, 582pp pp., Cambridge University Press, Cambridge, UK and New York, NY, USA. [1.1](#)
- Fine, C. M., R. H. Johnson, P. E. Ciesielski, and R. K. Taft (2016), The Role of Topographically Induced Vortices in Tropical Cyclone Formation over the Indian Ocean, *Monthly Weather Review*, 144(12), 4827–4847, doi: 10.1175/MWR-D-16-0102.1. [6.2.2](#)
- Gadgil, S., and K. R. Kumar (2005), The Asian monsoon - agriculture and economy, in *The Asian Monsoon*, edited by B. Wang, chap. 18, pp. 651–683, Springer-Verlag, Berlin, Heidelberg, New York. [2.3](#)
- Ghosh, S., M. Pant, and B. Dewan (1978), Influence of the Arabian Sea on the Indian summer monsoon, *Tellus*, 30(2), 117–125, doi: 10.1111/j.2153–3490.1978.tb00,825x. [2.3.1](#), [5](#)

- Hodges, K. (1995), Feature tracking on the unit-sphere, *Monthly Weather Review*, 123(12), 3458–3465, doi: 10.1175/1520–0493(1995)123<3458:FTOTUS>2.0.CO;2. [6.2.2](#)
- Hodges, K. (1999), Adaptive constraints for feature tracking, *Monthly Weather Review*, 127(6), 1362–1373, doi: 10.1175/1520–0493(1999)127<1362:ACFFT>2.0.CO;2. [6.2.2](#)
- Hodges, K. I. (1994), A general method for tracking analysis and its application to meteorological data, *Monthly Weather Review*, 122(11), 2573–2586, doi: 10.1175/1520–0493(1994)122<2573:AGMFTA>2.0.CO;2. [6.2.2](#)
- Hodges, K. I., and R. Emerton (2015), The Prediction of Northern Hemisphere Tropical Cyclone Extended Life Cycles by the ECMWF Ensemble and Deterministic Prediction Systems. Part I: Tropical Cyclone Stage, *Monthly Weather Review*, 143(12), 5091–5114, doi: 10.1175/MWR-D-13-00385.1. [6.2.2](#)
- Hoskins, B., I. Draghici, and H. Davies (1978), A new look at the ω -equation, *Quarterly Journal of the Royal Meteorological Society*, 104(439), 31–38, doi: 10.1002/qj.49710443,903. [6.2.2](#)
- Houze Jr, R., L. McMurdie, K. Rasmussen, A. Kumar, and M. Chaplin (2017), Multi-scale Aspects of the Storm Producing the June 2013 Flooding in Uttarakhand, India, *Monthly Weather Review*, 145(11), 4447–4466, doi: 10.1175/MWR-D-17-0004.1. [1.1](#), [4](#), [5](#)
- Houze Jr, R. A., D. C. Wilton, and B. F. Smull (2007), Monsoon convection in the Himalayan region as seen by the TRMM Precipitation Radar, *Quarterly Journal of the Royal Meteorological Society*, 133(627), 1389–1411, doi: 10.1002/qj.106. [1.2](#), [2.1](#), [2.2](#), [2.3.1](#)
- Houze Jr, R. A., K. Rasmussen, S. Medina, S. Brodzik, and U. Romatschke (2011), Anomalous atmospheric events leading to the summer 2010 floods in Pakistan, *Bulletin of the American Meteorological Society*, 92(3), 291–298, doi: 0.1175 / 2010 BAM S3173.1. [1.1](#), [2.1](#), [4](#)
- Huffman, G. J., D. T. Bolvin, E. J. Nelkin, D. B. Wolff, R. F. Adler, G. Gu, Y. Hong, K. P. Bowman, and E. F. Stocker (2007), The TRMM multisatellite precipitation analysis (TMPA): Quasi-global, multiyear, combined-sensor precipitation estimates at fine scales, *Journal of Hydrometeorology*, 8(1), 38–55, doi: 10.1175/JHM560.1. [6.1](#)
- Ichiyanagi, K., M. D. Yamanaka, Y. Muraji, and B. K. Vaidya (2007), Precipitation in Nepal between 1987 and 1996, *International Journal of Climatology*, 27(13), 1753–1762, doi: 10.1002/joc.1492. [2.1](#), [2.3.2](#)
- Joseph, P., and S. Sijikumar (2004), Intraseasonal variability of the low-level jet stream of the Asian summer monsoon, *Journal of Climate*, 17(7), 1449–1458, doi: 10.1175/1520–0442(2004)017<1449:IVOTLJ>2.0.CO;2. [2.1](#), [2.3.2](#)

- Kansakar, S. R., D. M. Hannah, J. Gerrard, and G. Rees (2004), Spatial pattern in the precipitation regime of Nepal, *International Journal of Climatology*, 24(13), 1645–1659. [2.2](#), [2.2](#)
- Katz, R. W., M. B. Parlange, and P. Naveau (2002), Statistics of extremes in hydrology, *Advances in Water Resources*, 25(8–12), 1287–1304, doi: 10.1016/S0309-1708(02)00,056–8. [6.2.1](#)
- Koenker, R., and K. Hallock (2001), Quantile regression: An introduction, *Journal of Economic Perspectives*, 15(4), 43–56. [6.2.1](#)
- Krishnamurthy, V., and R. Ajayamohan (2010), Composite structure of monsoon low pressure systems and its relation to Indian rainfall, *Journal of Climate*, 23(16), 4285–4305, doi: 10.1175/2010JCLI2953.1. [2.2](#)
- Kumar, A., R. A. Houze Jr, K. L. Rasmussen, and C. Peters-Lidard (2014), Simulation of a flash flooding storm at the steep edge of the Himalayas, *Journal of Hydrometeorology*, 15(1), 212–228, doi: 10.1175/JHM-D-12–0155.1. [1.1](#), [2.1](#), [2.1](#), [4](#)
- Kumar, K. K., B. Rajagopalan, and M. A. Cane (1999), On the weakening relationship between the Indian monsoon and ENSO, *Science*, 284(5423), 2156–2159, doi: 10.1126/science.284.5423.2156. [2.1](#), [2.3.2](#)
- Läderach, A. (2016), Characteristic scales of atmospheric moisture transport, Ph.D. thesis, ETH Zurich. [2.3.1](#)
- Läderach, A., and H. Sodemann (2016), A revised picture of the atmospheric moisture residence time, *Geophysical Research Letters*, 43(2), 924–933, doi:10.1002/2015GL067449. [6.1](#), [6.2.2](#), [6.3](#)
- Lang, T. J., and A. P. Barros (2002), An investigation of the onsets of the 1999 and 2000 monsoons in central Nepal, *Monthly Weather Review*, 130(5), 1299–1316, doi: 10.1175/1520–0493(2002)130<1299:AIOTOO>2.0.CO;2. [1.2](#), [2.1](#), [2.2](#), [2.3.2](#)
- Laprise, R. (1992), The Euler equations of motion with hydrostatic pressure as an independent variable, *Monthly weather review*, 120(1), 197–207, doi: 10.1175/1520–0493(1992)120<0197:TEEOMW>2.0.CO;2. [6.2.2](#)
- Marahatta, S., B. S. Dangol, and G. B. Gurung (2009), Temporal and spatial variability of climate change over Nepal (1976–2005), *Tech. rep.*, Practical Action Nepal Office. [2.3.1](#)
- Martius, O., et al. (2013), The role of upper-level dynamics and surface processes for the Pakistan flood of July 2010, *Quarterly Journal of the Royal Meteorological Society*, 139(676), 1780–1797, doi: 10.1002/qj.2082. [5](#)
- Medina, S., R. A. Houze, A. Kumar, and D. Niyogi (2010), Summer monsoon convection in the Himalayan region: Terrain and land cover effects, *Quarterly Journal of the Royal Meteorological Society*, 136(648), 593–616, doi: 10.1002/qj.601. [2.1](#)

- Nandargi, S., and O. Dhar (2011), Extreme rainfall events over the Himalayas between 1871 and 2007, *Hydrological Sciences Journal*, 56(6), 930–945, doi: 10.1080/0262667.2011.595373. [1.2](#), [1.2](#), [2.1](#), [2.2](#)
- Nayava, J. L. (1980), Rainfall in Nepal, *Himalayan Review*, 12, 1–18. [2.3](#), [2.3.1](#)
- Press, W. H. (2007), *Numerical recipes 3rd edition: The art of scientific computing*, Cambridge university press, New York. [6.2.2](#), [6.2.2](#)
- Rajeevan, M., S. Gadgil, and J. Bhate (2010), Active and break spells of the Indian summer monsoon, *Journal of earth system science*, 119(3), 229–247, doi: 10.1007/s12,040–010–0019–4. [2.1](#), [2.3.2](#)
- Rasmussen, K., A. Hill, V. Toma, M. Zuluaga, P. Webster, and R. Houze (2015), Multiscale analysis of three consecutive years of anomalous flooding in Pakistan, *Quarterly Journal of the Royal Meteorological Society*, 141(689), 1259–1276, doi: 10.1002/qj.2433. [1.1](#), [2.1](#), [4](#)
- Rasmussen, K. L., and R. A. Houze Jr (2012), A flash-flooding storm at the steep edge of high terrain: disaster in the Himalayas, *Bulletin of the American Meteorological Society*, 93(11), 1713–1724, doi: 10.1175/BAMS-D-11-00,236.1. [1.1](#), [2.1](#), [2.1](#), [4](#)
- Renard, B., X. Sun, and M. Lang (2013), Bayesian Methods for Non-stationary Extreme Value Analysis, in *Extremes in a Changing Climate - Detection, Analysis, and Uncertainty*, edited by A. A. Kouchak, D. Easterling, K. Hsu, S. Schubert, and S. Sorooshian, chap. 3, pp. 39–95, Springer Science+Business Media Dordrecht, Dordrecht, Heidelberg, New York, London. [6.2.1](#)
- Romatschke, U., and R. A. Houze Jr (2011), Characteristics of precipitating convective systems in the South Asian monsoon, *Journal of Hydrometeorology*, 12(1), 3–26, doi: 10.1175/2010JHM1289.1. [1.2](#), [2.2](#)
- Romatschke, U., S. Medina, and R. A. Houze Jr (2010), Regional, seasonal, and diurnal variations of extreme convection in the South Asian region, *Journal of climate*, 23(2), 419–439, doi: 10.1175/2009JCLI3140.1. [1.2](#), [2.1](#), [2.2](#)
- Rousseeuw, P. J. (1987), Silhouettes: a graphical aid to the interpretation and validation of cluster analysis, *Journal of computational and applied mathematics*, 20, 53–65, doi: 10.1016/0377–0427(87)90,125–7. [6.2.1](#)
- Sawyer, J. (1947), The structure of the intertropical front over NW India during the SW monsoon, *Quarterly Journal of the Royal Meteorological Society*, 73(317-318), 346–369, doi: 10.1002/qj.49707331,709. [2.1](#), [2.1](#)
- Shrestha, A. B., S. R. Bajracharya, A. R. Sharma, C. Duo, and A. Kulkarni (2016), Observed trends and changes in daily temperature and precipitation extremes over the Koshi river basin 1975–2010, *International Journal of Climatology*, doi: 10.1002/joc.4761, 37(2). [1.1](#)
- Shrestha, K. L. (2005), Global change impact assessment for himalayan mountain regions for environmental management and sustainable development, *Global Environmental Research*, 9(1), 69–81. [1.1](#)

- Shrestha, M. (2000), Interannual variation of summer monsoon rainfall over Nepal and its relation to Southern Oscillation Index, *Meteorology and Atmospheric Physics*, 75(1-2), 21–28, doi: 10.1007/s007030070,012. [2.1](#), [2.3.2](#)
- Sigdel, M., and M. Ikeda (), Summer monsoon rainfall over nepal related with large-scale atmospheric circulations, *Journal of Earth Science & Climatic Change*, 2012, doi: 10.4172/2157-7617.1000112. [2.1](#), [2.3.2](#)
- Sillmann, J., V. V. Kharin, X. Zhang, F. W. Zwiers, and D. Branaugh (2013a), Climate extremes indices in the CMIP5 multimodel ensemble: Part 1. Model evaluation in the present climate, *Journal of Geophysical Research: Atmospheres*, 118(4), 1716–1733, doi: 10.1002/jgrd.50,203. [1.1](#)
- Sillmann, J., V. V. Kharin, F. W. Zwiers, X. Zhang, and D. Branaugh (2013b), Climate extremes indices in the CMIP5 multimodel ensemble: Part 2. Future climate projections, *Journal of Geophysical Research: Atmospheres*, 118(6), 2473–2493, doi: 10.1002/jgrd.50,188. [1.1](#)
- Skamarock, W. C., and J. B. Klemp (2008), A time-split nonhydrostatic atmospheric model for weather research and forecasting applications, *Journal of Computational Physics*, 227(7), 3465–3485, doi: 10.1016/j.jcp.2007.01.037. [6.1](#), [6.2.2](#)
- Skamarock, W. C., J. B. Klemp, J. Dudhia, D. O. Gill, D. M. Barker, M. G. Duda, X.-Y. Huang, W. Wang, and J. G. Powers (2008), A description of the Advanced Research WRF version 3. NCAR Tech. Note NCAR/TN-4751STR, http://www.mmm.ucar.edu/wrf/users/docs/arw_v3.pdf. [6.1](#), [6.2.2](#)
- Sodemann, H., C. Schwierz, and H. Wernli (2008), Interannual variability of Greenland winter precipitation sources: Lagrangian moisture diagnostic and North Atlantic Oscillation influence, *Journal of Geophysical Research: Atmospheres*, 113(D3), doi: 10.1029/2007JD008503. [2.3.1](#), [2.3](#), [6.2.2](#), [6.3](#)
- Sørland, S. L., and A. Sorteberg (2015a), The dynamic and thermodynamic structure of monsoon low-pressure systems during extreme rainfall events, *Tellus A*, 67, doi: 10.3402/tellusa.v67.27039. [2.2](#), [6.2.2](#)
- Sørland, S. L., and A. Sorteberg (2015b), Low-pressure systems and extreme precipitation in central India: sensitivity to temperature changes, *Climate Dynamics*, 47(1-2), 465–480, doi: 10.1007/s00382-015-2850-4. [6.2.2](#)
- Stiller-Reeve, M. A., M. A. Syed, T. Spengler, J. A. Spinney, and R. Hossain (2015), Complementing scientific monsoon definitions with social perception in Bangladesh, *Bulletin of the American Meteorological Society*, 96(1), 49–57, doi: 10.1175/BAMS-D-13-00,144.1. [2.3.1](#)
- Stocker, T., et al. (2013), IPCC, 2013: climate change 2013: the physical science basis. Contribution of working group I to the fifth assessment report of the intergovernmental panel on climate change. [1.1](#)

- Stohl, A., C. Forster, A. Frank, P. Seibert, and G. Wotawa (2005), Technical note: The Lagrangian particle dispersion model FLEXPART version 6.2, *Atmospheric Chemistry and Physics*, 5(9), 2461–2474, doi:10.5194/acp-5-2461-2005. [6.1](#), [6.2.2](#)
- Talchhabadel, R., R. Karki, and B. Parajuli (2016), Intercomparison of precipitation measured between automatic and manual precipitation gauge in Nepal, *Measurement*, 106, 264–273, doi: 10.1016/j.measurement.2016.06.047. [6.1](#)
- Thompson, G., R. M. Rasmussen, and K. Manning (2004), Explicit forecasts of winter precipitation using an improved bulk microphysics scheme. Part I: Description and sensitivity analysis, *Monthly Weather Review*, 132(2), 519–542, doi: 10.1175/1520-0493(2004)132<0519:EFOWPU>2.0.CO;2. [6.2.2](#)
- Thompson, G., P. R. Field, R. M. Rasmussen, and W. D. Hall (2008), Explicit forecasts of winter precipitation using an improved bulk microphysics scheme. part ii: Implementation of a new snow parameterization, *Monthly Weather Review*, 136(12), 5095–5115, doi: 10.1175/2008MWR2387.1. [6.2.2](#)
- Tibshirani, R., G. Walther, and T. Hastie (2001), Estimating the number of clusters in a data set via the gap statistic, *Journal of the Royal Statistical Society: Series B (Statistical Methodology)*, 63(2), 411–423. [6.2.1](#), [6.2.1](#), [6.2.1](#)
- Trenberth, K. E. (1997), The Definition of El Niño, *Bulletin of the American Meteorological Society*, 78(12), 2771–2777, doi:10.1175/1520-0477(1997)078<2771:TDOENO>2.0.CO;2. [2.1](#), [2.3.2](#)
- Trenberth, K. E., D. P. Stepaniak, and K. M. Caron (2000), The Global Monsoon as Seen through the Divergent Atmospheric Circulation, *Journal of Climate*, 13(22), 3969–3993, doi: 10.1175/1520-0442(2000)013<3969:TGMAST>2.0.CO;2. [2.3.1](#)
- Trenberth, K. E., J. W. Hurrell, and D. P. Stepaniak (2005), The Asian monsoon: Global perspectives, in *The Asian Monsoon*, edited by B. Wang, chap. 2, pp. 67–87, Springer-Verlag, Berlin, Heidelberg, New York. [2.3.1](#)
- Tyagi, A., P. Asnani, U. De, H. Hatwar, and A. Mazumdar (2012), The Monsoon Mono-graph, Vols. 1 and 2, *Indian Meteorological Department*. [6.2.2](#)
- Wagstaff, K. (2004), Clustering with missing values: No imputation required, in *Classification, Clustering, and Data Mining Applications. Studies in Classification, Data Analysis, and Knowledge Organisation.*, edited by Banks D., McMorris F.R., Arabie P., and Gaul W., pp. 649–658, Springer, Berlin, Heidelberg. [6.2.1](#)
- Waldron, K. M., J. Paegle, and J. D. Horel (1996), Sensitivity of a spectrally filtered and nudged limited-area model to outer model options, *Monthly weather review*, 124(3), 529–547, doi: 10.1175/1520-0493(1996)124<0529:SOASFA>2.0.CO;2. [6.2.2](#)
- Wang, J. X., and D. J. Gaffen (2001), Late-twentieth-century climatology and trends of surface humidity and temperature in China, *Journal of Climate*, 14(13), 2833–2845, doi: 10.1175/1520-0442(2001)014<2833:LTCCAT>2.0.CO;2. [2.3.1](#)

- Wang, S.-Y., and R. R. Gillies (2013), Influence of the Pacific quasi-decadal oscillation on the monsoon precipitation in Nepal, *Climate Dynamics*, 40(1-2), 95–107, doi: 10.1007/s00382-012-1376-2. [2.3.2](#)
- Webster, P. J., V. O. Magana, T. Palmer, J. Shukla, R. Tomas, M. Yanai, and T. Yasunari (1998), Monsoons: Processes, predictability, and the prospects for prediction, *Journal of Geophysical Research: Oceans*, 103(C7), 14,451–14,510, doi: 10.1029/97JC02719. [2.3](#), [2.3.1](#), [2.3.1](#), [2.3.2](#)
- Wicker, L. J., and W. C. Skamarock (2002), Time-splitting methods for elastic models using forward time schemes, *Monthly weather review*, 130(8), 2088–2097, doi: 10.1175/1520-0493(2002)130<2088:TSMFEM>2.0.CO;2. [6.2.2](#)
- Winschall, A., S. Pfahl, H. Sodemann, and H. Wernli (2014), Comparison of Eulerian and Lagrangian moisture source diagnostics—the flood event in eastern Europe in May 2010, *Atmospheric Chemistry and Physics*, 14(13), 6605–6619, doi:10.5194/acp-14–6605–2014. [6.2.2](#)
- Yang, S., and W. K.-M. Lau (2005), Interannual variability of the Asian monsoon, in *The Asian Monsoon*, edited by B. Wang, chap. 6, pp. 258–293, Springer-Verlag, Berlin, Heidelberg, New York. [2.3.2](#)